4.1.4 PAPER 3: Industrialization and Thermal Performance of a New Unitized Water Flow Glazing Facade

Overview

Water flow glazing (WFG), as an advanced facade technology, combines passive (coatings and polyvinyl butyral (PVB) layers) and active solutions (variable water mass flow rate) to absorb or reject infrared radiation and reduce the temperature of the interior glass pane. Flowing water captures most of the solar infrared radiation, while a significant part of the visible component goes through the glazing. WFG radiant panels can be used as components of a heating or cooling hydronic system with little difference between the water and the indoor temperature. Finally, WFG can work as an integrated solar collector to provide water heating in warm seasons, and the excess of hot water can be stored in buffer tanks. The use of the facade and interior partitions as radiant heating and cooling devices have advantages compared with convective cooling systems. The *Sofia prototype* showed some of the accomplishments of the research project: "Industrialized Development of Water Flow Glazing Systems" (InDeWag), supported by program Horizon 2020. An effort was made on industrializing a new WFG unitized facade and its introduction in the architecture, engineering, and construction (AEC) industry. The water flow glazing unitized facade was made of three components: glazing, circulating device, and aluminum frame. The glazing comprises different layers and interfaces according to determined spectral and thermal properties. The circulating device includes a water pump moving the fluid in a closed circuit, a heat exchanger, and temperature and flow sensors to monitor and control the heat. Finally, the aluminum frame provides the unitized module with structural stability.

After validating the simulation results in the first paper and after proving the ability to reject energy in the second paper, the next goal was to explore the potential of WFG to achieve an nZEB standard in an actual building. The design of new light envelopes for zero-energy buildings must integrate disciplines such as architectural design, building simulation, HVAC systems, and the curtain wall industry. This article showed a WFG unitized facade ready for architecture, engineering, and construction industries. In addition, the outputs were validated with an actual test facility placed in Sofia, Bulgaria. The design of new light envelopes for zero-energy buildings must integrate different disciplines such as architectural design, building simulation, HVAC systems, and the curtain wall industry. This article developed a methodology for selecting WFG solutions for different facades and tested its performance using real data. Case 1 was a triple glazing with the water chamber facing outdoors. Case 2 was made of triple glazing with water chamber indoors and Low-E coating. Case 3 had a high reflective coating on face 2 and a water chamber indoors. Hence, it was essential to *(i)* simulate the steady state to select the optimum WFG

in each orientation at the first stage of the design process, *(ii)* validate the first results by including transient boundary conditions, *(iii)* analyze the performance of the selected glazing in a real facility, and *(iv)* estimate the final energy savings, the potential renewable energy production, and CO_2 emissions in summer and winter conditions.

Dynamic properties of WFG allowed considering options for different orientations and the internal loads, which depend on the building use. The thermal transmittance (U) ranged from 1 W/m^2 K ($\dot{m} = 0$) to 0.06 W/m^2K ($\dot{m} = 2$ L/min m^2). A mass flow rate ($\dot{m}$) above 2 L/min m^2 (0.029 Kg/s m^2) did not impact the water–energy absorption. The position of the gas and water cavities and the spectral properties of glass panes and coatings affected the performance of the WFG. Simulation results at steady conditions showed that Case 2 had the best performance for energy absorption in winter (226.6 W/m^2). Case 1 showed the highest energy absorption in summer (603.3 W/m^2). Case 3 showed the lowest energy absorption, both in summer (131.9 W/m^2) and winter (11.5 W/m^2).

The difficulties identified were related to the high initial cost and the need for an energy management system integrated with the rest of the equipment conditioned the WFG system. After the first year of monitoring, there are uncertainties and system issues that must be addressed. Firstly, the control unit must integrate the ventilation system to reduce condensation risks. Secondly, the presented simulation tool must be integrated into commercial building performance simulation software. Finally, further research on the deployment is needed to bring down payback periods. Although considerable efforts have been made in the industrialization process, there is still low market penetration because of the limited information between professionals and consumers. With economies of scale a price comparable to triple-pane glazing systems equipped with automated exterior shading can be achieved.

Published Paper

sustainability

MDPI

Article

Industrialization and Thermal Performance of a New Unitized Water Flow Glazing Facade

Belen Moreno Santamaria [1], Fernando del Ama Gonzalo [2,*], Danielle Pinette [2], Benito Lauret Aguirregabiria [1] and Juan A. Hernandez Ramos [3]

[1] Department of Construction and Architectural Technology, Technical School of Architecture of Madrid, Technical University of Madrid (UPM), Av. Juan de Herrera 4, 28040 Madrid, Spain; belen.moreno@upm.es (B.M.S.); benito.lauret@upm.es (B.L.A.)

[2] Department of Sustainable Product Design and Architecture, Keene State College, 229 Main St., Keene, NH 03435, USA; pinetteda@gmail.com

[3] Department of Applied Mathematics, School of Aeronautical and Space Engineering, Technical University of Madrid (UPM), Plaza Cardenal Cisneros 3, 28040 Madrid, Spain; juanantonio.hernandez@upm.es

* Correspondence: fernando.delama@keene.edu

Received: 9 August 2020; Accepted: 11 September 2020; Published: 14 September 2020

Abstract: New light envelopes for buildings need a holistic vision based on the integration of architectural design, building simulation, energy management, and the curtain wall industry. Water flow glazing (WFG)-unitized facades work as transparent and translucent facades with new features, such as heat absorption and renewable energy production. The main objective of this paper was to assess the performance of a new WFG-unitized facade as a high-performance envelope with dynamic thermal properties. Outdoor temperature, variable mass flow rate, and solar radiation were considered as transient boundary conditions at the simulation stage. The thermal performance of different WFGs was carried out using simulation tools and real data. The test facility included temperature sensors and pyranometers to validate simulation results. The dynamic thermal transmittance ranged from 1 W/m^{2}K when the mass flow rate is stopped to 0.06 W/m^{2}K when the mass flow rate is above 2 L/min m^2. Selecting the right glazing in each orientation had an impact on energy savings, renewable energy production, and CO_2 emissions. Energy savings ranged from 5.43 to 6.46 KWh/m^2 day in non-renewable energy consumption, whereas the renewable primary energy production ranged from 3 to 3.42 KWh/m^2 day. The CO_2 emissions were reduced at a rate of 1 Kg/m^2 day. The disadvantages of WFG are the high up-front cost and more demanding assembly process.

Keywords: building energy management; water flow glazing; unitized facade

1. Introduction

The residential and commercial building sector accounts for almost 40% of the European Union final energy consumption [1]. Thus, the goal of achieving a highly energy-efficient building stock by 2050 was set by The Energy Performance of Buildings Directive (EPBD 2018) [2]. In the United States, recent studies have shown that heating and cooling account for more than 30% of energy consumption in buildings [3]. Other non-OECD countries, including China and India, will be responsible for half of the global increase in energy consumption until 2040 [4]. The development of new materials, new heating and ventilation technologies, and energy-saving measures have improved the thermal performance of buildings in winter conditions [5]. However, in summer conditions, the increasing standards of life and the affordability of air-conditioning technologies have contributed to increasing the energy needs for cooling over the last decade [6]. Nowadays, air conditioning in office and commercial facilities accounts for 15% of the total electricity consumption

in the world [7–9]. Occupants and equipment are responsible for internal heat gains, and large glass areas increase solar radiation gains, especially in warm climates, thus leading to the increased total electricity consumption for the purposes of cooling [10,11].

The design of advanced glazed facades is the most promising component in building design with the highest impact on building performance [12]. In this paper, advanced facades refer to a broad spectrum of constructive solutions that allow for the dynamic response of the building envelope. They can actively manage the heat flow and energy transfer between the building and its external environment, leading to a potentially significant reduction in heating and cooling loads [13]. Advanced glazed facades include passive solutions, such as Low-E coatings, which reflect the indoor heat when the outdoor temperature is low [14], and highly selective coatings that reflect direct and diffuse solar heat radiation in summer. Scientific literature has confirmed this potential energy reduction [15,16]. However, the most promising results can be accomplished with dynamic technologies that can adapt to different outdoor conditions. Polymer dispersed liquid crystal (PDLC), Suspended Particle Devices (SPDs), and electrochromic (EC) glass switch from transparent to colored or vary transmission and reflection parameters [17,18]. The system is limited by its high initial cost and the need for an energy management system integrated with the rest of the equipment, especially the ventilation system. Controlling the relative humidity is essential in radiant panels to prevent condensation issues, especially in summer. The integrated piping does not allow movable panels, so its use is limited to buildings with mechanical ventilation [19]. Nevertheless, the measures to improve the energy performance of buildings do not focus only on the building envelope. Building designers must consider all technical and mechanical systems in a building, such as passive elements; heating, ventilation, air conditioning (HVAC); the energy use for lighting and ventilation; and other measures to improve thermal and visual comfort [20].

Water flow glazing (WFG), as an advanced facade technology, combines passive (coatings and polyvinyl butyral (PVB) layers) and active solutions (variable water mass flow rate) to absorb or reject infrared radiation and reduce the temperature of the interior glass pane [21,22]. Flowing water captures most of the solar infrared radiation, while a significant part of the visible component goes through the glazing [23,24]. WFG radiant panels can be used as components of a heating or cooling hydronic system with little difference between the water and the indoor temperature [25]. Finally, WFG can work as an integrated solar collector to provide water heating in warm seasons, and the excess of hot water can be stored in buffer tanks [26]. The use of the facade and interior partitions as radiant heating and cooling devices have advantages compared with convective cooling systems. Using radiant ceilings or walls can reduce energy consumption between 10% to 70% compared with all-air systems [27]. This article showed some of the accomplishments of the research project: "Industrialized Development of Water Flow Glazing Systems" (InDeWag), supported by program Horizon 2020–the EU.3.3.1: Reducing energy consumption and carbon footprint by smart and sustainable use. The water flow glazing unitized facade is made of three components: glazing, circulating device, and aluminum frame [28]. The glazing comprises different layers and interfaces according to determined spectral and thermal properties. The circulating device includes a water pump moving the fluid in a closed circuit, a heat exchanger, and temperature and flow sensors to monitor and control the heat. Finally, the aluminum frame provides the unitized module with structural stability.

Despite the fast pace of product innovation, a gap has been created between the new advanced facades and the available building simulation tools to model and assess building energy performance [29]. Monitoring activities are essential to support simulation models, especially in transient state [30], when changing the boundary conditions can affect the results of dynamic simulations by more than 30% [31]. Although there are commercial building energy simulation tools that include dynamic simulations [32], very few include WFG [33,34]. The authors of this paper developed a set of equations that take into account multiple direct and diffuse reflections between the glazing surfaces, the absorptance of glass and water layers, the spectral properties of coatings, and the convective heat transfer coefficient [35,36]. Then, a simulation tool was developed to allow building designers to make decisions on the glazing type. Finally, the equations and the simulation tool were validated

through the real results taken from a demonstrator placed in Sofia, Bulgaria. In addition to an accurate simulation tool, the actual challenge was to develop a monitoring system to reveal characteristic patterns of users, and to finally discover relevant design criteria that might be applicable to different orientations throughout the year. The monitoring system applied in this case study has been tested in other facilities over the last few years, and results were shown in previous articles [37,38].

This paper focused on a methodology to select and assess the performance of different WFG configurations in a test facility in Sofia, Bulgaria. Hence, to achieve this goal, it was essential to (i) simulate the steady state to select the optimum WFG in each orientation at the first stage of the design process, (ii) validate the first results by including transient boundary conditions, (iii) analyze the performance of the selected glazing in a real facility, and (iv) estimate the final energy savings, the potential renewable energy production, and CO_2 emissions in summer and winter conditions.

2. Materials and Methods

Commercial building energy simulation (BES) software does not consider WFG as a component of the heating and cooling systems. It is essential to provide building designers with a simple method to select the correct glazing and evaluate its performance at the beginning of the design stage. The first subsection defines three tested WFGs in terms of spectral properties. The second subsection shows the mathematical model that defined the dynamic thermal properties of the glazing. The third subsection describes the components and industrialization process of the unitized WFG.

2.1. Determination of Spectral Properties

The International Glazing DataBase (IGDB) is a collection of optical data for glazing products. Spectral transmittance and reflectance are measured in a spectrophotometer and contributed to the IGDB by the manufacturer of the glazing product, subject to a careful review. The IGDB currently only allows the inclusion of specular glazing materials without patterns, such as monolithic glass, plastic, laminates, applied films on glass, or thin-film coated glass. The products included in the WFG catalog are low-emissivity (Low-E) glass, high selective glass, and solar polyvinyl butyral (PVB) interlayers to increase sun energy absorbance. The solar energy spectrum can be divided into the ultraviolet (UV) light, visible light, and infrared (IR) light, depending on the wavelength. The wavelengths of the ultraviolet light range from 310 to 380 nanometers. The visible light ranges from 380 to 780 nanometers. The infrared light spectrum is transmitted as heat into a building and begins at wavelengths of 780 nanometers. Solar heat radiation has shortwave energy, and it is known as near-infrared (NIR), whereas the heat radiating off warm objects has higher wavelengths and is known as far-infrared (FIR). Three different WFGs were tested:

- Case 1 was made of the following layers: Planiclear (8 mm), 2 Saflex R solar (SG41), Planiclear (8 mm), water chamber (24 mm), Planiclear (8 mm), Planiclear (8 mm), 4 Saflex R standard clear (RB11), Planiclear (8 mm), a low-emissivity coating Planitherm XN, an argon chamber (16 mm), Planiclear (6 mm), 4 Saflex R standard clear (RB11), Planiclear (6 mm).
- Case 2 was made of the following layers: diamant glass (10 mm), an argon chamber (16 mm), a low-emissivity coating Planitherm XN, Planiclear (8 mm), 2 Saflex R solar (SG41), Planiclear (8 mm), water chamber (24 mm), Planiclear (8 mm), 4 Saflex R standard clear (RB11), Planiclear (8 mm).
- Case 3 was made of the following layers: diamant glass (10 mm), a highly reflective coating Xtreme 60.28, an argon chamber (16 mm), Planiclear (8 mm), 4 Saflex R standard clear (RB11), Planiclear (8 mm), water chamber (24 mm), Planiclear (8 mm), 4 Saflex R standard clear (RB11), Planiclear (8 mm).

Figure 1 shows the front and back reflectance (R), transmittance (T), and absorptance (A), as a function of the angle of incidence. It illustrates the glass panes, coatings, and the position of the air and water chambers. Case 1 showed the highest infrared absorptance (A), the lowest front reflectance (R), and the lowest infrared transmittance (T). It seemed the best option to heat up water. Case 2

showed a high near-infrared (NIR) absorptance, low far-infrared (FIR) absorptance, and high front far-infrared (FIR) reflectance. The absorptance was not as high as in Case 1, but its ability to reflect heat made it the right solution for large glass areas in warm climates. Case 3 showed very low infrared absorptance and very high infrared front reflectance. This case would have been the best option to reject energy and prevent heat from entering the indoor space, but it would not have been appropriate to heat up water.

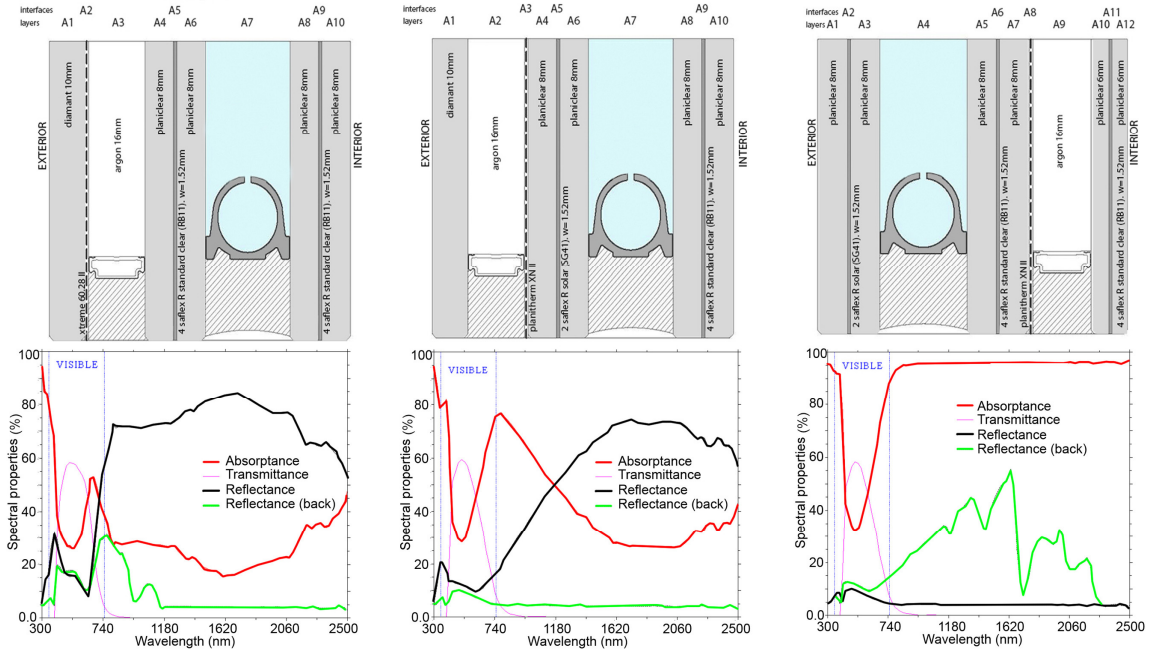

Figure 1. Spectral properties as a function of the solar wavelength. Description of the layers and coatings. (**a**) Case 1: 8 + 8/24 w /8 + 8/16 a /6 + 6. (**b**) Case 2: 10/16 a/Low-E8 + 8/24 w/8 + 8. (**c**) Case 3: 10XNII/16 a/8 + 8/24 w/8 + 8.

2.2. Determination of Heat Transfer Coefficients (h) and Dynamic Thermal Transmittance (U)

Water absorbs the solar near-infrared radiation and increases the temperature as it flows through the window. The mass flow rate and the thermal properties of glass panes must be studied to allow designers to apply energy-management strategies. Sometimes it might be interesting to increase the water temperature and store that energy for heating purposes. Other times it might be appropriate to reject as much solar radiation as possible without heating the water. The thermal transmittance (U) measures the heat transfer through the glazing and the European Standard determines its value [39,40]. Figure 2 illustrates the heat transfer coefficients (h_i, h_w, h_g, and h_e), the temperature distribution in the WFG layers (θ_i, θ_1, θ_2, θ_3, θ_w, θ_e), and the absorptance of layers (A_1, A_2, A_w, A_3).

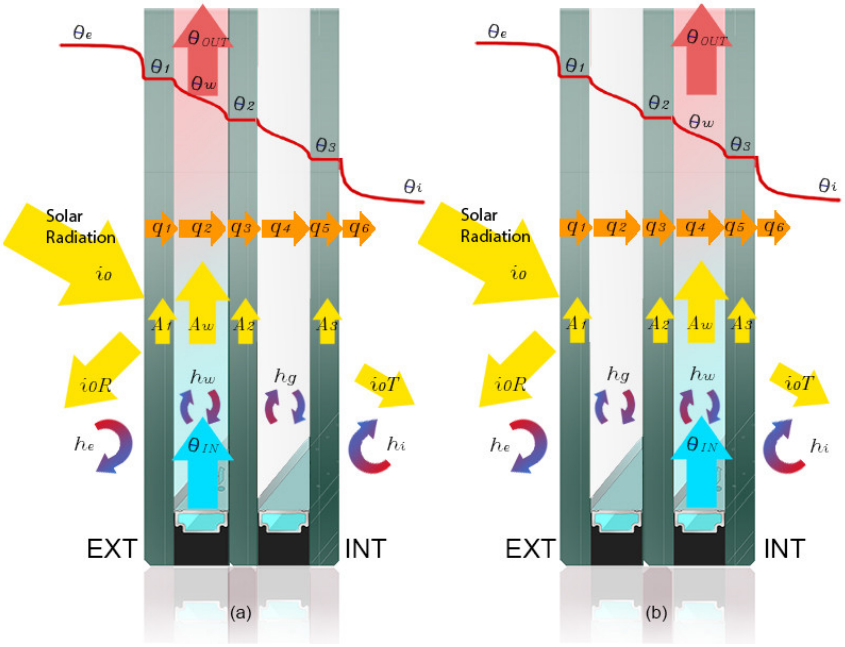

Figure 2. Temperature distribution in a triple water flow glazing (WFG) at a specific height, with heat transfer coefficients (h_i, h_w, h_g, h_e), heat fluxes through a triple WFG (q_1, q_2, q_3, q_4, q_5, q_6), solar radiation and absorptance of layers (A_1, A_2, A_w, A_3). (**a**) Triple WFG with water chamber outdoors. (**b**) Triple WFG with water chamber indoors.

The Equation (1) gives the outdoor heat flux:

$$q_e = h_e(\theta_e - \theta_1), \quad (1)$$

where h_e is the outdoor convective coefficient, θ_1 is the superficial temperature of the outermost glass pane, and θ_e is the outdoor temperature. The beam solar irradiance, diffuse irradiance, and the angle of incidence should be given. Regarding indoor boundary conditions, the indoor heat flux is given by the Equation (2):

$$q_i = h_i(\theta_3 - \theta_i), \quad (2)$$

where *hi* is the indoor convective coefficient, θ_3 is the superficial temperature of the inner glass pane, and θ_i is the indoor temperature that can be a constant value or calculated solving the indoor thermal problem. Newton's law also models the heat transfer inside gas chambers. The heat flux in a gas chamber between two parallel surfaces is expressed by Equation (3):

$$q_i = h_g(\theta_i - \theta_{i+1}), \quad (3)$$

where h_g is the heat transfer coefficient of gas chambers, this coefficient considers the radiative heat transfer between the parallel glass panes and the natural convective transport. This value can be constant or calculated, knowing the emissivity of the two glass planes and an experimental correlation for the natural convective transport. In the water chamber, the situation is different. Heat flux is proportional to the temperature difference between the water temperature θ_w and the glass pane temperatures. This coefficient takes into account the heat transport mechanism forced by the water flow inside the chamber. Since the water is opaque to far-infrared, the radiative heat transfer mechanism is not present in the water chamber. Hence, the heat flux through glass panes in contact with the water chamber is expressed in Equation (4) for glass panes outside the water chamber, and Equation (5) when the glass pane is after the water chamber:

$$q_i = h_w(\theta_{i-1} - \theta_w), \quad (4)$$

$$q_{i+1} = h_w(\theta_w - \theta_i), \quad (5)$$

where h_w is the heat transfer coefficient for the water chamber. By default $h_w = 50$.

When it comes to considering the absorptance of layers (A_i), the heat flux can be expressed as in Equation (6).

$$q_{i+1} = q_i + A_i\, i_0\,. \tag{6}$$

Spectral and thermal properties of WFG have been explained in previous articles [35]. The authors used data from commercial software and developed equations to evaluate the influence of water flowing through glass panes. Equation (7) considers the energy balance at each layer and Newton's definition of heat flux.

$$q_i = q_{i-1} + A_w\, i_0 + \dot{m}c(\theta_{IN} - \theta_{OUT}). \tag{7}$$

Equations (8)–(17) show the heat flux of WFG with water chamber indoors.

$$q_1 = h_e\,(\theta_e - \theta_1), \tag{8}$$

$$q_2 = q_1 + A_1\, i_0\,, \tag{9}$$

$$q_2 = h_g\,(\theta_1 - \theta_2), \tag{10}$$

$$q_3 = q_2\,, \tag{11}$$

$$q_4 = h_w\,(\theta_2 - \theta_w), \tag{12}$$

$$q_4 = q_3 + A_2\, i_0\,, \tag{13}$$

$$q_5 = h_w\,(\theta_w - \theta_3), \tag{14}$$

$$q_5 = q_4 + A_w\, i_0 + \dot{m}c(\theta_{IN} - \theta_w), \tag{15}$$

$$q_6 = h_i\,(\theta_3 - \theta_i), \tag{16}$$

$$q_6 = q_5 + A_3\, i_0\,, \tag{17}$$

where h_i is the interior heat transfer coefficient; h_e, the exterior heat transfer coefficient; h_g, the air-cavity heat transfer coefficient; and h_w, the water heat transfer coefficient. The thermal transmittances (U_e, U_i) depend on the heat transfer coefficients. Equations (18) and (19) refer to WFG with the water chamber outdoors (Case 1), and Equations (20) and (21) show the expressions for WFG with a water chamber indoors (Cases 2, 3).

$$\frac{1}{U_e} = \frac{1}{h_e} + \frac{1}{h_w}, \tag{18}$$

$$\frac{1}{U_i} = \frac{1}{h_i} + \frac{1}{h_g} + \frac{1}{h_w}, \tag{19}$$

$$\frac{1}{U_e} = \frac{1}{h_e} + \frac{1}{h_g} + \frac{1}{h_w}, \tag{20}$$

$$\frac{1}{U_i} = \frac{1}{h_i} + \frac{1}{h_w}. \tag{21}$$

U represents the thermal transmittance between the room and outdoors, and U_w represents the thermal transmittance between the water chamber and indoors. The thermal transmittance (U) is almost zero when the flow rate is the design flow rate because the water chamber isolates the building from outdoor conditions. When the water flow stops, the thermal transmittance depends mainly on the air chamber. Equations (22) and (23) show the expressions for U and U_w, respectively:

$$U_w = \frac{U_i \dot{m}c}{\dot{m}c + U_e + U_i}, \tag{22}$$

$$U = \frac{U_e U_i}{\dot{m}c + U_e + U_i}, \tag{23}$$

where $\dot{m}$ is the mass flow rate and c is the specific heat of water.

Table 1 shows a complete description of the different layers and the selected glazing average values. Visual transmittance (T_v) is the measurement of visible light (380 to 780 nm) passing through the glazing. The thermal parameters depended on the mass flow rate. If the water was flowing, the *g*-factor became lower. When the water chamber was stopped, the amount of energy entering the building increased. The thermal transmittance (U) was almost zero at the design flow rate (2 L/min m^2). When $\dot{m}$ = 0, U depended on the air chamber. The thermal transmittance (U_w) as defined in Equation (22) measures the heat losses or gains between the water chamber and the indoor air. U_w = 0 when $\dot{m}$ = 0. At the working flow rate, its value was high (6.4 W/m^{2}K) when the water chamber was close to indoors, and it was low (0.9 W/m^{2}K) when the water chamber was outdoors. The first case had the water chamber outdoors and a low-emissivity coating in face 4. When $\dot{m}$ = 0, the U value was 1.041 W/m^{2}K, and the *g*-factor was 0.25. At the operating $\dot{m}$, the *g*-factor became 0.22 and the U value, 0.128 W/m^{2}K. The visual transmittance (T_v = 0.51) was the lowest of the selected cases. The second case had a water chamber facing indoors. A low-emissivity coating was placed in face 3 and a solar PVB layer in the central pane. The U value ranged from 0.066 to 1.041 W/m^{2}K and a variable *g*-factor was 0.24 when the flow was ON, and 0.59 when the flow was OFF, adapting to the outdoor environment in both summer and winter conditions. The visual transmittance was 0.53. The third case had a highly selective coating in face 2. It yielded a U value of 0.995 W/m^{2}K when the flow was OFF, and 0.063 W/m^{2}K when the flow was ON. The *g*-value varied between 0.22 and 0.27. The visual transmittance (T_v = 0.55) was the highest of the selected cases. The energy transmittance (T), did not show significant variations, and it ranged from 0.20 in Case 1 to 0.21 in Cases 2 and 3.

Table 1. Spectral and thermal properties of the studied WFGs.

	Spectral Properties [1]		**Thermal Properties** [2]					
			$\dot{m}$ **= 0 L/min m^2**			$\dot{m}$ **= 2 L/min m^2**		
Glazing	T_v	T	U **(W/m^{2}K)**	U_w **(W/m^{2}K)**	g	U **(W/m^{2}K)**	U_w **(W/m^{2}K)**	g
Case 1: P8 (2SG41) P8/24water /P8 (4RB11)P8 (plaXNII) /16argon/P8 (4RB11) P8	0.51	0.20	1.041	0.0	0.25	0.128	0.977	0.22
Case 2: D10/16argon /(plaXNII) P8(2RB11) P8 /24water/P8 (4RB11) P8	0.53	0.21	1.041	0.0	0.59	0.066	6.459	0.24
Case 3: D10 Xtreme /16argon /(plaXNII) P8(2SG41) P8 /24water/P6 (4RB11) P6	0.55	0.21	0.995	0.0	0.27	0.063	6.462	0.22

[1] Visual transmittance (T_v), energy transmittance (T). [2] Thermal transmittance from water chamber to interior (U_w), Thermal transmittance of triple glazing (U), g-factor (g).

2.3. Description of the WFG Unitized Module

All the test cases were triple glazing with a 16 mm argon cavity and a 24 mm water cavity. The water cavity spacer was designed to lead the design flow rate. The circulating device was made of a plate heat exchanger and a solar water pump. The WFG units were manufactured and assembled in the glass factory and prepared for deployment on-site with an aluminum frame that enclosed the circulating device. The maximum dimension of the panel was 3000 mm high by 1300 mm width. The circulating device main components were a plate heat exchanger and a solar water pump. Its design allowed hydraulic and electrical independence of the modules with a reduced size. The operating flow rate was set to 8 l/min for a 4 m^2 module. The circulating device was made of a water pump, selected according to the desired flow rate, and a plate heat exchanger based on the glazing heat capacity. Figure 3 shows a drawing of the circulator with its materials and primary components. Inlet and outlet temperatures were measured using one-wire temperature probes, and a flow meter was placed just before the glazing inlet.

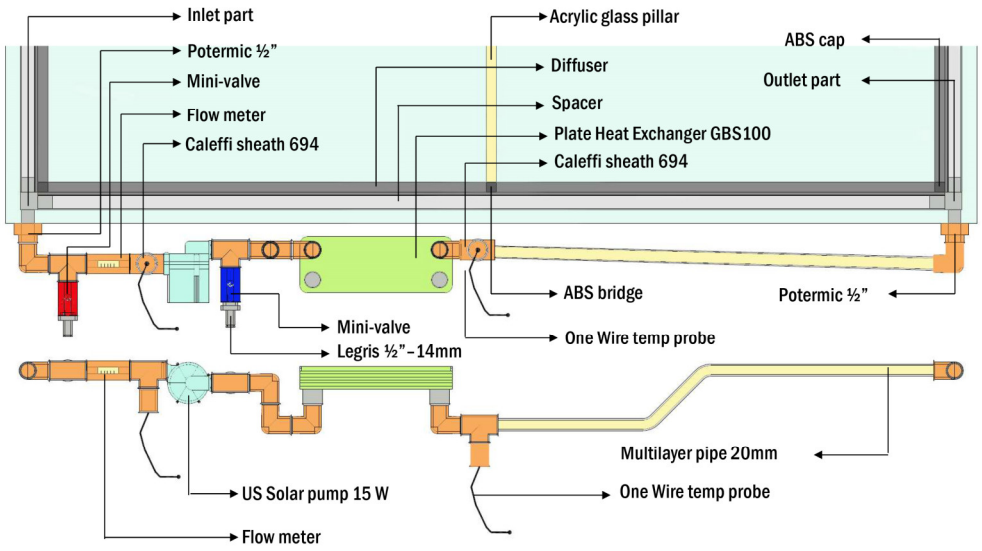

Figure 3. Description and general dimensions of the circulating device.

The modular unit hid the complexity of the hydraulic installation, so it became a plug and play product with essential advantages from the product marketing point of view. Depending on the glass selection, the WFG modules offered a broad spectrum of capabilities depending on the location, facade orientation, and use of the building.

3. Results

The objective of this section is to compare the thermal performances of different glazings using simulation tools and real data. The heat transfer coefficients (h_g, h_w) define convective heat transfer mechanisms of the air and water chambers. Optics and Window software tools were used to validate the absorptance and transmittance of commercial glass panes [41]. Optics allows analyzing the spectral properties at normal incidence, whereas Window considers spectral properties of glazing using different angles of incidence. In order to validate the simulation of the complete thermal problem, isolated glazing was considered. The assumption that indoor air temperature was constant and diffuse indoor irradiance was zero simplified the problem. Two different cases were tested: steady and transient boundary conditions.

3.1. Steady Boundary Conditions

If boundary conditions do not vary with time, the steady state does not depend on thermal mass and specific heat of components. Hence, a benchmark test case based on constant boundary conditions was the easiest way to start with validation. The study comprised three different cases of WFG. When the system was circulating, the design flow rate was 2 L/min m^2, and the inlet temperature was set at a constant value θ_{IN}. When the flow rate was stopped, the outlet temperature of the water chamber θ_{OUT} was called the stagnation temperature. The outputs of these test cases were the thermal power transported by the flow rate and the water heat gain. Figure 4 shows the dynamic U and U_w values defined in Equations (22) and (23). The red line represents the design flow rate (2 L/min m^2 = 0.029 Kg/s m^2). If the flow rate were above the design value, it would not affect the transmittances.

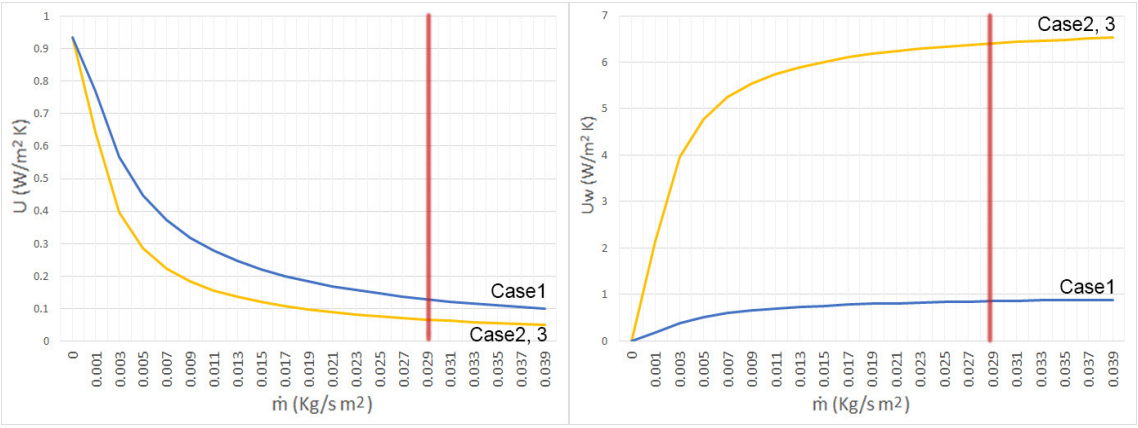

(**a**) (**b**)

Figure 4. Thermal transmittances of three WFG case studies depending on the mass flow rate, $\dot{m}$. (**a**) Thermal transmittance of the WFG modular units (U). (**b**) Thermal transmittance between the water chamber and indoors (U_w).

Equation (24) shows the absorptance, A_v, that depends on the energy absorbed by the glass panes and by the water:

$$A_v = A_1\left(\frac{U_e}{h_e}\right) + A_2\left(\frac{1}{h_g} + \frac{1}{h_e}\right)U_e + A_3\left(\frac{U_e}{h_i}\right) + A_w. \quad (24)$$

Equation (25) shows that the g-factor for WFG also depends on the mass flow rate:

$$g = \left(\frac{U_i}{\dot{m}c + U_e + U_i}\right)A_v + A_i + T, \quad (25)$$

where A_i is the secondary internal heat transfer factor. The direct solar energy transmittance (T) is related to the visible and NIR wavelengths. A_i is negligible when the water chamber is facing indoors, but if it is facing outdoors and with high values of h_w, A_i can be calculated With Equation (26).

$$A_i = A_3\left(1 - \frac{U_i}{h_i}\right). \quad (26)$$

Table 2 shows the thermal transmittance of WFG at the design flow rate. The interior or exterior convective heat transfer mechanism can be modeled by constant values or by more elaborate models given by the norm ISO 15099:2003. By default, constant values of h_i = 8 and h_e = 23 were used. However, by selecting the ISO model, h_i and h_e could be determined precisely using the European Standard [40]. A typical value for the heat transfer coefficient of the water chamber, h_w, was 50 W/m²K. The heat transfer coefficient of an argon chamber was h_c = 1.16 W/m²K. The air chamber emissivity was very low, so the heat transfer coefficient due to radiation, h_r, could be neglected. Therefore, the heat transfer coefficient of the argon chamber, $h_g = h_c + h_r$, was 1.16 W/m²K. The specific heat capacity of the fluid was c = 3600 J/kg K. A_1 is the absorptance of the exterior glass pane, A_2, is the absorptance of the middle glass pane, and A_3 is the absorptance of the interior one. A_w is the absorptance of the water chamber. The highest A_i (0.01) is shown in Case 1, when the water chamber was placed outdoors.

Table 2. Absorptances and thermal transmittances of WFG ($\dot{m}$ = 2 L/min m²).

Glazing	A_1	A_2	A_3	A_w	A_v	A_i	U_i (W/m²K)	U_e (W/m²K)	U (W/m²K)	U_w (W/m²K)
Case 1	0.685	0.033	0.012	0.004	0.51	0.01	0.99	15.75	0.128	0.977
Case 2	0.069	0.432	0.019	0.002	0.44	0.001	6.89	1.08	0.066	6.459
Case 3	0.291	0.028	0.019	0.001	0.06	0.001	6.89	1.08	0.063	6.462

Absorptances of glass panes (A_j), Absorptances of water layer (A_w), Total absorptance of water flow glazing (A_v), Interior thermal transmittance (U_i), Exterior thermal transmittance (U_e), Thermal transmittance of triple glazing (U), Thermal transmittance from water chamber to interior (U_w).

Equation (27) results from solving the equations (9)–(28):

$$\theta_{OUT} = \frac{i_0 A_v + U_i\theta_i + U_e\theta_e + \dot{m}c\theta_{IN}}{\dot{m}c + U_e + U_i}. \quad (27)$$

Equation (28) shows the analytical expression of water heat gain (P).

$$P = \dot{m}c(\theta_{OUT} - \theta_{IN}), \quad (28)$$

where θ_{OUT} and θ_{IN} are the temperatures of water leaving and entering the glazing, respectively; $\dot{m}$ is the mass flow rate, and c is the specific heat of the water. By combining Equations (27) and (28), Equation (29) shows the power as a function of absorptance (A_v) and thermal transmittances (U_i, U_e).

$$P = \frac{\dot{m}c}{\dot{m}c + U_e + U_i}(i_0 A_v + U_i(\theta_i - \theta_{IN}) + U_e(\theta_e - \theta_{IN})), \quad (29)$$

where A_v comes from Equation (24). When the system reaches a steady state, the boundary conditions do not change with time. The assumption that solar radiation is perpendicular to the interfaces makes the absorptance of each layer non-dependent of the angle of incidence. When the mass flow rate is high enough ($\dot{m}c >> Ue + Ui$), the absorbed power (P) reaches its peak value (P_{max}). Table 3 shows constant input values in winter and summer conditions. Indoor air temperature (θ_i), outdoor air temperature (θ_e), interior and exterior heat transfer coefficients (h_i, h_e), and solar irradiance (I). Equations (29)–(32) were used to calculate U_e and U_i.

Table 3. Constant input parameters in winter and summer.

Season	θ_e (°C)	θ_i (°C)	h_e (W/m²K)	h_i (W/m²K)	I (W/m²)	$\dot{m}$ (L/min m²)	θ_{IN} (°C)	h_g (W/m²K)	h_w (W/m²K)
Winter	0	21	23	8	600	2	21	1.16	50
Summer	35	28	23	8	800	2	17	1.16	50

Once the glazing reaches the steady state in winter and in summer, thermal performances are determined. Using Equations (27) and (29), and considering the inputs in Table 3, Table 4 shows the following outputs in winter and summer, respectively. P is the water heat gain, T is the transmittance of the glazing, θ_{OUT} is the outlet temperature when the flow rate is $\dot{m}$ = 2 L/min m², and θ_s is the stagnation temperature when $\dot{m}$ = 0.

Table 4. Simulation outputs. Steady state in winter and summer conditions.

Glazing	P_{winter} (W/m²)	θ_{OUT} (°C)	θ_s (°C)	T_{winter} (W/m²)	P_{summer} (W/m²)	θ_{OUT} (°C)	θ_s (°C)	T_{summer} (W/m²)
Case 1	22.9	20.78	19.41	123.7	603.3	22.77	58.8	164.9
Case 2	226.6	23.17	51.57	128.4	418.7	21.01	73.5	171.2
Case 3	11.5	19.81	4.69	129.2	131.9	18.26	34.81	172.3

If energy management in winter is based on energy harvesting, Case 2 showed the best performance. Its water heat gain in winter was ten times as high as in Case 1. On the other hand, if energy management in summer is based on energy rejection, Case 3 was the best choice. In summer, the water heat gain of Case 1 was 1.5 times as much as Case 2. When it came to cooling capacity, Case 3 showed the best performance. It had to dissipate around 131.9 W/m², whereas Case 2 had to dissipate 418.7 W/m². Case 3 showed excellent properties for energy rejection strategies in warm climates because it showed the least absorbed power in summer, whereas the transmittance (T) was not much higher than in other cases.

Considering the simulation results in a steady state, Case 2 showed the best performance for water heat absorption throughout the year. It was selected for the south elevation. Case 3 showed the best performance for energy rejection, and it was selected for east and west facades. The next subsection studies the simulation results of the selected cases in transient conditions.

3.2. Transient Boundary Conditions

Transient behavior is expected when boundary conditions such as outdoor temperature and solar irradiance vary during the day. In these following test cases, the indoor temperature was a given indoor boundary condition, and transport coefficients remained constant to avoid uncertainties in the validation process. These test cases were simulated in Sofia, and the weather file was the standard EPW file (EnergyPlus Weather). Regarding the water flow glazing, the flow rate and the inlet temperature were constant values given by Table 3. Two simulations in winter and summer were accomplished. The simulation period ran from 7 January to 11 January in winter and from 14 July to 18 July in summer. Figure 5 illustrates the thermal behavior of Case 2 and Case 3. In summer, the solar irradiance peak value was 500 W/m^2, and the maximum outdoor temperature was slightly above 26 °C on 14 July 2020. The goal of rejecting energy was met, and the water heat gain, measured by the difference between inlet and outlet temperatures, was not above 1 °C on five sample summer days. The peak solar radiation in winter on the eastern facade was 180 W/m^2 on 10 January 2020. Due to the high infrared reflectance (above 70%) of the selected glazing and the low outdoor temperature (below 5.5 °C), the water heat gains were negligible. According to the steady-state analysis, Case 2 showed the best performance to heat water, as measured by the solar irradiance on the southern facade, the outdoor temperature, and the difference between inlet and outlet temperatures in southern WFG modules. In summer, the peak solar radiation was 400 W/m^2, and the maximum temperature was above 26.5 °C on 15 July 2020. On that day, the maximum outlet water temperature was 22 °C when the inlet temperature was 20 °C, and there were water heat gains during the central hours of the day. In winter, the peak solar radiation was above 250 W/m^2, and that made the water absorb heat, although the outdoor temperature was low.

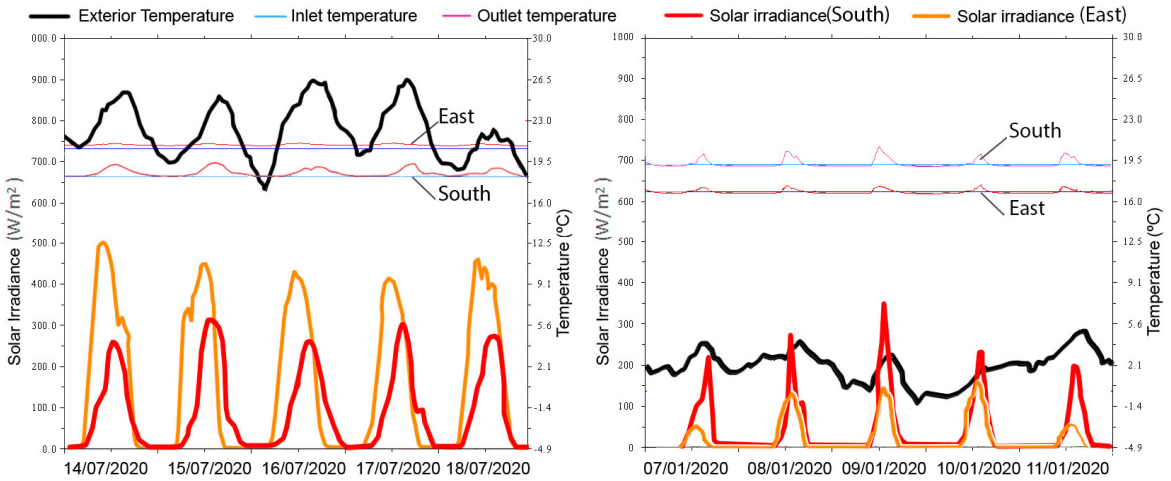

Figure 5. Simulation results of WFG Case 2 on the southern facade and Case 3 on the eastern facade with transient boundary conditions. (**a**) Summer. (**b**) Winter.

Figure 6 shows a summary of the water heat gains on two sample days in summer and winter. Case 3 was selected for eastern and western facades because it showed the least heat absorption in summer (17 KWh), whereas Case 2 showed the highest absorption in summer (34 KWh). To reject energy, the best choice for eastern and western facades was Case 3. Case 2 had the highest heat

absorption on a winter day (21 KWh) and a good value in summer (30.5 KWh). Case 2 confirmed its excellent performance on southern facades.

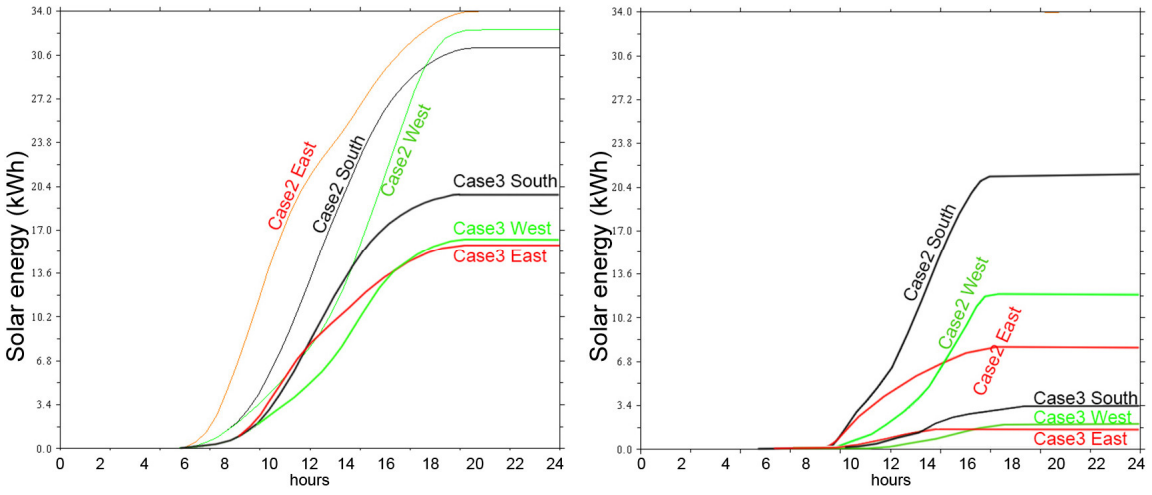

Figure 6. Accumulated energy of WFG case studies with transient boundary conditions. (**a**) Summer sample day 14 July 2020. (**b**) Winter sample day 8 January 2020.

3.3. Real Results in Sofia, Bulgaria

An experimental setup was placed in Sofia, Bulgaria (42°39′1″ North, 23°23′26″ East, Elevation: 590 m a.s.l.), to test the performance of isolated WFG modules throughout a year. Figure 7 shows the outdoor temperature. On the coldest winter days, the minimum temperature was below −10 °C, and the average daily temperature was 0 °C. During the hottest months, the maximum temperature reached 32 °C and the average temperature was 25 °C. The southern solar radiation reached a peak value of 400 W/m² on 21 December 2019, whereas the eastern and western were 160 W/m² and 270 W/m², respectively, on 21 June 2019. On summer days, the highest values were on the east and west facades (500 W/m²) because the sun angle was almost perpendicular to the vertical walls. The south facade received little radiation (200 W/m²).

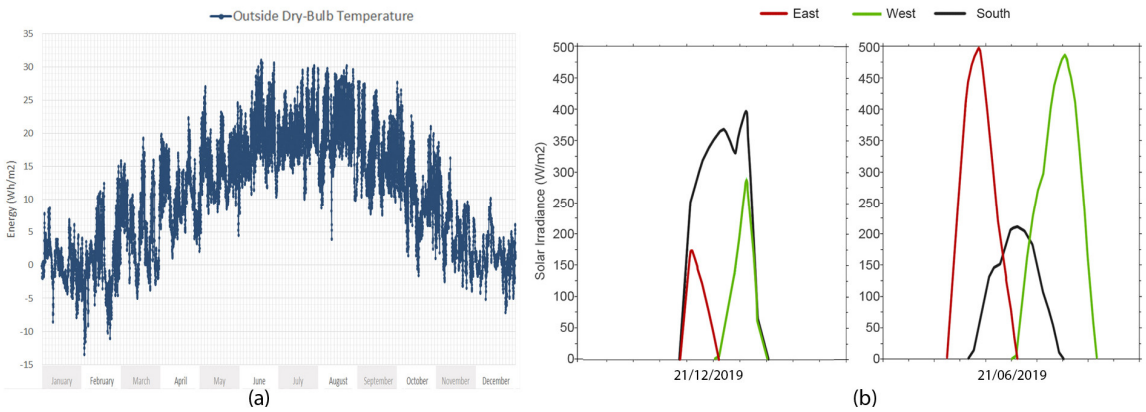

Figure 7. (**a**) Outdoor dry bulb temperature in Sofia, Bulgaria (EnergyPlus Weather file). (**b**) Eastern, western, and southern solar radiation on facades. Sample winter day 21 December 2019 and sample summer day 21 June 2019.

Based on the outdoor simulation data, and the thermal and spectral properties of the studied WFG in Table 4, the best option for the southern facade was Case 2. It showed the highest potential

for heat absorption in winter (226.6 W/m²) with the highest outlet temperature (23.17 °C). In summer, the maximum southern solar radiation was 200 W/m², whereas the absorption potential was 418 W/m², so the fluid could absorb the heat without heating the interior face of the glazing. Due to the high solar radiation in summer, the best option for eastern and western facades was Case 3. It showed the lowest absorption in summer (131.9 W/m²) with the lowest outlet temperature (18.26 °C). Figure 8 shows the prototype plan, with five modules facing east, five modules facing west, and five more modules on the southern facade. Unitized WFG modules were placed in three different orientations (east, south, and west) with a pyranometer measuring solar radiation on each facade. Each heat plate exchanger of the circulating device was connected to inlet and outlet water distribution systems.

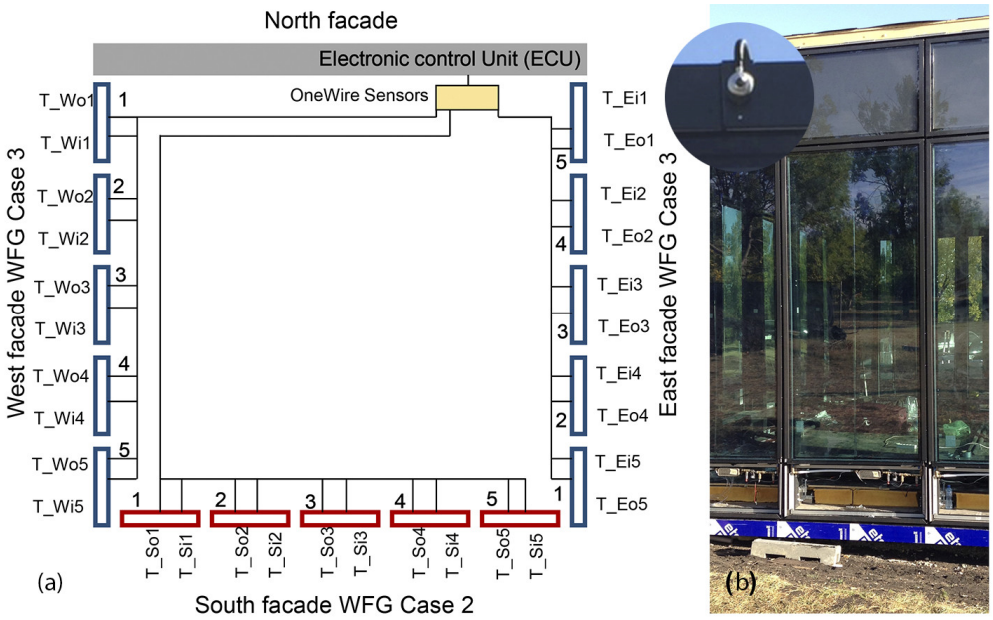

Figure 8. (**a**) Prototype plan. Position of WFG and electronic control unit. (**b**) Pictures of the unitized module in the actual facility with the pyranometer.

The output signals were collected by one-wire probes and sent to an electronic control unit (ECU), where the developed software processed the calculations and elaborated the energy outputs. The temperature sensor network was installed in both the inlet and outlet of the plate heat exchanger. Flux meters were added to the monitoring equipment to keep a steady mass flow rate through all the modules. The temperature difference in the external WFG elements could reach 10 °C, depending on the exterior conditions. Glass selection for renewable production on the southern facade (Case 2) absorbed the maximum incident solar radiation and at the same time reduced indoor solar heat gains. A heat pump was used to control the inlet temperature. Figure 9 illustrates the outdoor air temperature (*T_out*), inlet (*T_Ei5*) and outlet (*T_Eo5*) temperatures in two eastern WFG modules in summer conditions. The maximum temperature difference occurred from 7:00 a.m. to 10:00 a.m., when the solar radiation reached its peak value on the east facade. The southern modules' inlet and outlet temperatures (*T_Si5*, *T_So5*) reflected the solar radiation and outdoor temperature, and there were two peak values at 11:00 a.m. and 4:00 p.m. The maximum temperature difference between *T_So5* and *T_Si5* was 2 °C. The maximum temperature difference between the inlet (*T_Wi3*) and outlet (*T_Wo3*) temperatures in two western WFG modules occurred at 4:30 p.m., when the solar radiation reached its peak value on the west facade. The real measurements confirmed the simulation results because, despite the high solar radiation values on the eastern and western facades (700 W/m²), the temperature difference between inlet and outlet was 1 °C. However, in the southern modules, the temperature difference was 2 °C when the maximum solar radiation was 470 W/m².

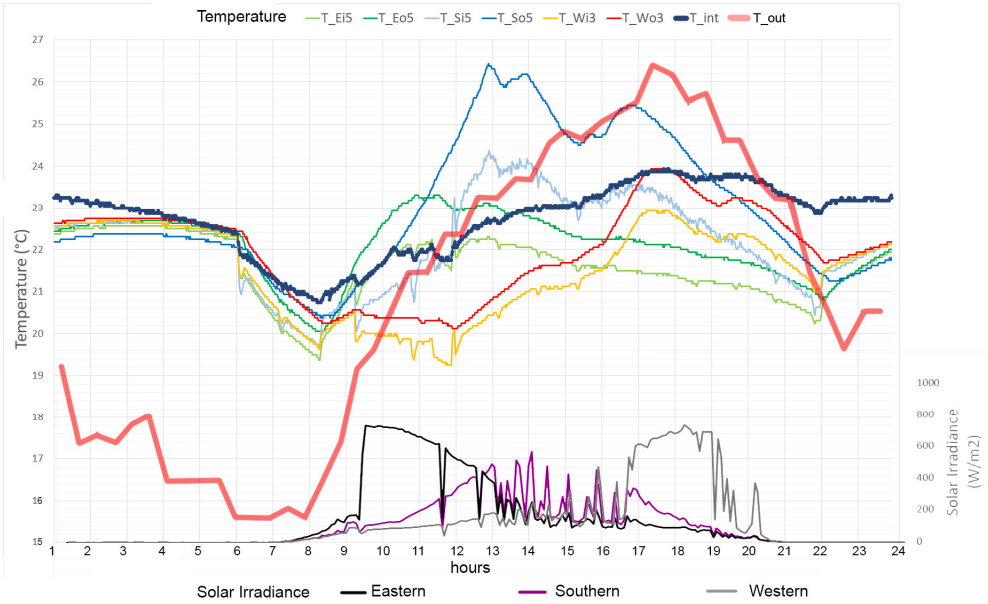

Figure 9. Inlet and outlet temperatures of eastern WFG. Sample summer day 14 July 2020. (**a**) Module E5. (**b**) Module E1.

In winter, heat absorption does not depend directly on solar radiation due to the severity of climatic conditions. The difference between indoor and outdoor temperatures affected energy performance more than the solar radiation on the eastern and western facades. Figure 10 illustrates the outdoor air temperature (*T_out*), the inlet (*T_Ei5*) and outlet (*T_Eo5*) temperatures in two eastern WFG modules. The southern WFG performance showed heat losses in the morning and in the afternoon. From 10:00 a.m. to 5:00 p.m., the outlet temperature (*T_So5*) was higher than the inlet (*T_Si5*), and the maximum difference reached 2.5 °C at 1:30 p.m. In western modules, the inlet (*T_Wi3*) and outlet (*T_Wo3*) temperatures showed that there were heat losses in the morning with no solar radiation and low outdoor temperature. The simulation results were validated with little energy absorption on eastern and western facades, and heat gains in the southern modules.

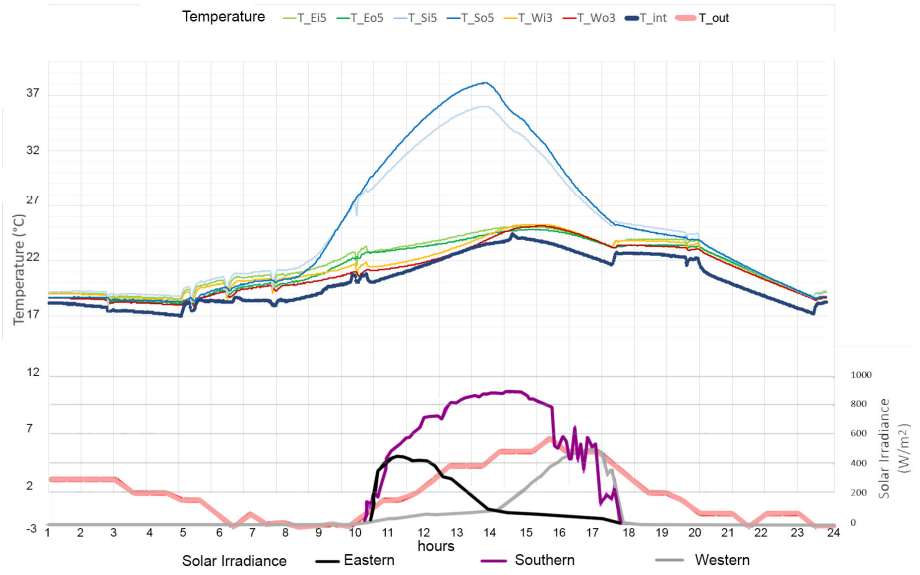

Figure 10. Inlet and outlet temperatures of eastern WFG. Sample winter day 8 January 2020. (**a**) Module E4. (**b**) Module E3.

4. Discussion

The next step was to analyze the results in terms of potential energy savings. Firstly, the results of the simulation tool were validated. Secondly, the heat absorbed by water in summer can be both subtracted from the cooling loads and considered as renewable energy production. According to the Energy Performance of Buildings Directive (EPDB 2018) recommendations [2], primary energy factors (PEFs) were used to assess the energy performance.

4.1. Validation of Energy Performance

To validate the selection of WFG, the daily absorbed energy per unit of area was calculated using Equation (29). Figure 11 shows the performance of two WFG panels in winter in three orientations. As expected, the eastern and western panels' energy absorption was not relevant. Most of the time there were heat losses due to the little radiation and the low outdoor temperature. A different performance was shown in the southern panels, where the daily absorbed energy was 21.3 kWh in 7.8 m², so the ratio of energy per area was 2.73 kWh/m².

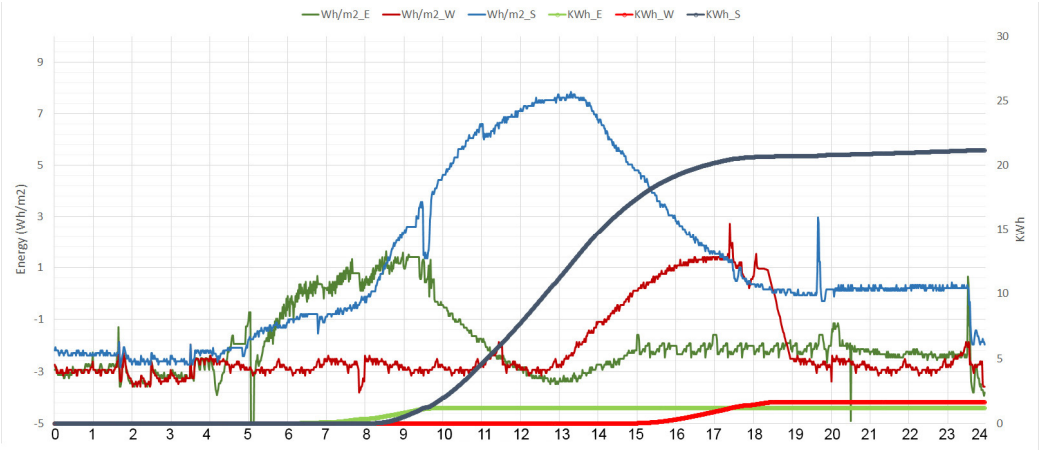

Figure 11. Energy absorption on eastern, southern, and western WFG facades. Sample winter day 8 January 2020.

Figure 12 shows the energy performance on a sample summer day (14 July 2020). The total absorbed energy was 30 KWh in two southern WFGs, 18.6 KWh in two western WFGs, and 15.9 KWh in two eastern WFGs. The energy-to-area ratio was 3.85 kWh/m² in the south, 2.38 kWh/m² in the west, and 2.04 kWh/m² in the east.

Figure 12. Energy absorption on eastern, southern, and western WFG facades. Sample summer day 14 July 2020.

The goal of rejecting energy in the east and west was met. Despite the high solar radiation, the water heated up by 2 °C, and most of the infrared energy was rejected. On the south facade, the energy absorption was similar in winter and summer, and the water heated up around 3 °C. The reliability of the simulation tool was tested by developing real prototypes. Figure 13 illustrates the comparison between the results of the real data and the simulation data. The daily energy absorption on southern facades in winter and summer were taken from Figures 11 and 12 and compared with the simulated results from Figure 6.

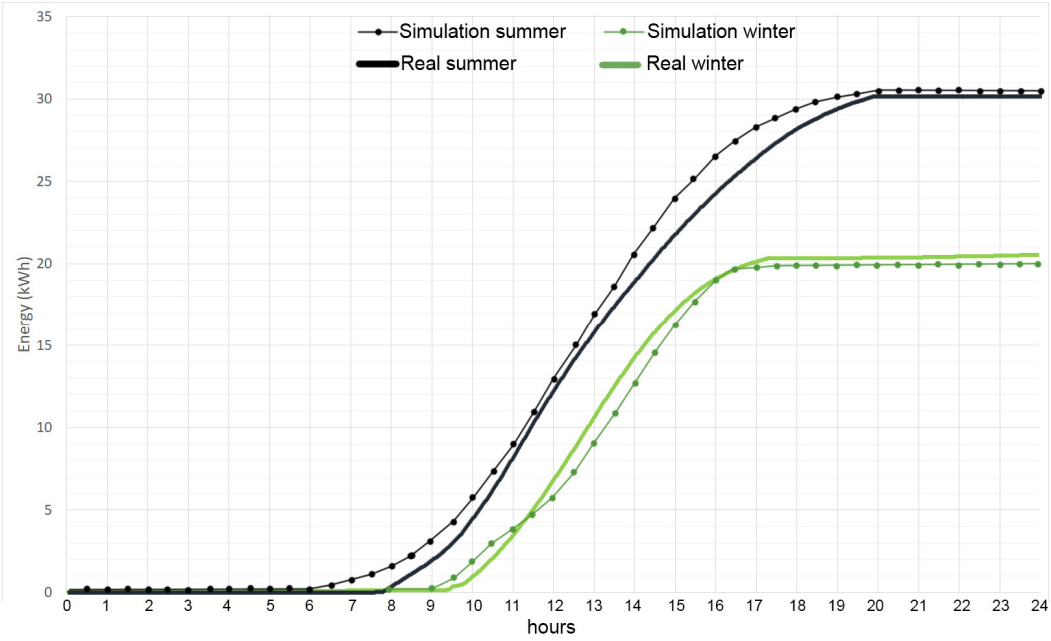

Figure 13. Accumulated energy absorption on southern WFG facades. Sample days 14 July 2020 and 8 January 2020. Comparison between simulated and real data.

The Mean Error (*ME*), shown in Equation (24), is the difference between the measured value and simulation results. The total number of measurements was $n = 2872$.

$$ME = \frac{1}{n}\sum_{i=1}^{n}|E_{Si} - E_{Ri}|, \quad (30)$$

where E_{Si} is the simulated energy absorption, and E_{Ri} is the measured energy absorption. By computing *ME* on 14 July 2020 the value was 0.78. When it came to the energy absorption on 8 January 2020, the *ME* was 0.67. The reason for this might be the uncertainties about the inlet and indoor temperatures. Although the accumulated energy values were quite similar in the simulation and the real conditions, the intermediate values differed at some times of the day. The simulation tool could not work with variable inlet and indoor temperatures, which is the main goal for further research.

4.2. Primary Energy Consumption

Figure 14 shows the outdoor air temperature and the accumulated energy throughout five days in summer. WFG absorbed solar energy and prevented it from entering the building. The amount of energy absorbed by the water could be connected to the district heating network, geothermal boreholes, or to domestic hot water devices. In the final energy balance, the accumulated energy was subtracted from the cooling loads and added to the renewable energy production.

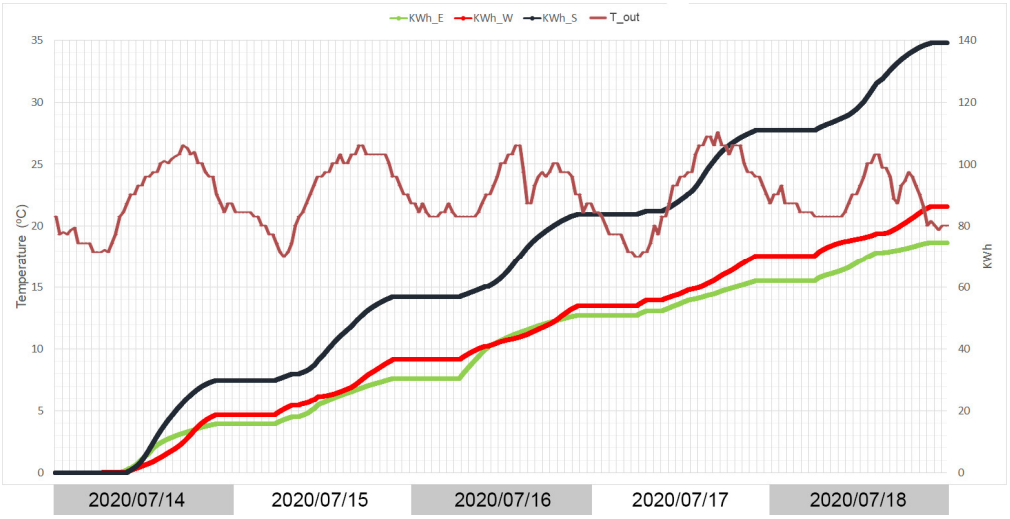

Figure 14. Energy absorption on eastern, southern, and western WFG facades. Sample summer days from 14 July 2020 to 18 July 2020.

Article 41 of the Energy Performance of Buildings Directive (EPDB 2018) recommended the use of primary energy factors to calculate the energy parameters of building envelopes [2]. Table 5 shows these energy factors, such as cooling energy demand (CED in kWh/m²), final energy consumption (FEC in kWh/m²), non-renewable primary energy consumption (NRPEC in kWh/m²). The energy absorbed by the water was considered as renewable primary energy production (RPE in kWh/m²) and CO_2 emissions (kg CO_2/m²). The electricity consumption of the circulation water pumps was not considered because they were connected to photovoltaic panels. The circulation pump was working 24 h per day. The primary energy factor (PEF) is the inverse of electricity production efficiency from fuel source to electricity at the building, taken from official European Union documents [42,43], if the energy was produced using heat pumps, considering a Coefficient of Performance (COP) of 2.5 and a conversion factor between final energy and non-renewable primary energy (KWh NRPE/KWh FE) of 1.954. The factor of emitted CO_2 for electricity was 0.331.

Table 5. Primary energy balance of WFG in summer.

	Cooling Energy Demand (CED) kWh/m² day	Final Energy Consumption (FEC) kWh/m² day	Non-Renewable Primary Energy Consumption (NRPEC) kWh/m² day	Renewable Primary Energy (RPE) kWh/m² day	CO_2 Emissions kgCO_2/m² day
Day 1	8.27	3.31	6.46	3.42	1.09
Day 2	7.60	3.04	5.94	3.15	1.01
Day 3	8.24	3.29	6.44	3.41	1.09
Day 4	6.95	2.78	5.43	2.88	0.92
Day 5	7.25	2.9	5.67	3.00	0.96
Total	38.31	15.32	29.94	15.86	5.07

Table 6 shows the estimated winter heating loads over the working hours. Indoor ($T_{\_int}$) and outdoor ($T_{\_ext}$) temperatures were taken from Figure 10 with a surface area of 3.9 m². The same procedure was repeated to calculate the values on five sample days. A high-performance triple glass made of three glass panes with an argon chamber and Low-E coating was compared with the selected WFG cases. The triple-glass U value was taken from a glazing catalog [41], whereas the U value of the WFG was defined in Table 1. The total heat losses through the passive triple glazing and the WFG were 288.38 Wh/m² and 15.31 Wh/m². The energy savings per day was 273.07 Wh/m². In addition, the WFG was able to produce renewable energy.

Table 6. Winter heating loads on 14 January 2020.

			Triple Glass		*WFG*	
	T_{int} (C) [1]	T_{ext} (C) [1]	U *(triple glazing)* (W/m²K) [2]	$\sum UA(T_{int}-T_{ext})$ (Wh/m²)	U *(WFG)* (W/m²K)	$\sum UA(T_{int}-T_{ext})$ (Wh/m²)
7–8 h	18	−3	1.3	23.73	0.06	1.26
8–9 h	18	−3	1.3	23.73	0.06	1.26
9–10 h	21.5	−3	1.3	27.69	0.06	1.47
10–11 h	21.8	0	1.3	24.63	0.06	1.31
11–12 h	18.8	1.5	1.3	19.55	0.06	1.04
12–13 h	20	3.1	1.3	19.10	0.06	1.01
13–14 h	22.7	4.5	1.3	20.57	0.06	1.09
14–15 h	23	5.1	1.3	20.23	0.06	1.07
15–16 h	23.1	6	1.3	19.32	0.06	1.03
16–17 h	23.5	5.6	1.3	20.23	0.06	1.07
17–18 h	22.2	3.6	1.3	21.02	0.06	1.12
18–19 h	22	2	1.3	22.60	0.06	1.20
19–20 h	22	−1	1.3	25.99	0.06	1.38
TOTAL				288.38		15.31

[1] Values are taken from Figure 10; [2] values are taken from [41].

Table 7 illustrates the primary energy savings, the reduction of CO_2 emissions, and renewable energy production of WFG in five winter days.

Table 7. Primary energy balance of WFG in winter.

	CED kWh/m²	FEC kWh/m²	NRPEC kWh/m²	RPE kWh/m²	EM kgCO_2/m²
Day 1	0.226	0.090	0.177	2.40	0.030
Day 2	0.225	0.090	0.176	2.55	0.030
Day 3	0.222	0.089	0.174	2.46	0.029
Day 4	0.222	0.089	0.174	2.46	0.029
Day 5	0.227	0.091	0.177	2.57	0.030
Total	0.116	0.449	0.877	12.44	0.149

4.3. Cost Considerations

The ideal project for these advanced facades would be a large tower-type office building with limited site access. The facade should consist of repetitive geometry that can be divided easily into panels. The system would not be fit to have movable windows, so special modules for openings and mechanical ventilation systems are required. A literature review was carried out to assess the cost and the performance of advanced facades [44–46]. The unit costs of the components included the material, production, and assembly costs. These values are the average of the unit costs taken from two different passive curtain wall systems [47]. The cost analysis for the WFG-unitized facade considered a triple glass described in Case 2, the total estimated costs for aluminum production, module fabrication, on-site transportation, and facade assembly. The energy values were calculated with the indoor and outdoor temperatures shown in Figures 9 and 10 for sample summer and winter days, respectively. The energy parameters and construction costs calculated for all the alternatives are shown in Table 8.

Table 8. Energy and cost parameters.

System Description	Glazing	U W/m²K	FEC kWh/m²		RPE kWh/m²		EM kgCO_2/m²	Cost EUR/m²
			S	*W*	*S*	*W*		
Aluminum frame fixed to slab	Triple glazed	1.3 [1]	2.42	0.64	-	-	1.01	620 [1]
Unitized facade Aluminum frame	WFG (Case 2)	0.066	0.94	0.30	3.42	2.73	0.41	1375

[1] Values taken from [47].

The initial costs of the WFG made up of the triple glazing, the circulating device, and the unitized aluminum frames were high, compared to passive glazing systems. However, a holistic approach should include energy savings, energy production, and CO_2 emissions. The total final energy consumption was 3.06 kWh/m² for the standard triple-glazed lightweight enclosure and 1.24 kWh/m² for the WFG. When it came to CO_2 emissions, the standard curtain wall solution would account for 2.5 times as much CO_2 as the studied WFG.

5. Conclusions

The design of new light envelopes for zero-energy buildings must integrate different disciplines such as architectural design, building simulation, HVAC systems, and the curtain wall industry. This article developed a methodology for selecting WFG solutions for different facades and tested its performance using real data. Case 1 was a triple glazing with the water chamber facing outdoors. Case 2 was made of triple glazing with water chamber indoors and Low-E coating. Case 3 had a high reflective coating on face 2 and a water chamber indoors.

1. Dynamic properties of WFG allowed considering options for different orientations and the internal loads, which depend on the building use. The thermal transmittance (U) ranged from 1 W/m²K ($\dot{m}$ = 0) to 0.06 W/m²K ($\dot{m}$ = 2 L/min m²). A mass flow rate ($\dot{m}$) above 2 L/min m² (0.029 Kg/s m²) did not impact the water–energy absorption.
2. The position of the gas and water cavities and the spectral properties of glass panes and coatings affected the performance of the WFG. Simulation results at steady conditions showed that Case 2 had the best performance for energy absorption in winter (226.6 W/m²). Case 1 showed the highest energy absorption in summer (603.3 W/m²). Case 3 showed the lowest energy absorption, both in summer (131.9 W/m²) and winter (11.5 W/m²).
3. The primary energy factor (PEF) was used to assess building energy performance. Energy savings ranged from 5.43 to 6.46 KWh/m² day in non-renewable energy consumption, whereas the renewable primary energy production ranged from 3 to 3.42 KWh/m² day. The CO_2 emissions were reduced at a rate of 1 Kg/m² day.
4. In the cold winter season, the absorbing south facade heated water (2.73 kWh/m²), whereas eastern and western facades received very little solar radiation.
5. In summer, eastern and western facades rejected most of the solar radiation, and the flowing water was heated without surpassing the comfort temperature. The maximum outlet temperature was 24 °C on 14 July 2020. The daily absorbed energy was 3.84 KWh/m² in the southern WFG, 2.38 KWh/ m² in WFG, and 2.04 KWh/ m² in WFG.

This article showed an industrialized water flow glazing unitized facade ready to be used in the architecture, engineering, and construction industries. The authors developed a simulation tool to be used at the first stage of the design process. The outputs were validated with an actual test facility placed in Sofia, Bulgaria. The difficulties identified were related to the limitations of the software for simulating the dynamic properties of WFG. The high initial cost and the need for an energy management system integrated with the rest of the equipment conditioned the WFG system. After the first year of monitoring, there are uncertainties and system issues that must be addressed. Firstly, the control unit must integrate the ventilation system to reduce condensation risks. Secondly, the

presented simulation tool must be integrated into commercial building performance simulation software. Finally, further research on the deployment is needed to bring down payback periods.

With economies of scale a price comparable to triple-pane glazing systems equipped with automated exterior shading can be achieved.

Author Contributions: Conceptualization, B.M.S., F.d.A.G., J.A.H.R.; methodology, B.M.S., F.d.A.G.; software, J.A.H.R.; formal analysis, B.M.S., F.d.A.G.; data curation, J.A.H.R.; writing—original draft preparation, B.M.S., F.d.A.G., J.A.H.R.; writing—review and editing, F.d.A.G., D.P.; visualization, B.M.S., F.d.A.G., B.L.A.; supervision, J.A.H.R., B.L.A.; project administration, B.M.S.; funding acquisition, F.d.A.G. All authors have read and agreed to the published version of the manuscript.

Funding: This article has been funded by a KSC Faculty Development Grant (Keene State College, New Hampshire, USA).

Acknowledgments: This work was supported by program Horizon 2020-EU.3.3.1: Reducing energy consumption and carbon footprint by smart and sustainable use, project Ref. 680441 (InDeWaG: Industrialized Development of Water Flow Glazing Systems). Special thanks to the Central Laboratory of Solar Energy and New Energy Sources of the Bulgarian Academy of Science (CL SENES–BAS) for providing measured data of the solar radiation on the different facades of the test facility in Sofia, Bulgaria.

Conflicts of Interest: The authors declare that they have no conflict of interest.

Nomenclature

Symbol	Meaning
A_j	Absorptance of glass layers
A_w	Absorptance of water
A_v	Total absorptance of water flow glazing
h_i	Interior heat transfer coefficient (W/m^{2}K)
h_w	Water heat transfer coefficient (W/m^{2}K)
h_g	Air chamber heat transfer coefficient (W/m^{2}K)
h_e	Exterior heat transfer coefficient (W/m^{2}K)
q_j	Heat fluxes through the different layers of the glazing
i_0	Normal incident solar irradiance (W/m^2)
θ_i	Interior temperature (K)
θ_e	Exterior temperature (K)
θ_j	Temperature of the glass layer (K)
θ_{IN}	Inlet temperature of the water chamber (K)
θ_{OUT}	Outlet temperature of the water chamber (K)
θ_w	Temperature of the water (K)
θ_S	Stagnation temperature of the water when $\dot{m}$ = 0 (K)
U	Thermal transmittance (W/m^{2}K)
U_i	Interior thermal transmittance (W/m^{2}K)
U_e	Exterior thermal transmittance (W/m^{2}K)
U_w	Thermal transmittance (water chamber–interior) (W/m^{2}K)
T	Transmittance of the glazing
R	Reflectance of the glazing
$\dot{m}$	Mass flow rate (kg/s m^2)
c	Specific heat of the water (J/Kg K)
P	Heat gain in the water chamber (W)

References

1. Stenqvist, C.; Nielsen, S.B.; Bengtsson, P.-O. A Tool for Sourcing Sustainable Building Renovation: The Energy Efficiency Maturity Matrix. *Sustainability* **2018**, *10*, 1674.
2. European Union. Directive (EU) 2018/844 of the European Parliament and of the Council of 30 May 2018. Amending Directive 2010/31/EU on the Energy Performance of Buildings and Directive 2012/27/EU on Energy Efficiency, 2018. Available online: https://eur-lex.europa.eu/legal-content/EN/TXT/PDF/?uri=CELEX:32018L0844&from=EN (accessed on 24 July 2020).

3. DOE/EIA. *International Energy Outlook*; US Energy Information Administration, US Department of Energy: Washington, DC, USA, 2016.
4. Chin, J.; Lin, S.-C. A Behavioral Model of Managerial Perspectives Regarding Technology Acceptance in Building Energy Management Systems. *Sustainability* **2016**, *8*, 641.
5. Prieto, A.; Knaack, U.; Klein, T.; Auer, T. 25 Years of cooling research in office buildings: Review for the integration of cooling strategies into the building facade (1990–2014). *Renew. Sustain. Energy Rev.* **2017**, *71*, 89–102, doi:10.1016/j.rser.2017.01.012.
6. Santamouris, M.; Kolokotsa, D. Passive cooling dissipation techniques for buildings and other structures: The state of the art. *Energy Build.* **2013**, *57*, 74–94.
7. Sudhakar, K.; Winderl, M.; Shanmuga Priya, S. Net-zero building designs in hot and humid climates: A state-of-art. *Case Stud. Therm. Eng.* **2019**, *13*, 100400, doi:10.1016/j.csite.2019.100400.
8. Fernandez-Antolin, M.-M.; del-Río, J.-M.; Gonzalez-Lezcano, R.-A. Influence of Solar Reflectance and Renewable Energies on Residential Heating and Cooling Demand in Sustainable Architecture: A Case Study in Different Climate Zones in Spain Considering Their Urban Contexts. *Sustainability* **2019**, *11*, 6782.
9. Ürge-Vorsatz, D.; Cabeza, L.F.; Serrano, S.; Barreneche, C.; Petrichenko, K. Heating and cooling energy trends and drivers in buildings. *Renew. Sustain. Energy Rev.* **2015**, *41*, 85–98, doi:10.1016/j.rser.2014.08.039.
10. Bustamante W; Vera S; Prieto A; Vasquez, C. Solar and Lighting Transmission through Complex Fenestration Systems of Office Buildings in a Warm and Dry Climate of Chile. *Sustainability* **2014**, *6*, 2786–2801.
11. Ozel, M. Influence of glazing area on optimum thickness of insulation for different wall orientations. *Appl. Therm. Eng*. **2019**, *147*, 770–780.
12. López-Ochoa, L.M.; Las-Heras-Casas, J.; López-González, L.M.; García-Lozano, C. Energy Renovation of Residential Buildings in Cold Mediterranean Zones Using Optimized Thermal Envelope Insulation Thicknesses: The Case of Spain. *Sustainability* **2020**, *12*, 2287.
13. Ulpiani, G., Giuliani, D., Romagnoli, A., di Perna, C. Experimental monitoring of a sunspace applied to a NZEB mock-up: Assessing and comparing the energy benefits of different configurations, *Energy and Buildings* **2017**, *152*, 194–215, doi:10.1016/j.enbuild.2017.04.034.
14. Hermanns, M.; del Ama, F.; Hernández, J.A. Analytical solution to the one-dimensional non-uniform absorption of solar radiation in uncoated and coated single glass panes. *Energy Build.* **2012**, *47*, 561–571.
15. Ascione, F.; de Masi, R.F.; de Rossi, F.; Ruggiero, S., Vanoli, G.P. Optimization of building envelope design for nZEBs in Mediterranean climate: Performance analysis of residential case study. *Appl. Energy* **2016**, *183*, 938–957, doi:10.1016/j.apenergy.2016.09.027.
16. Manz, H.; Menti, U.P. Energy performance of glazings in European climates. *Renew. Energy* **2012**, *37*, 226–232, doi:10.1016/j.renene.2011.06.016.
17. Allen, K.; Connelly, K.; Rutherford, P.; Wu, Y. Smart windows—Dynamic control of building energy performance. *Energy Build*. **2017**, *139*, 535–546, doi:10.1016/j.enbuild.2016.12.093.
18. Ghosh, A.; Norton, B.; Duffy, A. Measured overall heat transfer coefficient of a suspended particle device switchable glazing. *Appl. Energy* **2015**, *159*, 362–369, doi:10.1016/j.apenergy.2015.09.019.
19. Casini, M. Smart windows for energy efficiency of buildings. *Int. J. Civ. Struct. Eng. IJCSE* **2015**, *2*, 230–238, doi:10.15224/978-1-63248-030-9-56.
20. Gueymard, C.; duPont, W. Spectral effects on the transmittance, solar heat gain, and performance rating of glazing systems. *Solar Energy* **2009**, *83*, 940–953.
21. Gutai, M.; Kheybari, A.G. Energy consumption of water-filled glass (WFG) hybrid building envelope. *Energy Build.* **2020**, *218*, 110050, doi:10.1016/j.enbuild.2020.110050.
22. Gil-Lopez, T., Gimenez-Molina, C. Influence of double glazing with a circulating water chamber on the thermal energy savings in buildings. *Energy Build.* **2013**, *56*, 56–65, doi:10.1016/j.enbuild.2012.10.008.
23. Chow, T.T.; Li, C.; Lin, Z. Thermal characteristics of water-flow double-pane window. *Int. J. Therm. Sci.* **2010**, *50*, 140–148, doi:10.1016/j.ijthermalsci.2010.10.006.
24. Li, C.; Chow, T.T. Water-filled double reflective window and its year-round performance. *Proc. Environ. Sci*. **2011**, *11*, 1039–1047.
25. Chow, T.T.; Li, C. Liquid-filled solar glazing design for buoyant water-flow. *Build. Environ.* **2013**, *60*, 45–55, doi:10.1016/j.buildenv.2012.11.010.

26. Ji, J.; Luo, C.; Chow, T.T.; Sun, W.; He, W. Thermal characteristics of a building-integrated dual-function solar collector in water heating mode with natural circulation. *Energy* **2011**, *36*, 566–574, doi:10.1016/j.energy.2010.10.004.
27. Lanzisera, S.; Dawson-Haggertym, S.; Cheung, H.; Taneja, J.; Culler, D.; Brown, R. Methods for detailed energy data collection of miscellaneous and electronic loads in a commercial office building, *Build. Environ.* **2013**, *65*, 170–177, doi:10.1016/j.buildenv.2013.03.025.
28. Nikolaeva-Dimitrova, M.; Stoyanova, M.; Ivanov, P.; Tchonkova, K.; Stoykov, R. Investigation of thermal behaviour of innovative water flow glazing modular unit. *Bulg. Chem. Commun*. **2018**, *50*, 21–27.
29. Dagdougui, Y.; Ouammi, A.; Benchrifa, R. Energy Management-Based Predictive Controller for a Smart Building Powered by Renewable Energy. *Sustainability* **2020**, *12*, 4264.
30. Gan, V.J.L.; Lo, I.M.C.; Ma, J.; Tse, K.T.; Cheng, J.C.P.; Chan, C.M. Simulation Optimisation towards Energy Efficient Green Buildings. *J. Clean. Prod.* **2020**, *254*, 120012, doi:10.1016/j.jclepro.2020.120012.
31. Chiesa, G.; Grosso, M. The influence of different hourly typical meteorological years on dynamic simulation of buildings. *Energy Procedia* **2015**, *78* 2560–2565.
32. Loonen, R.; Favorino, F.; Hensen, J.; Overend, M. Review of current status, requirements and opportunities for building performance simulation of adaptive facades. *J. Build. Perform. Simul.* **2016**, *1493*, 1–19.
33. Bambardekar, S.; Poerschke, U. The architect as performer of energy simulation in the early design stage. In Proceedings of the IBPSA 2009—International Building Performance Simulation Association 2009, Eleventh International IBPSA Conference, Glasgow, UK, 27–30 July 2009; pp. 1306–1313
34. Fernandez-Antolin, M.; del-Rio, J.M.; del Ama Gonzalo, F.; Gonzalez-Lezcano, R. The Relationship between the Use of Building Performance Simulation Tools by Recent Graduate Architects and the Deficiencies in Architectural Education. *Energies* **2020**, *13*, 1134, doi:10.3390/en13051134.
35. Sierra, P.; Hernandez, J.A. Solar heat gain coefficient of water flow glazing. *Energy Build.* **2017**, *139*, 133–145.
36. Chow, T.; Chunying, L.; Clarke, J.A. Numerical prediction of water-flow glazing performance with reflective coating. In Proceedings of Building Simulation 2011, 12th Conference of International Building Performance Simulation Association, Sydney, Australia, 14–16 November 2011.
37. Moreno Santamaria, B.; del Ama Gonzalo, F.; Pinette, D.; Gonzalez-Lezcano, R.-A.; Lauret Aguirregabiria, B.; Hernandez Ramos, J.A. Application and Validation of a Dynamic Energy Simulation Tool: A Case Study with Water Flow Glazing Envelope. *Energies* **2020**, *13*, 3203.
38. Moreno Santamaria, B.; del Ama Gonzalo, F.; Lauret Aguirregabiria, B.; Hernandez Ramos, J.A. Experimental Validation of Water Flow Glazing: Transient Response in Real Test Rooms. *Sustainability* **2020**, *12*, 5734.
39. German Institute for Standardization. *Glass in Building—Determination of Thermal Transmittance (U Value)—Calculation Method*; EN 673; German Institute for Standardization: Berlin, Germany, 2011.
40. German Institute for Standardization. *Glass in Building—Determination of Luminous and Solar Characteristics of Glazing*; EN 410; German Institute for Standardization: Berlin, Germany, 2011.
41. Finlayson, E.; Arasteh, D.; Huizenga, C.; Rubin, M.; Reilly, M. *WINDOW 4.0:Documentation of Calculation Procedures*; University of California, Lawrence Berkeley Laboratory: Berkley, CA, USA, 1993.
42. Baranzelli, C.; Lavalle, C.; Sgobbi, A.; Aurambout, J.; Trombetti, M.; Jacobs, C.; Cristobal Garcia, J.; Kancs, D.; Kavalov, B. *Regional Patterns of Energy Production and Consumption Factors in Europe—Exploratory Project EREBILAND—European Regional Energy Balance and Innovation Landscape*; EUR 27697; Publications Office of the European Union: Luxembourg, 2016; doi:10.2788/357099.
43. Edwards, R.; Larivé, J.F.; Rickeard, D.; Weindorf, W. *Well-To-Tank Report Version 4.a. Well-to-Wheels Analysis of Future Automotive Fuels and Powertrains in the European Context*; Publications Office of the European Union: Luxembourg, 2014; doi:10.2790/95629.
44. Vanhoutteghem, L.; Skarning, G.C.J.; Hviid, C.A.; Svendsen, S. Impact of façade window design on energy, daylighting and thermal comfort in nearly zero-energy houses. *Energy Build.* **2015**, *102*, 149–156, doi:10.1016/j.enbuild.2015.05.018.
45. Casini, M. 7-Advanced insulation glazing. In *Smart Buildings*; Casini, M., Ed.; Woodhead Publishing: Cambridge, MA, USA, 2016; pp. 249–277.

46. Kralj, A.; Drev, M.; Žnidaršič, M.; Černe, B.; Hafner, J.; Jelle, B.P. Investigations of 6-pane glazing: Properties and possibilities. *Energy Build.* **2019**, *190*, 61–68.
47. Tam, V.W.Y.; Le, K.N.; Wang, J.Y. Cost Implication of Implementing External Facade Systems for Commercial Buildings. *Sustainability* **2018**, *10*, 1917.

4.2 Validation of Objective 2

4.2.1 Context of papers and References

This paper evaluated the thermal comfort through the Predicted Mean Vote (PMV) in summer conditions. The study comprised the energy performance of water flow glazing (facade and internal partitions) of the DMAIA prototype (office room), coupled with an energy management system.

This paper has been published in *Sustainability*, which is an international, cross-disciplinary, scholarly, peer-reviewed and open access journal of environmental, cultural, economic, and social sustainability of human beings. It provides an advanced forum for studies related to sustainability and sustainable development, and is published semimonthly online by MDPI.

Sustainability is indexed in JCR, with an Impact Factor of 3.251 (2020) Q2, and in Scopus, with a CiteScore of 3.9 (2020) Q1.

Paper:

Sustainability

PAPER 4: *Moreno Santamaria, B.; Ama Gonzalo, F.; Lauret Aguirregabiria, B.; Hernandez Ramos, J.A. Evaluation of Thermal Comfort and Energy Consumption of Water Flow Glazing as a Radiant Heating and Cooling System: A Case Study of an Office Space. Sustainability 2020, 12, 7596.*

4.2.2 PAPER 4: Evaluation of Thermal Comfort and Energy Consumption of Water Flow Glazing as a Radiant Heating and Cooling System: A Case Study of an Office Space

Overview

This paper has studied the energy performance of water flow glazing (facade and internal partitions), coupled with an energy management system, and the relationships with steady and transient parameters. The energy management system was composed of a heat pump and an air heat exchanger to deliver heat or cold to a buffer tank. The energy management system received inputs from temperature and relative humidity sensors. The results included actual indoor air and glazing

temperatures, heating and cooling energy consumption, and the influence of WFG on the mean radiant temperature and comfort.

The main conclusion drawn from this paper is that a radiant system such as WFG interior partitions can achieve occupants' comfort at indoor temperatures between $25°C$ and $27°C$ and thus improve the energy performance of air-to-water heat pumps.

Radiant panels improve the performance of air-to-water heat pumps. The energy efficiency ratio (EER) reached 3.62 when the water temperature was 18 $°C$, and the coefficient of performance (COP) was 4.5 when the water temperature was 35 $°C$ in heating mode. Using WFG as a radiant cooling facade and indoor partitions effectively reduced the operative temperature to comfortable levels when the indoor air temperature was between 25 and 27.5 $°C$.

$$MRT = T_1\ F_p - 1 + T_2\ F_p - 2 + ... + T_N\ F_p - N, \tag{4.1}$$

The mean radiant temperature (MRT) has a strong influence on human thermal comfort because the occupant body transfers heat to the hot or cold surface. MRT is calculated as the average value of the surrounding temperatures weighted according to the angle factors (F_{p-N}), as it is showm in Equation 4.1. The predicted mean vote (PMV) model uses six key factors to address thermal comfort: metabolic rate, clothing insulation, air temperature, radiant temperature, airspeed, and humidity.

The Predicted Mean Vote (PMV) in summer conditions was between 0 and -0.5 in working hours, within the recommended values of ASHRAE-55 standard. The MRT ranged from 19.3 to 23 $°C$, and the indoor air temperature ranged from 25.2 to 29.1 $°C$.

Water-Flow Glazing was evaluated as a component of a hydronic radiant heating and cooling system. It showed final energy-saving potential, provided thermal comfort, and was considered a valid option for office retrofitting.

The system is limited by its high initial cost and the need for an energy management system integrated with the rest of the equipment, especially the ventilation and heat pumps.

Published Paper

sustainability

MDPI

Article

Evaluation of Thermal Comfort and Energy Consumption of Water Flow Glazing as a Radiant Heating and Cooling System: A Case Study of an Office Space

Belen Moreno Santamaria [1], Fernando del Ama Gonzalo [2,*], Benito Lauret Aguirregabiria [1] and Juan A. Hernandez Ramos [3]

[1] Department of Construction and Architectural Technology, Technical School of Architecture of Madrid, Technical University of Madrid (UPM), 28040 Madrid, Spain; belen.moreno@upm.es (B.M.S.); benito.lauret@upm.es (B.L.A.)
[2] Department of Sustainable Product Design and Architecture, Keene State College, Keene, NH 03435, USA
[3] Department of Applied Mathematics, School of Aeronautical and Space Engineering, Technical University of Madrid (UPM), 28040 Madrid, Spain; juanantonio.hernandez@upm.es
* Correspondence: fernando.delama@keene.edu

Received: 19 July 2020; Accepted: 11 September 2020; Published: 15 September 2020

Abstract: Large glass areas, even high-performance glazing with Low-E coating, could lead to discomfort if exposed to solar radiation due to radiant asymmetry. In addition, air-to-air cooling systems affect the thermal environment indoors. Water-Flow Glazing (WFG) is a disruptive technology that enables architects and engineers to design transparent and translucent facades with new features, such as energy management. Water modifies the thermal behavior of glass envelopes, the spectral distribution of solar radiation, the non-uniform nature of radiation absorption, and the diffusion of heat by conduction across the glass pane. The main goal of this article was to assess energy consumption and comfort conditions in office spaces with a large glass area by using WFG as a radiant heating and cooling system. This article evaluates the design and operation of an energy management system coupled with WFG throughout a year in an actual office space. Temperature, relative humidity, and solar radiation sensors were connected to a control unit that actuated the different devices to keep comfortable conditions with minimum energy consumption. The results in summer conditions revealed that if the mean radiant temperature ranged from 19.3 to 23 °C, it helped reduce the operative temperature to comfortable levels when the indoor air temperature was between 25 and 27.5 °C. The Predicted Mean Vote in summer conditions was between 0 and −0.5 in working hours, within the recommended values of ASHRAE-55 standard.

Keywords: building energy management; Water Flow Glazing; mean radiant temperature; final energy consumption

1. Introduction

Obsolete equipment, design flaws, and inappropriate use can account for up to 20% of the energy that buildings use over the operation period [1]. Dwellings, offices, educational facilities, and commercial buildings show different consumption patterns. For example, commercial buildings exhibit high energy consumption associated with heating, ventilation, and air conditioning (HVAC) systems and lighting [2]. Office buildings have a high amount of energy use by computers and monitors, while educational buildings have significantly more energy consumption for lighting [3]. Office buildings are likely to have higher cooling demands due to the impact of internal gains from

occupants and IT equipment [4]. The European air conditioning (AC) market is essential in raising awareness about primary energy utilization. Over the last two decades, all members of the European Union (EU) have been committed to increasing the production of renewable energy, decreasing greenhouse gas (GHG) emissions, and reducing the final energy consumption by 20% from 1990 levels by 2020. The goal of reducing the emissions of GHG by 40% by 2030 has been set. Furthermore, the EU members have committed to reducing GHG emissions by 80–95% by 2050, and the fulfillment of the Paris Conference of the Parties 21 agreement will require a further reduction of GHG emissions [5]. In this regard, some studies show that electricity demand for cooling is increasing, especially in colder European countries [6]. If the electricity demand exceeds the projected renewable capacity, the goal of reducing GHG emissions will not be met.

An energy management system (EMS) assures that the building's energy demand is accomplished without compromising the air quality and comfort levels of its occupants [7]. The EMS can collect measurements at a specified time interval at designated measurement points. The accurate and diverse data, deployment without affecting the building operation, communication protocol, and cost influence the selection of the EMS [8]. Engineers tend to overestimate the internal heat gains in office buildings, which results in the specification of cooling systems that exceed the needed capacity. As a result, there is an energy waste over long periods of inefficient operation [9,10]. The Energy Consumption Guide (ECG) shows patterns and benchmarks for electricity consumption in office buildings [11]. Energy consumption schedules, occupants' habits, and the diversity of electric loads have a significant impact on office building energy behavior [12,13]. An energy management system allows owners to understand building performance, improve energy efficiency, and take appropriate actions [14,15].

Power load density is used to assess expected peak power demand, taking into account internal heat gains [16,17]. The building envelope materials contribute decisively to reducing the heating and cooling loads. Windows and curtain walls play a crucial role in the energy efficiency of office buildings due to solar heat gains. Although solar radiation may help reduce heating loads in the cold season, summer heat gains have to be avoided [18,19]. In this regard, the extensive use of glass in facades in office buildings has led to an 8.7% increase in the AC market in Europe over the last decade, especially in Mediterranean countries [20,21]. Despite the growth of the market, other factors like the increasing price of electricity in the European Union (17% from 2008 to 2019) [22] and new government regulations have forced manufactures to develop energy-efficient products, such as inverter technologies and new refrigerants [23]. The energy performance of heating and AC systems is measured by the energy efficiency ratio (EER) in the cooling mode and the coefficient of performance (COP) in the heating mode. The seasonal energy efficiency ratio and the seasonal coefficient of performance (SEER, SCOP) designate the total heat supplied or removed from areas ($Q_{heat/cold,\ season}$) divided by the total work input over the same period ($W_{electricity,\ season}$) [24]. By product type, split systems, coupled with air-to-air heat pumps, account for the majority of AC units per type [25]. Air-to-water and water-to-water heat pumps can be coupled with fan coil units (FCUs) and radiant panels in walls, floors, and ceilings. The EER and COP of heat pumps depend on the source and load side temperatures, so assessing the energy performance of each type requires analyzing the outdoor and indoor operating temperatures [26].

When it comes to defining thermal comfort conditions, six main factors must be taken into account: metabolic rate, clothing insulation, air temperature, radiant temperature, airspeed, and humidity [27]. Fanger's Predicted Mean Vote (PMV) method was developed to consider the different variables that influence the comfort assessment in a working environment [28,29]. The international organization for standardization document ISO 7726 defined local thermal discomfort as the thermal dissatisfaction caused by unwanted cooling or heating of one particular part of the body. It mainly affects people developing light sedentary activities [30]. The mean radiant temperature (MRT) has a strong influence on human thermal comfort because occupant bodies transfers heat to hot or cold surfaces [31]. In office buildings with convective heating and cooling systems, such as split units, and facades with extensive glazing, users experience a lack of comfort caused by the inhomogeneity in indoor surfaces and air temperatures [32]. For example, windows with high thermal transmittance and without Low-E

coatings can lead to high radiant temperature asymmetry and the local dissatisfaction of some body parts [33]. An effective way to improve the comfort conditions in these buildings would be to use temperature-controlled surfaces or radiant panels as the principal source of sensible cooling and heating in the conditioned space. Radiant panels provide a comfortable indoor environment without lowering the room air's moisture content. Occupants in an area heated or cooled by radiant panels are comfortable at lower air temperatures in winter and higher air temperatures in summer. Indoor partitions and facades with Water-Flow Glazing (WFG) are considered active radiant panels that control their temperature by circulating water, and can be used to control the surface temperatures and provide an acceptable thermal environment [34]. In facades exposed to solar radiation, the water flows between two glass panes and captures most of the solar infrared radiation, and the visible component enters the building [35]. Since the WFG is a dynamic envelope, the solar heat transmitted through the material depends on the flow rate. When the water flows, the transmitted solar heat is low, and when the water flow stops, the solar radiation enters the building [36]. In interior partitions, WFG panels can supply the needed power at a rate of 120 W/m^2 if the difference between the circulating water and the indoor air temperature is 10 °C [37].

This paper focused on assessing the performance of WFG envelopes in commercial buildings by analyzing power demand patterns through measured data obtained from a testing facility. Hence, to achieve this goal, it was essential to: (i) validate the energy management system to enhance the thermal performance of the building, (ii) estimate the final energy consumption of the office space in summer and winter conditions, and (iii) evaluate the comfort conditions and the influence of the mean radiant temperature in the Predicted Mean Vote over the office space working hours.

2. Materials and Methods

Commercial building energy simulation (BES) tools do not include Water-Flow Glazing as an option, so it is necessary to validate its behavior in real facilities. This section described the office space layout, the description of the envelope and the Water-Flow Glazing, the energy management system components, and the electronic control unit logic operation.

2.1. Description of the Facility

The testing facility was an office space of the Department of Applied Mathematics in the School of Aeronautics and Space Engineering in Madrid, Spain (40,44389° N, −3,7261972° E). Two faculty members occupy the room from 8:00 a.m. to 8:00 p.m., and there are meetings with students during office hours. The occupancy is limited to six people at a time. The facility validated the WFG behavior as a component of the heating and cooling system. Figure 1 illustrates the floor plan. Four transparent WFG panels (WFG1, WFG2, WFG3, and WFG4) separated the corridor from the office. The thermal and spectral properties of these transparent panels were carefully selected to absorb the maximum heat from the beam solar radiation, which entered through the main glazed facade, impinging into the WFG in the afternoon for four to five hours, depending on the season. The northeast facade was an insulated opaque wall, and the rest of the interior partitions were translucent WFG (WFG_TP01 to WFG_TP09). In all, there were thirteen WFG panels of 1500 mm height by 1300 mm width. The energy management system is placed outdoors, in the north-east facade. The electronic control unit (ECU) monitored the temperatures of the WFG and the indoor, corridor, and outdoor temperatures.

Table 1 shows the thermal transmittance and areas of the office envelope. The opaque internal partitions were modular walls with melamine panel finish (0.5 cm) and rock–wool acoustic insulation (3 cm). The northeast facade was an insulated opaque wall made up of a zinc plate external finish (1 mm), ventilated air chamber (3 cm), a brick wall (11 cm), rock–wool thermal insulation (6 cm), air chamber (5 cm), and a plaster board (12 mm). The roof was composed of a zinc plate external finish (1 mm), ventilated air chamber (3 cm), metal deck with concrete (10 cm), air chamber (10 cm), rock–wool thermal insulation (6 cm), and a plaster board (12 mm). The thermal transmittances met the requirements of the Spanish Building Code [38].

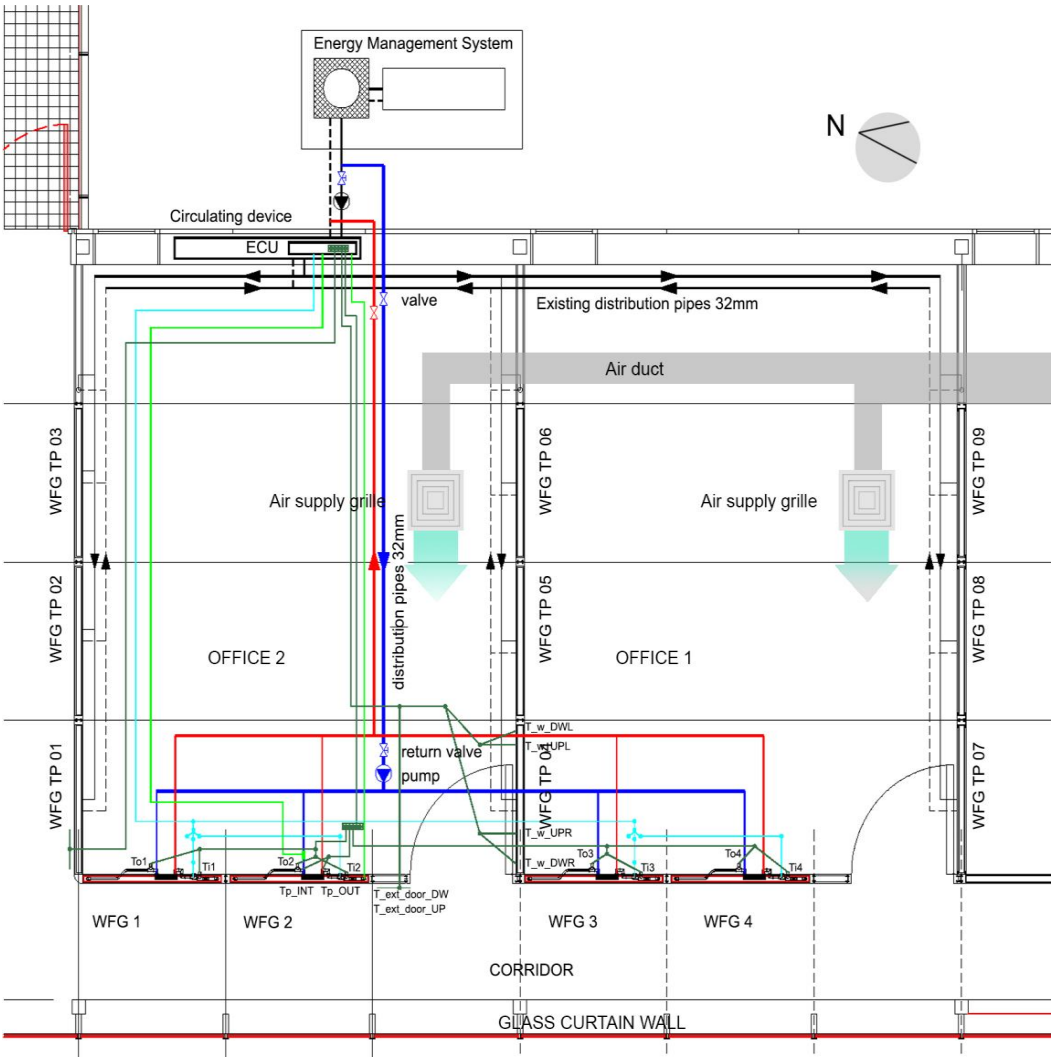

Figure 1. Plan view of the office spaces. The transparent Water-Flow Glazing (WFG) was connected directly to the primary circuit. The translucent interior partitions were connected in parallel to the circulating device.

Table 1. Parameters of the office envelope.

Thermal and Geometric Parameters	Roof	N-E Wall	N-E Window	Int Wall	Int Glass	Floor
U (W/m^2K) [1]	0.3	0.3	2.9	0.7	5.2	0.6
A (m^2)	40	22.5	2.2	19.6	7.8	40
∑UA (W/K)	12	6.75	6.38	13.72	40.56	24

[1] Values meet the Spanish Building Code (CTE DB HE1) requirements [38].

Figure 2 shows the space with transparent WFG (a) facing south-west and translucent interior partitions (b). The former was double glazed; each glass pane was composed of 8 mm planiclear, 1.54 mm saflex Rsolar SG41, 8 mm planiclear, and a 20 mm water chamber. The latter was double glazed; each glass pane was formed of 10 mm planiclear, 1 mm translucent Polyvinyl butyral (PVB) 000A CoolWhite, 3 mm planiclear, and a 16 mm water chamber. The mass flow rate through the transparent WFG was set to be 2 L/min, and through the translucent glazing, it was 1 L/min. The transparent panes were exposed to western solar radiation and had to absorb a large amount of heat. In contrast, the translucent panes were designed to deliver heat or cold in winter or summer.

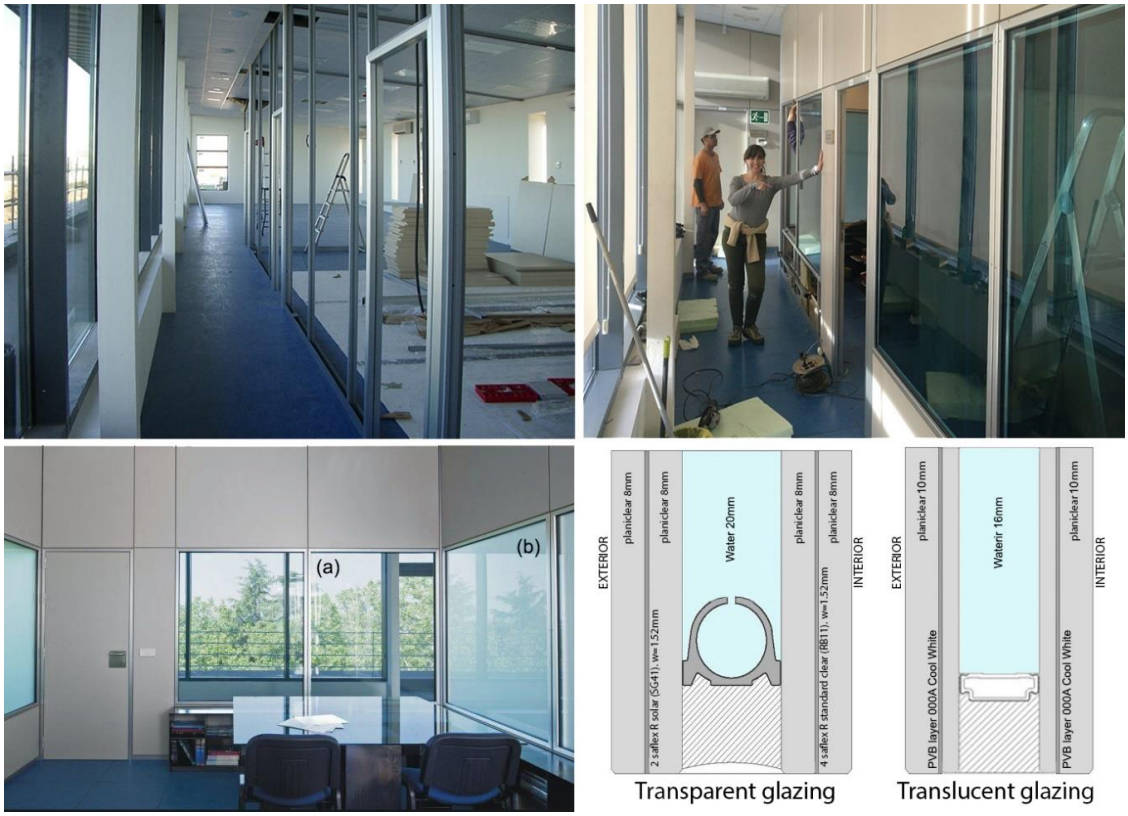

Figure 2. Top: View from the access corridor during the construction process. Bottom: Glass configuration of the office space. (**a**) Transparent Water-Flow Glazing (corridor), (**b**) translucent Water-Flow Glazing (interior partitions).

Table 2 shows the estimated heating and cooling loads in the office space. Ventilation loads (*Vent*) and internal loads (*IL*) were calculated for an occupancy of six people and average office equipment [38,39]. The total glazed surface was 7.8 m^2 of transparent WFG and 17.55 m^2 of translucent interior partitions. The wall-to-window ratio of the wall exposed to solar radiation was 40%. The total area of WFG radiant panels was 25.35 m^2, with a floor area of 40 m^2. The expected power delivered by WFG was 130 W/m^2 when the difference between the circulating water and the indoor air temperature was 13 °C. The dew point temperature for the indoor air temperature was at 27 °C and relative humidity at 40% was 12 °C. Therefore, keeping the WFG inlet temperature above 12 °C, the indoor air temperature at 27 °C, and the average water temperature at 14 °C, the delivered cooling power would be 130 W/m^2. The total WFG surface area was 25.35 m^2 and the total cooling power was 3295 W, which was above the predicted cooling loads shown in Table 2. The cost of the system depends on a few different factors, including the dimensions of the glass, thickness, and distance between the energy management system and the panels. A typical 2 m^2 double glass panel costs 900 USD (around 450 USD/m^2), including the piping and individual circulating devices. Installation of WFG requires a professional team, which could run 50 to 70 USD per hour.

Table 2. Estimation of heating and cooling loads in the offices.

Operating Condition	$T_{\_int}$ (°C)	$T_{\_ext}$ (°C) [1]	$T_{\_ext\_C}$ (°C)	n	$\sum UA(T_{\_int}-T_{\_ext})$ (W)	$\sum UA(T_{\_int}-T_{\_ext\_C})$ (W)	Vent (W)	IL (W)	SR (W)	Total (W)
Heating	22	4	22	2	452.34	-	1620	-	-	2018.16
Cooling	23	35	30	6	301.56	379.26	1080	1400	82.5	3243.42

[1] Values are taken from CTE DB HE1 [38].

Figure 3 shows the schematics of both circuits. The energy management circuit consisted of a 370 L buffer tank, an expansion tank, an air-to-water heat pump, and an air heat exchanger. The heat pump's (Saunier Duval Genia Air 8/1 Power A7/W35 = Power A35/W18) nominal power was 7.60 kW in winter (at an outdoor air temperature of 7 °C and inlet water temperature of 35 °C) and summer (at an outdoor air temperature of 35 °C and inlet water temperature of 18 °C). The heat pump was selected for commercial reasons, regarding availability and budget constraints. Some malfunctions and operating issues related to the oversized cooling and heating power are addressed in the following sections. The air heat exchanger works when the outdoor air temperature is low enough to cool down water. This cooling mode can only be used when outdoor ambient air temperatures are below 12 °C. When the air heat exchanger is used for free cooling, the control system uses valves to isolate the heat pump from the rest of the loop, and the heat exchanger is used like a chiller. Once the buffer tank is heated or cooled down, the water flows to transfer heat or cold to the circulating device. Then, the secondary circuit transports the heated or cooled water to thirteen radiant WFG units. A control system with a thermostat based on the indoor temperature turned the heat pump and the flow rate ON and OFF. The secondary circuit was made up of two branches—one that transferred heat or cold to translucent partitions and another one for the transparent WFG modules. Each transparent WFG module had a circulating device (*CDi*). The mass flow rate through the transparent modules was set to $\dot{m}$ = 2 L/min m^2 when the system was ON. All the translucent WFG panels were connected to the same circulating device (*CD TP*), and the flow rate was $\dot{m}$ = 1 L/min m^2. The influence of the mass flow rate on the ability to deliver or absorb heat and the recommended values have been studied in previous articles [37]. Transparent WFG panels are exposed to solar radiation, so the mass flow rate had to be higher to absorb heat in summer and keep the water temperature within acceptable values. The electronic control unit actuated the WFG circulating devices, the heat pump, and the air heat exchanger using the basic commands of ON and OFF, with the control logic explained in Table 3. There was a mechanical ventilation system that met the requirements of the Spanish Regulation of Thermal Installations in Buildings (RITE) for ventilation of office spaces (12.5 L per second per person) [40]. The mechanical ventilation provided conditioned air and operated over the working hours (8:00 a.m. to 8:00 p.m.) at a constant air volume. However, it was not a component of the controlled energy management system. The lack of control of the ventilation device was one of the system's uncertainties because high relative humidity can cause condensation in radiant panels when operating in cooling mode, and can affect the latent loads.

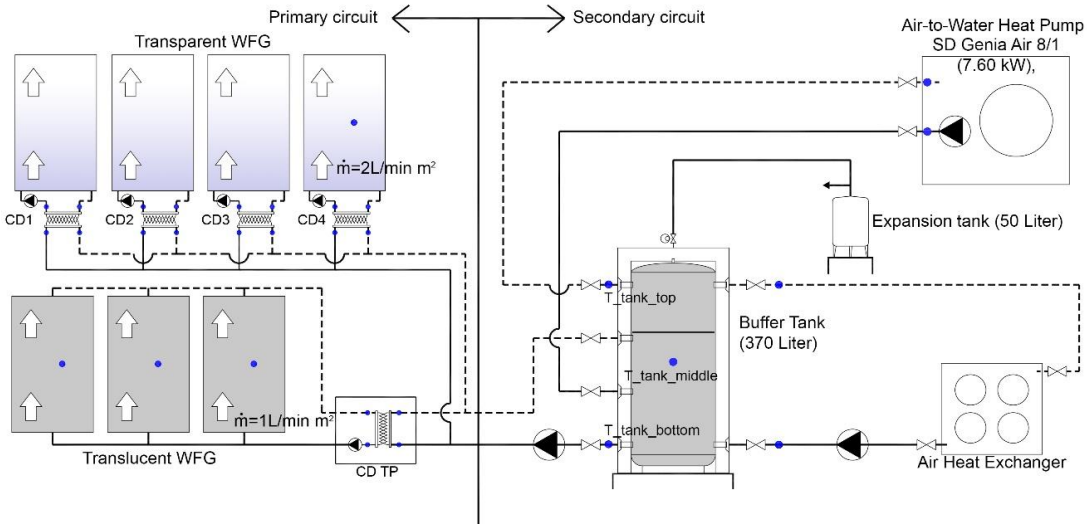

Figure 3. Schematics of the testing facility. The primary circuit connects the energy management devices (heat pump, air heat exchanger, and buffer tank). The secondary circuit goes from the buffer tank to the WFG.

Table 3. Energy management system in cooling mode.

Device	HP	AHX	WFG	WFG_HP
Condition 1	$T_{\_int} > 25$ °C	-	$T_{\_int} > 25$ °C	
Condition 2	$(T_{\_tank\_top} - T_{\_ext}) < 10$ °C	$(T_{\_tank\_top} - T_{\_ext}) > 10$ °C	$(T_{\_int} - T_{\_tank\_bottom}) > 10$ °C	
8:00 p.m.–7:00 a.m.	-	ON	ON	ON
7:00 a.m.–8:00 p.m.	ON	-	ON	ON

Tables 3 and 4 show the proposed energy management strategy in the heating and cooling modes. The heat pump (*HP*) was set to operate during working hours, whereas the air heat exchanger (*AHX*) operated only in cooling mode during non-working hours. The first condition was related to the indoor air temperature ($T_{\_int}$) and the second condition depended on the difference between the outdoor air temperature ($T_{\_ext}$) and the tank temperatures ($T_{\_tank\_top}$, $T_{\_tank\_bottom}$).

Table 4. Energy management system in heating mode.

Device	HP	AHX	WFG	WFG_HP
Condition 1	$T_{\_int} < 20$ °C		$T_{\_int} < 20$ °C	
Condition 2	-		$(T_{\_tank\_bottom} - T_{\_int}) > 10$ °C	
8:00 p.m.–7:00 a.m.	-	-	ON	ON
7:00 a.m.–8:00 p.m.	ON	-	ON	ON

2.2. Description of the Sensors

To measure the water heat gain of the WFG panels, flow meters and inlet and outlet digital thermometers were installed in the primary and secondary circuits. The DS18B20-PAR digital thermometer communicated over a one-wire bus with the energy control unit (ECU). They had an operating temperature range of −55 to +100 °C and an accuracy of ±0.5 °C. A pyranometer Delta Ohm LP PYRA 03, placed on the vertical south-western facade, allowed measurement of the solar irradiance. It is a second-class pyranometer according to ISO 9060 standards and the World Meteorological Organization (WMO); it had to be placed outdoors because obstacles and reflections can affect the measurements. The same monitoring equipment has been described in other articles [37]. Figure 4 shows the position of the temperature sensors in the WFG and the circulating device. The flow meter (s) measures the flow rate at the inlet of the WFG panels. The flow meter (p) measures the flow rate of the primary circuit. The temperature sensors, T_{i2} and T_{o2}, measure the inlet and outlet temperatures in the WFG 2, respectively, and T_{p2} and T_{p2} measure the temperatures at the primary circuit.

Every WFG module had a circulator that comprised a water pump, a plate heat exchanger, and two one-wire sensors inserted into two pocket wells to measure the inlet and outlet temperatures of the glazing. In addition, one module was monitored with a digital flow meter for the primary circuit and another digital flow meter for the secondary circuit. Together with the inlet and outlet temperatures, these flow meters allowed validation of the design flow rate of the glazing as well as having precise actual values for the water heat gain of each WFG panel. The one-wire digital thermometers were inserted into the pocket wells. Each sensor had a unique 64-bit serial number etched into it, and allowed the housing of a considerable number of sensors to be used on one data bus. There were four transparent WFG modules and two thermometers per module, plus the inlet and outlet temperatures for the primary circuit, measured with the same data bus. Thermostats and timers controlled the heating and cooling system. All indoor temperatures were measured 150 cm above the floor level. The main objective of this strategy was to maintain a comfortable indoor temperature and to minimize energy consumption using solar energy harvesting and free cooling. Table 5 presents a description of the sensors and parameters that have been measured. The WFG transparent panels were located in a

corridor with south-west orientation. When the solar radiation impinged on the glazing, the water absorbed the energy. After analyzing the indoor temperature, the EMS decided whether to store the heat or to distribute it through the rest of the translucent interior partitions. The energy surplus could be stored in the buffer tank. If there was no solar energy to harvest or there was not enough energy harvested in the buffer tank, the heat pump would work to satisfy the demand. Generally, an office building demands cold throughout the year due to its high internal heat load. In winter, the outdoor temperature is low enough to dissipate the internal heat load utilizing an air heat exchanger. The heat pump electricity consumption was not measured. The electricity consumption was estimated with the heat pump thermal power, the coefficient of performance, and the energy efficiency ratio provided by the manufacturer.

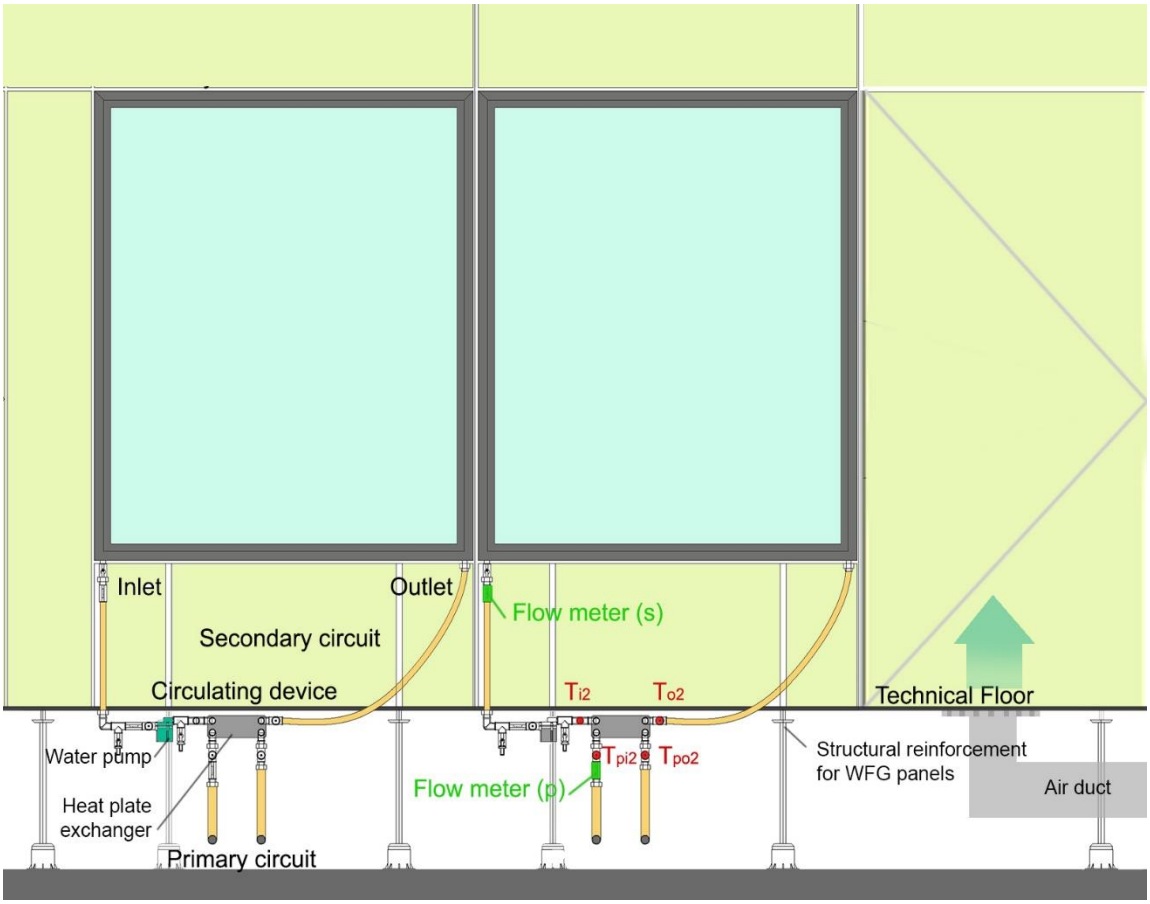

Figure 4. Front view of the transparent WFG in the corridor facing south-west. Location of the circulating device underneath the technical floor. Location of inlet and outlet temperature probes and flow meters for the primary and secondary circuits of the WFG.

Table 5. Nomenclature and description of sensors.

Sensor	Description
T_{ik}	Inlet temperature of the transparent WFG [1] (°C)
T_{ok}	Outlet temperature of the transparent WFG [1] (°C)
T_{s_IN}	Inlet temperature of the translucent WFG partitions (°C)
T_{s_OUT}	Outlet temperature of the translucent WFG partitions (°C)
$T_{\_ext}$	Outside temperature (°C)
$T_{\_int}$	Indoor air temperature (°C)
$T_{\_tank\_bottom}$	Temperature at the bottom of the buffer tank (°C)
$T_{\_tank\_middle}$	Temperature in the middle of the buffer tank (°C)
$T_{\_tank\_top}$	Temperature at the top of the buffer tank (°C)
$T_{\_ext\_C}$	Temperature of the corridor right outside the door (°C)
T_{floor}	Surface temperature of the floor (°C)
T_{wall}	Surface temperature of opaque walls (°C)
$T_{ceiling}$	Surface temperature of the ceiling (°C)
T_{WFG}	Surface temperature of transparent WFG (°C)
T_{WFG_TP}	Surface temperature of WFG translucent partitions (°C)
Sun_rad	Solar irradiance on vertical surface (W/m^2)
kWh_HP	Thermal heating/cooling energy by the heat pump (kWh)
kWh_AXH	Thermal cooling energy by the air heat exchanger (kWh)
kWh_WFG	Heating/cooling energy delivered by transparent WFG (kWh)
kWh_WFG_TP	Heating/cooling energy delivered by WFG translucent partitions (kWh)
RH	Indoor Relative Humidity (%)

[1] k is the module number from 1 to 4.

3. Results

This section presents monitoring temperatures and the power efficiency of WFG modules. The implementation of different energy strategies was validated. By analyzing the system's performance, the energy strategy is improved, achieving significant energy savings. Finally, the power performance of the WFG module is obtained by measuring the inlet and outlet temperatures and flow rate of each WFG panel.

3.1. Analysis in Summer Conditions

Figure 5 shows the system temperatures and the irradiance curve of a sample summer week from 10 July 2019 to 16 July 2019. T_{i2} and T_{o2} illustrate the inlet and outlet temperatures of the WFG. T_int is the indoor temperature, and T_ext is the exterior temperature. T_ext_C corresponds to the temperature in the corridor between the office and the exterior. The first day, 10 July 2019, was clear, with some evolution clouds between 16:30 and 18:00. On clear days, direct beam radiation prevailed over diffuse radiation. The typical irradiance curve (*Sun_rad*) reached maximum levels above 700 W/m^2. From 9:00 a.m. to 1:00 p.m., the south-west facade was shaded due to geometrical obstructions, and the irradiance was mainly diffuse, reaching values around 200 W/m^2. However, in the afternoon, the facade was exposed to direct solar radiation, and the corridor temperature rose to 35 °C. On 11 July 2019, the indoor and outdoor temperatures showed a similar performance, although the oscillations of the inlet and outlet temperatures were different from those of the previous day. On 12 July 2019, the solar irradiance showed irregular values because of clouds, and it affected the temperature of the corridor, which was slightly above 30 °C. Over the weekend, on 13 July 2019 and 14 July 2019, the mass flow rate was 0 and the heat pump did not operate. Inlet and outlet temperatures of the WFG (T_{i2} and T_{o2}) did not show any difference and reached peak values of 32 °C. The indoor air temperature reached a maximum of 34 °C, whereas the temperature in the corridor (T_ext_C) was 39 °C. A WFG circuit is a closed loop and there are two cases, mass flow rate $\dot{m}$ = 0 or $\dot{m}$ = design flow rate. Over the weekend, the mass flow rate was 0 and the heat pump was not in operation. After two weekend days, the indoor temperature rose to 32 °C, making it necessary to cool down the office temperature. Figure 5 shows

that the inlet and outlet temperatures dropped on Sunday 14/07/2019 before 7:00 a.m., although the heating pump did not operate that day. The same behavior was shown on Monday, 15/07/2019, before 7:00 a.m. The reason was that the air heat exchanger operated both days for two hours when the difference between the top tank water temperature (T_{tank_top}) and the outdoor air temperature (T_{ext}) was above 10 °C.

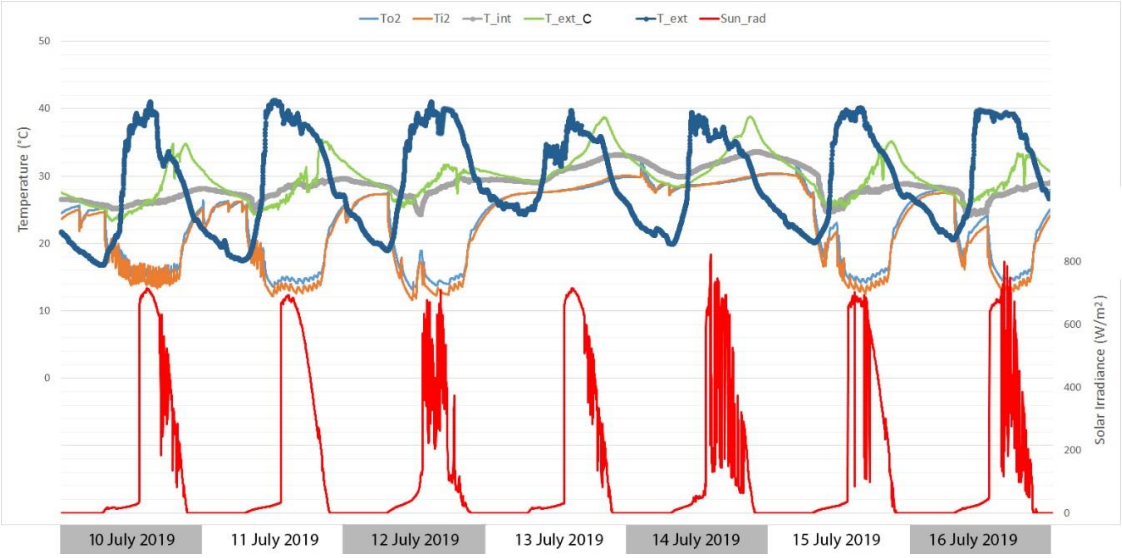

Figure 5. Solar irradiance and indoor and outdoor temperatures—sample summer week of 10 July 2019 to 16 July 2019.

Figure 6 shows the detailed evolution of temperatures on two consecutive days. Figure 6a shows that the irradiance curve on 10 July 2019 had some oscillations in the afternoon, and the outdoor temperature declined, which indicated the existence of clouds. The inlet and outlet temperatures (T_{i2}, T_{o2}) showed that the heat pump worked at three cycles per hour. The heat pump parameters were fixed to meet the manufacturer's requirement for minimum cycle times. Figure 6b showed that the minimum time between starts was, at least, forty minutes. On 10 July 2019 at 7:00 p.m., there was a peak in the corridor temperature (T_{ext_C}), and this peak did not occur on 11 July 2019. The corridor had a cooling system that was not monitored or controlled by the studied energy management system, and its temperature was a boundary condition of the studied space. The indoor air temperature rose to 27 °C on 10 July 2019 and to 29.5 °C on 11 July 2019. Although the temperatures might seem too high, due to the effect of radiating panels and a low mean radiant temperature, there is thermal comfort in the space, as shown in the discussion section.

3.2. Analysis in Winter Conditions

Figure 7 shows the temperatures and the irradiance curve of a sample winter week from 08 January 2020 to 14 January 2020. On sunny working days (from 08 January 2020 to 10 January 2020), the outdoor temperature showed typical values of winter in Madrid, with a minimum temperature slightly below 0 °C and a maximum temperature between 10 and 15 °C. The solar radiation impinged on the south-west facade as of 11:00 a.m. with a peak value of 300 W/m^2. The indoor air temperature (T_{int}) was below comfort until 7:00 p.m. because the heating system was off. In the morning, the heat pump started working, and the radiant WFG panels were delivering heat. In the afternoon, the temperature in the corridor (T_{ext_C}) rose to 30 °C, which helped to heat the office space air temperature (T_{int}) to 22 °C. The solar radiation in the afternoon made the heat delivered by the WFG unnecessary. Over the weekend (11 January 2020 and 12 January 2020), the heat pump was not operating, and the indoor air temperature declined and reached its lowest value (14 °C) on Monday 13 July 2020 at 7:00 a.m. Due to the solar radiation, the temperature in the corridor rose to 28 °C. On weekend days, the heat pump did

not operate in the morning, so the indoor temperature continued to drop until the afternoon, when the solar radiation and the corridor overheating contributed to raising the indoor air temperature from 17 to 19 °C on 11 January 2020 and from 15 to 17 °C on 12 January 2020. Nevertheless, the indoor temperature on 11 January 2020 at 7:00 a.m. was 18 °C, and on 13 January 2020, it was 14 °C after two days without operating the heat pump. On working days, the indoor air temperature was above 18 °C at the beginning of the working hours. On 13 July 2020 and 14 July 2020, the solar irradiance was low, and the outdoor temperature variation over the day was only 5 °C. The heat pump operated most of the working hours, unlike on sunny days, when it operated only in the morning.

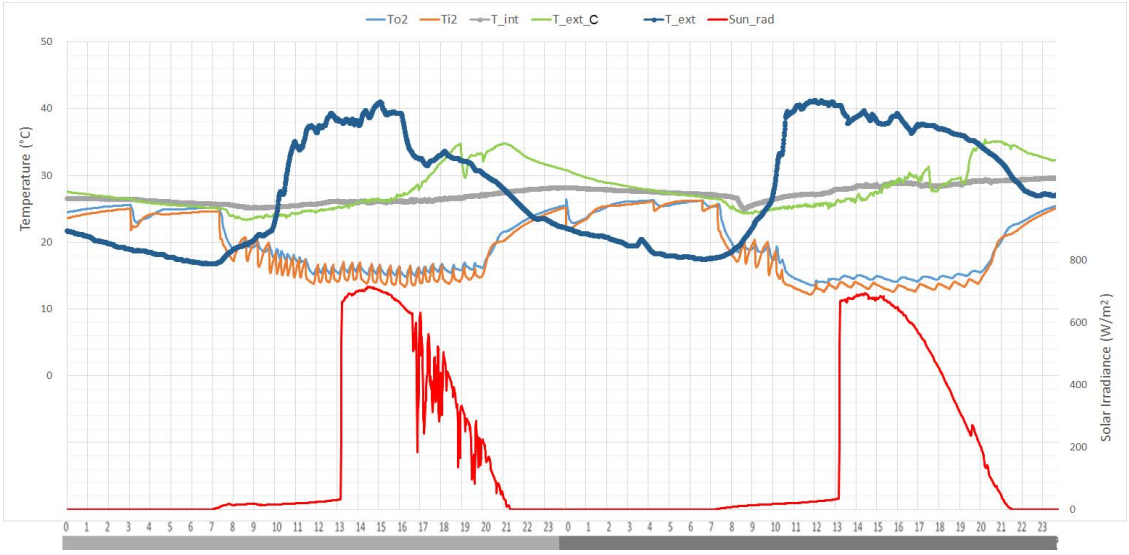

(**a**) (**b**)

Figure 6. Solar irradiance and indoor and outdoor temperatures—summer sample days (**a**) 10 July 2019 and (**b**) 11 July 2019.

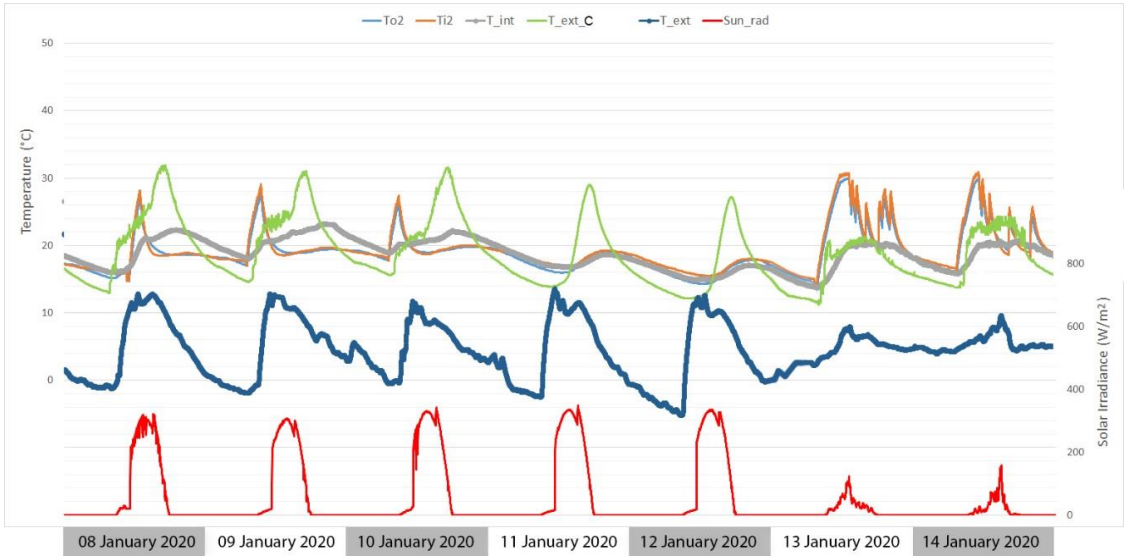

Figure 7. Solar irradiance and indoor and outdoor temperatures—sample winter week of 08 January 2020 to 14 January 2020.

Figure 8 details the parameters on two winter days with different outdoor conditions. Figure 8a illustrates a sunny winter day when the solar irradiance reached a peak value of 300 W/m^2, and the

outdoor temperature ranged from −1 to 11 °C. The WFG started working in heating mode from 7:00 a.m., when the indoor air temperature was 18 °C, to 9:30 a.m., when the indoor air temperature reached 20 °C. The indoor air temperature continued to rise to 22 °C because the corridor air temperature reached a peak of 30 °C. Figure 8b shows a winter day with little solar radiation and an outdoor temperature that ranged from 4 to 10 °C. The WFG started working in heating mode at 7:00 a.m., when the indoor air temperature was 16 °C. It took the system four hours to increase the indoor air temperature to 20 °C. The heat pump was connected to the buffer tank, so the heating time seemed too long due to the thermal inertia. Starting the heat pump four hours before the working hours would be an excellent strategy to improve comfort conditions on winter days after the holidays.

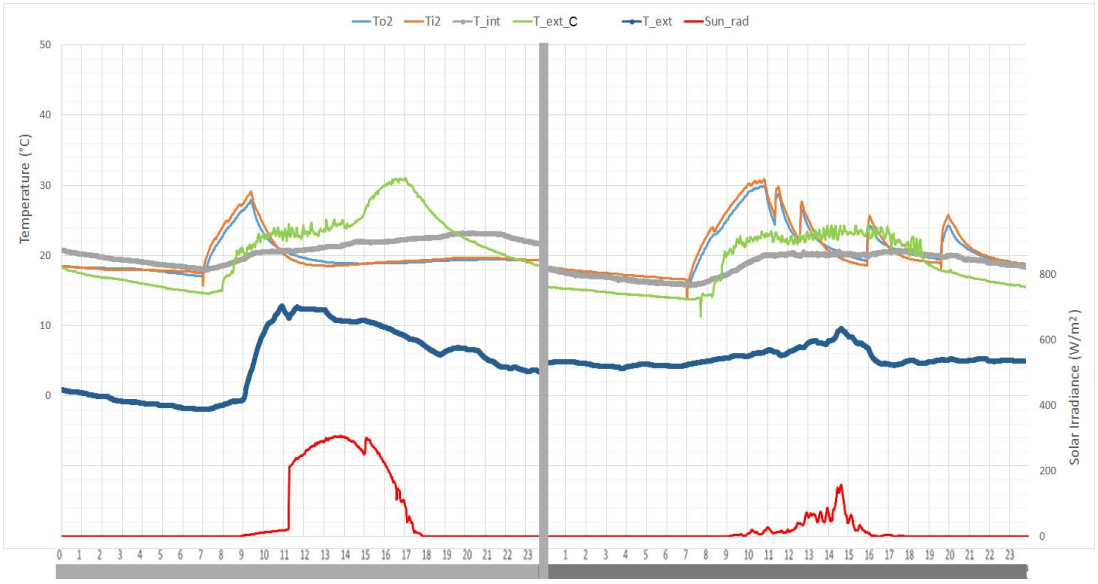

(**a**) (**b**)

Figure 8. Solar irradiance and indoor and outdoor temperatures—sample winter days (**a**) 09 January 2020 and (**b**) 14 January 2020.

Figure 9 presents a sample week of February, from 19 February 2020 to 25 February 2020. The minimum outdoor air temperature was 0 °C on 20 February 2020, and the maximum temperature was 21 °C on 24 February 2020. The indoor air temperature (T_int) in the office space maintained comfortable conditions operating in a free-floating temperature regime with zero energy consumption. The WFG circuit was never empty. During the free-floating regime, the mass flow rate was 0 and the heat pump was not in operation. Temperature in the corridor (T_ext_C) showed peak values above 32 °C in the afternoon. The solar irradiance on the west facade (Sun_rad) reached a peak of 480 W/m^2.

Figure 10 illustrates the performance on two consecutive February days. Although the minimum outdoor air temperature was 0 °C on 19 February 2020 and 20 February 2020, the peak solar radiation (440 W/m^2) increased the temperature inside the studied office in the afternoon. When the indoor air temperature reached 25 °C, the water inlet temperature dropped, and the outlet temperature was above the inlet. As stated in Table 3, the heat pump was set to operate in cooling mode when indoor temperature was above 25 °C. The heat pump cooled down water three times between 5:00 p.m. and 7:00 p.m. on 19 February 2020, and only once at 6:30 p.m. on 20 February 2020.

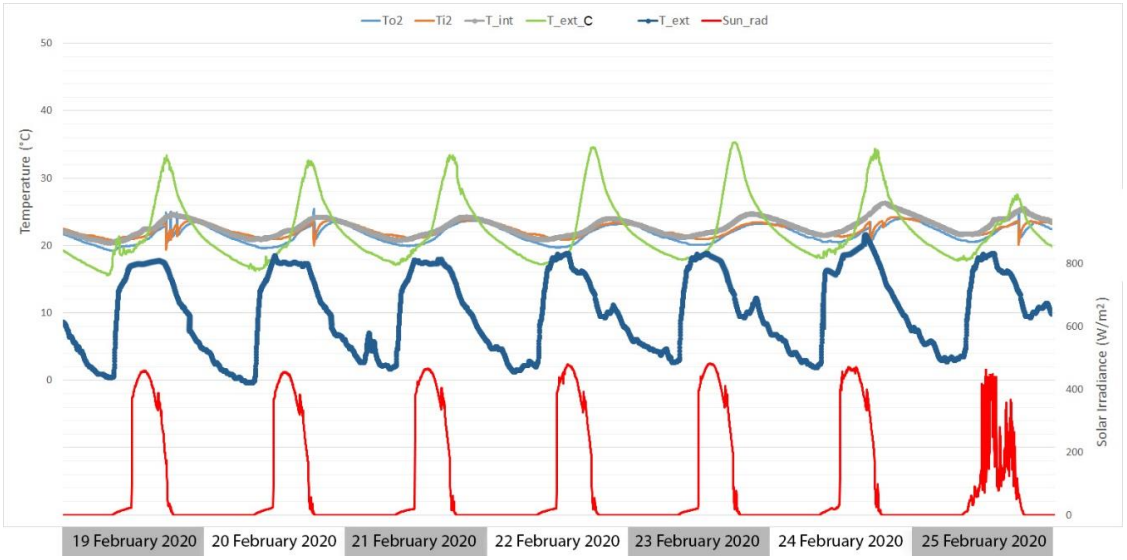

Figure 9. Solar irradiance and indoor and outdoor temperatures—sample week in February from 19 February 2020 to 25 February 2020.

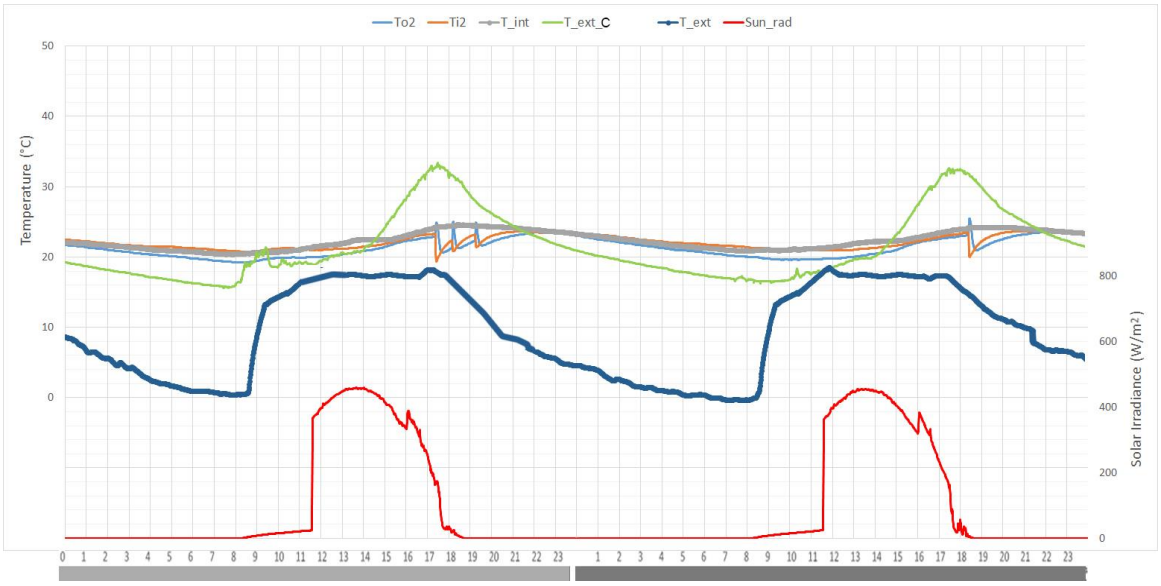

(**a**) (**b**)

Figure 10. Solar irradiance and indoor and outdoor temperatures—sample February days (**a**) 19 February 2020 and (**b**) 20 February 2020.

Table 6 shows a summary of the energy performance on four days in different seasons. On 10 July 2019, the system was working in cooling mode. The heat removed from the office space by the transparent WFG (*kWh_WFG*) and by the translucent partitions (*kWh_WFG_TP*) was 4.9 KWh. The transparent WFG absorbed the most significant amount of heat during the working hours because of the high mass flow rate ($\dot{m}$ = 2 L/min m^2), whereas the translucent interior partitions performed better during the night. The contribution of the air heat exchanger (*kWh_AXH*) during the night was negligible compared with the heat pump, which operated from 7:00 a.m. to 8:00 p.m.

Table 6. Thermal energy summary on four sample days.

Date	10 July 2019			09 January 2020			14 January 2020			20 February 2020		
hour	0–7	7–20	20–24	0–7	7–20	20–24	0–7	7–20	20–24	0–7	7–20	20–24
kWh_WFG [1]	−0.3	−4.3	−0.3	3.4	-	-	-	8.6	-	-	−2.3	-
kWhWFGTP [1]	−1.6	−2.0	−1.3	3.2	11.3	4.1	1.7	17.4	5.6	−2.5	−1.1	−1.2
kWh_HP [1]	-	−21	-	-	7.12	-	-	15.0	-	-	−0.6	-
kWh_AXH [1]	−0.7	-	-	-	-	-	-	-	-	−0.1	-	−0.3

[1] Energy values in kWh.

On 09 January 2020, the heat delivered by the translucent WFG (*KWh_WFG_TP*) was 18.7 kWh, whereas the total amount of energy delivered by the transparent WFG (*KWh_WFG*) was 3.4 kWh. In the afternoon, the transparent WFG circuit was stopped to allow solar radiation to enter the office space. The translucent WFG supplied most of the heat during the working hours. The thermal energy delivered by the heat pump (*kWh_HP*) was 7.12 kWh from 7:00 a.m. to 11:00 a.m. In the afternoon, the thermal inertia of the tank and the solar radiation made it unnecessary to operate the heat pump again. On 14 January 2020, the contribution of the transparent WFG was higher because there was little solar radiation in the afternoon. The heat pump operated over the working hours and released twice as much thermal energy as on 09 January 2020.

On 20 February 2020, the system was working in cooling mode. The air heat exchanger (*kW_AXH*) was cooling down the buffer tank during the night, and the heat pump operated during the working hours. The heat removed by the translucent WFG (*kWh_WFG_TP*) was 4.8 kWh. The energy delivered by the heat pump was 0.6 kWh, and the thermal inertia of the buffer tank was enough to keep indoor temperature between 20 and 26 °C. In Section 4.4, these conditions are assessed to evaluate the occupants' comfort.

4. Discussion

Radiant WFG panels were part of the heating and cooling system. They impact the indoor air temperature and help reduce the mean radiant temperature and, therefore, the operative temperature. The thermal problem of the glazing is coupled with the thermal problem of the room, and the indoor temperatures should be measured.

4.1. Validation of Energy Management System

The power released or absorbed by the water (P) is measured in watts per square meter (W/m^2), and is shown in Equation (1).

$$P = \dot{m}c(T_O - T_i), \quad (1)$$

where $\dot{m}$ is the mass flow rate (Kg/s m^2), c (J/Kg °C)is the specific heat of the water, and T_o and T_i are the temperatures of water leaving and entering the glazing, respectively (°C). The mass flow rate is the mass of a fluid passing by a point over time. In summer conditions, the transparent WFG was set to operate during working hours. It had to absorb most of the solar radiation impinging on the glazing. Figure 11 illustrates the buffer tank temperatures and the thermal energy provided by the heat pump in a sample summer week. The top tank temperature ($T_{\_tank\_top}$) showed that the heat pump was set to work when $T_{\_tank\_top}$ was between 15 and 18 °C. On 10 July 2019, it worked at three cycles per hour. The following days, it was fixed to operate at a minimum time between starts of forty minutes. Over the weekend, the heat pump did not operate, and the buffer tank temperature reached 35 °C. The maximum power delivered by the heat pump (31.13 kWh) took place on 11 July 2019, when the solar irradiance reached its maximum value without any obstructions, according to Figure 5.

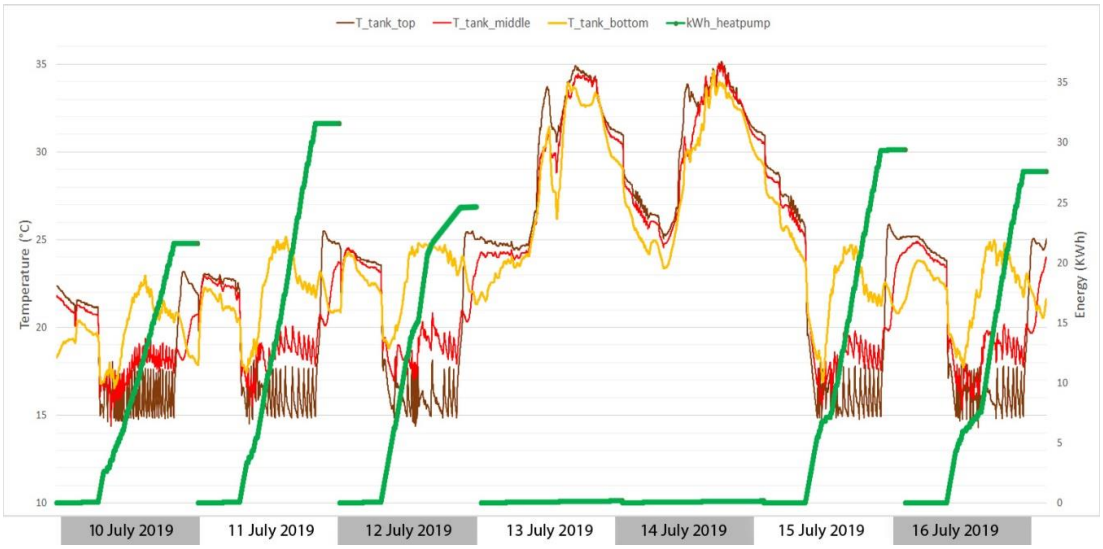

Figure 11. Tank temperatures and heat pump thermal power—sample summer week from 1 July 2019 to 16 July 2019.

When the heat pump was working in the heating mode in winter conditions, the transparent WFG was set to operate in the morning. It did not operate in the afternoon because the solar radiation on the south-west partition helped reduce the heating load. Figure 12 shows the tank temperatures (T_tank_top, T_tank_middle, T_tank_bottom) and the thermal consumption of the heat pump (*kWh_heatpump*) measured with the water flow rate and the difference of water temperature between the inlet and outlet in the heat pump. On sunny days, the heat pump operated mainly in the morning because the solar radiation heated up the office space in the afternoon. On 09 January 2020, when the outdoor air temperature ranged from −1 to 11 °C and a peak solar radiation of 300 W/m^2, the heat pump heated the buffer tank from 7:00 a.m. to 9:00 a.m. The thermal inertia of the tank and the solar radiation in the afternoon made it unnecessary to operate the heat pump again. The total energy consumption per day was 7.12 kWh. The average heat pump thermal energy was 7 kWh on 08 January 2020, 09 January 2020, and 10 January 2020, whereas on Monday 13 January 2020, a cloudy winter day after non-working days, the total energy consumption was 20.05 kWh. The warm-up response was too low, and it took four hours to raise the temperature to comfort conditions. Over the weekend, the tank temperature dropped, and this made it necessary to increase the energy supplied by the heat pump. The lack of solar radiation in the afternoon was the reason to operate the heat pump until the end of the working hours.

Figure 13 shows the tank temperatures (T_tank_top, T_tank_middle, T_tank_bottom) and the thermal consumption of the heat pump (*kWh_heatpump*) on six February days. The heat pump operated in cooling mode and cooled down the top tank temperature in the afternoon. On 21 February 2020 and 22 February 2020, the heat pump did not operate, and the buffer tank was in a free-floating regime. The average energy consumption per day was 1 kWh on working days. The difference between the heat pump consumption on 14 January 2020 (15 kWh) and on 20 February 2020 (1.1 kWh) can be explained because the peak solar radiation on 09 January 2020 was below 300 W/m^2, and the outdoor temperature was above 10 °C for four hours. On 20 February 2020, the peak solar radiation was 450 W/m^2, and the outdoor temperature was close to 18 °C for 7 h.

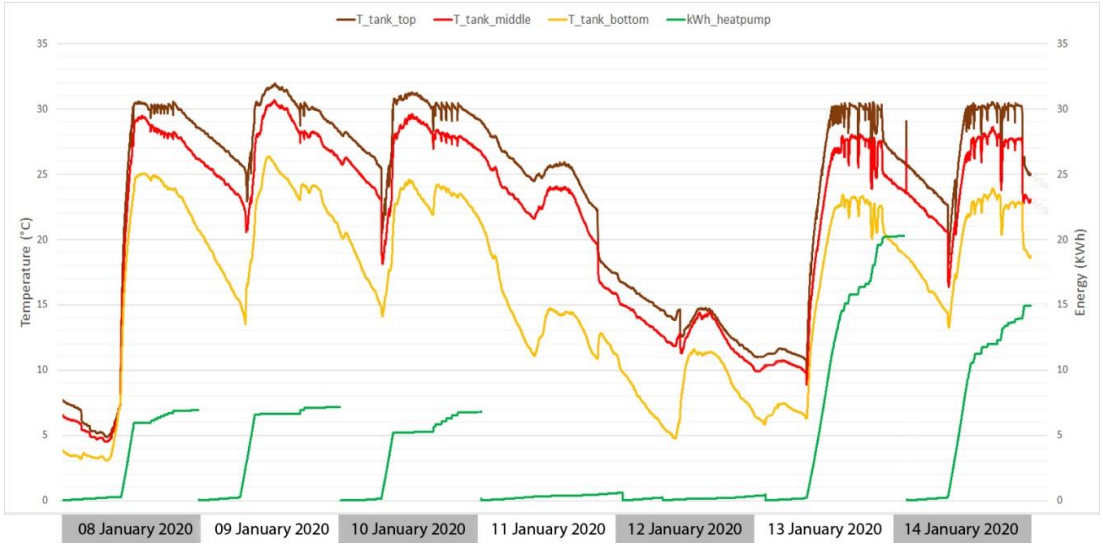

Figure 12. Tank temperatures and heat pump thermal power—sample winter week from 08 January 2020 to 14 January 2020.

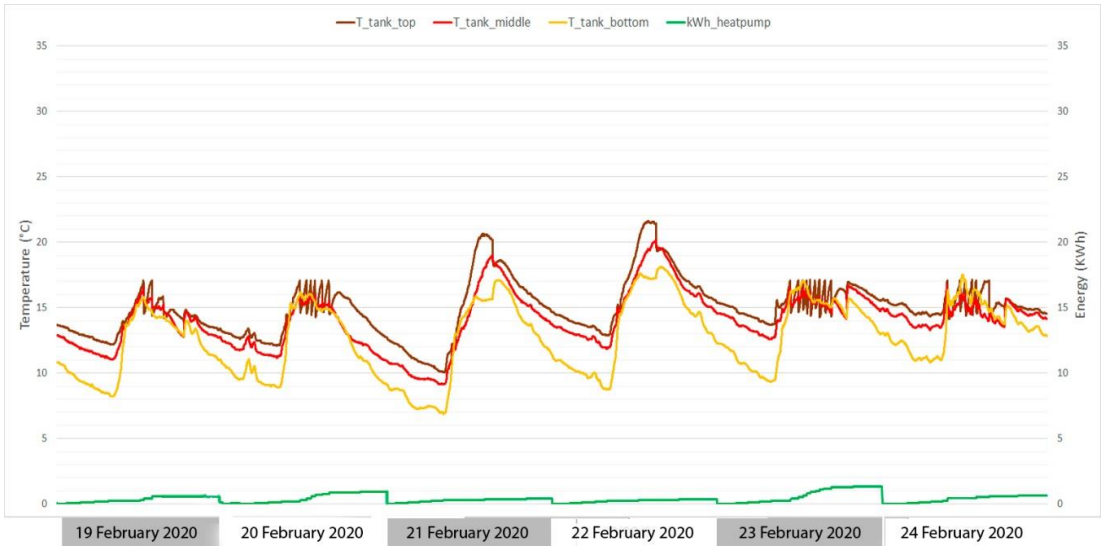

Figure 13. Tank temperatures and heat pump thermal power—ample February week from 19 February 2020 to 25 February 2020.

4.2. Estimation of Final Energy Consumption

Tables 7 and 8 show the estimated heating (positive) and cooling (negative) loads. Ventilation loads (*Vent*) were calculated with the number of occupants (*n*) at each hour. Internal loads (*IH*) are calculated with the number of occupants, the metabolic rate of typical office activity, and 20 W/m^2 for lighting and equipment. Solar radiation (*SR*) was taken from Figure 6a with a surface area of 7.8 m^2 and a solar heat gain coefficient of 0.5. The same procedure was repeated to calculate the values on five sample days.

Tables 9 and 10 compare the thermal energy consumption of the air-to-water heat pump with the calculated cooling and heating loads. The values are taken from Figures 11 and 12 (*kWh_heatpump*) and Tables 7 and 8 by adding the heating and cooling loads over the working hours.

Table 7. Summer cooling loads on 10 July 2019.

Hour	T_{int} (C)	T_{ext} (C) [1]	T_{ext_C} (C) [1]	n	$\sum UA(T_{int}-T_{ext})$ (Wh)	$\sum UA(T_{int}-T_{ext\_C})$ (Wh)	Vent (Wh)	IL (Wh)	SR (Wh)	Total (Wh)
7–8	23	18	24	0	−125.65	54.18	0	800	0	728.53
8–9	23	20	23.8	2	−75.39	43.34	−90	1000	0	877.95
9–10	23	21.5	23.7	2	−37.69	37.92	−45	1000	0	955.23
10–11	23	28	23.9	2	125.65	48.76	150	1000	0	1324.41
11–12	23	36	24	6	326.69	54.18	1170	1400	0	2950.87
12–13	23	38	24.2	6	376.95	65.01	1350	1400	0	3191.96
13–14	23	38.5	26	2	389.51	162.54	465	1000	510	2527.05
14–15	23	39.7	28	2	419.67	270.9	501	1000	521.2	2712.82
15–16	23	39.8	30	2	422.18	379.26	504	1000	510	2815.44
16–17	23	35	34	6	301.56	595.98	1080	1400	390	3767.54
17–18	23	32	33	6	226.17	541.8	810	1400	281.2	3259.22
18–19	23	31	34	2	201.04	595.98	240	1000	202.5	2239.52
19–20	23	29.5	32	2	163.34	487.62	195	1000	82.5	1928.45

[1] Values are taken from Figure 6.

Table 8. Winter heating loads on 14 January 2020.

Hour	T_{int} (C)	T_{ext} (C) [1]	T_{ext_C} (C) [1]	n	$\sum UA(T_{int}-T_{ext})$ (Wh)	$\sum UA(T_{int}-T_{ext\_C})$ (Wh)	Vent (Wh)	Total (Wh)
7–8 h	22	4	14	0	452.34	433.44	0	885.78
8–9 h	22	5	20	2	427.21	108.36	510	1045.57
9–10 h	22	6	22	2	402.08	0	480	882.08
10–11 h	22	7	23	2	376.95	−54.18	450	772.77
11–12 h	22	7	23	6	376.95	−54.18	1350	1672.77
12–13 h	22	8	24	6	351.82	−54.18	1260	1557.64
13–14 h	22	9	24	2	326.69	−54.18	390	662.51
14–15 h	22	10	24	2	301.56	−54.18	360	607.38
15–16 h	22	8	24	2	351.82	−54.18	420	717.64
16–17 h	22	4	24	6	452.34	−54.18	1620	2018.16
17–18 h	22	4	23	6	452.34	−54.18	1620	2018.16
18–19 h	22	5	21	2	427.21	54.18	510	991.39
19–20 h	22	5	18	2	427.21	216.72	510	1153.93

[1] Values are taken from Figure 8.

Table 9. Sample summer week energy consumption (kWh).

Date	10 July (kWh)	11 July (kWh)	12 July (kWh)	15 July (kWh)	16 July (kWh)	Total (kWh)
Cooling loads (WFG) [1]	21.60	31.13	23.90	29.40	27.6	133.63
Cooling loads (Aid-to-Air)	27.20	35.75	28.38	32.72	31.56	155.61

[1] Values are taken from Figure 11.

Table 10. Sample winter week energy consumption (kWh).

Date	08 January (kWh)	09 January (kWh)	10 January (kWh)	13 January (kWh)	14 January (kWh)	Total (kWh)
Heating loads (WFG) [1]	6.93	7.15	6.79	20.05	15.01	55.93
Heating loads (Ait-to-Air)	8.72	9.11	8.39	18.27	16.53	61.02

[1] Values are taken from Figure 12.

Final energy (FE) consumption, non-renewable final energy (NRFE) consumption, and the CO_2 emissions in kg are primary energy factors in calculating the energy performance of buildings, according to the Energy Performance of Buildings Directive (EPDB 2018) [39]. The Spanish regulation of building thermal systems (RITE) recommends a conversion factor between final energy (FE) and non-renewable

final energy (NRFE) of 1.954 [40]. The factor of emitted CO_2 for electricity is 0.331. The final energy consumption and CO_2 emissions were calculated with two different heat pumps. Table 11 illustrates the performance of the air-to-water heat pump in cooling and heating mode. The performance depends on the outlet temperature of the WFG (T_o = 15 °C in summer, T_o = 30 °C in winter) and the source inlet temperature in the heat pump ($T_{s,i}$ = 20–35 °C in summer, $T_{s,i}$ = 15–20 °C in winter). The outdoor temperature, T_ext, is shown in Figures 5 and 7, respectively. $T_{s,i}$ values were taken from the top tank temperatures (T_tank_top) shown in Figures 11 and 12. The air-to-water heat pump shows a better coefficient of performance (COP) when the water temperature is close to 35 °C and a better energy efficiency ratio (EER) when the water temperature is close to 18 °C. The top tank temperatures (T_tank_top) in Figures 11 and 12 confirmed the range of optimal operating temperatures. Although the actual heat pump electrical energy consumption has not been measured, the estimated COP and EER have been taken from [41].

Table 11. Final energy analysis. Air-to-water heat pump.

	Air-to-Water Heat Pump			
T_{ext_db} (°C)	Cooling 35 °C		Heating 7 °C	
$T_{s,i}$ (°C)	7 °C	18 °C	35 °C	45 °C
Energy consumption (kWh)	133.63	133.63	55.93	55.93
EER [1]/COP [2]	2.90 [1]	3.62 [1]	4.50 [2]	3.50 [2]
FE consumption (kWh)	46.08	36.91	12.43	15.98
NRFE consumption (kWh)	90.04	72.13	24.29	31.22
CO_2 emissions ($KgCO_2$)	15.25	12.22	4.11	5.29

[1] Energy efficiency ratio (EER)/[2] coefficient of performance (COP) values are taken from [41].

Air-to-air heat pumps were also analyzed using the cooling and heating loads from Tables 9 and 10. The parameters that influence air-to-air heat pump performance are the dry bulb exterior air temperature (T_ext_db) and the dry bulb interior return air temperature (T_{ri_db}). Table 12 shows the final energy (FE), non-renewable final energy (NRFE), and the emitted CO_2 for electricity of the air-to-air heat pump.

Table 12. Final energy analysis—air-to-air heat pump.

	Air-to-Air Heat Pump	
T_{ri_db} (°C)	Cooling 23 °C	Heating 22 °C
T_{ext_db} (°C)	35 °C	7 °C
Energy consumption (kWh)	155.61	61.02
EER [1]/COP [2]	3.25 [1]	3.72 [2]
FE consumption (kWh)	47.88	16.40
NRFE consumption (kWh)	93.56	32.05
CO_2 emissions ($KgCO_2$)	15.85	5.43

[1, 2] EER/COP values are taken from [41].

The radiant WFG panel system coupled with a buffer tank and air-to-water heat pump showed non-renewable final energy (NRFE) consumption of 72.13 kWh in cooling mode and 24.29 kWh in heating mode, whereas the expected values of an air-to-air system were 93.56 kWh and 32.05 kWh in the studied summer and winter weeks. This resulted in a final energy savings of 23% in summer and 24% in winter. The reductions of CO_2 emissions were 3.63 kg/week in summer and 1.32 kg/week in winter. As stated in Section 2.1, the ventilation device was not a component of the energy management system, and its performance was not controlled. The ventilation load was estimated by multiplying the air flow by the specific enthalpy (kJ/kg) difference between indoor and outdoor conditions. In summer, the specific enthalpy of outdoor air at 31.3 °C with 35% relative humidity was 58.8 kJ/kg. At 26 °C and 36% relative humidity, the indoor air specific enthalpy was 46.7 kJ/kg. At a ventilation air flow rate of

75 L per second, the total ventilation cooling load over 12 h was 10.8 kWh. In winter, the indoor and outdoor specific enthalpy were 37.11 kJ/kg and 16.36 kJ/kg, respectively, and the ventilation load over the working hours was 13.24 kWh. The electrical consumption of the ventilation device, including the engine and the fan, was 3.24 kWh [42].

The non-renewable energy consumption was 72 kWh in a summer week and 24 kWh in a winter week. The expected energy consumption projection throughout the year was 1700 kWh with a floor area of 40 m^2. Therefore, the yearly heating and cooling energy consumption per m^2 was 42.5 kWh/m^2 per year. If the average energy savings compared to an air-to-air heat pump with multi-split were 23%, the total non renewable energy consumption (NREC) savings accounted for 391 kWh/year. The average price of electricity in Spain is 0.12 EUR/kWh [22], and the system overcosts compared to traditional indoor wall partitions plus the split system can be 50 EUR/m^2. For 24 m^2 of radiant WFG panels, the expected payback period would be 20 years. WFG technology is not competitive nowadays, so future research is needed in industrialization and standardization to bring down the initial costs.

4.3. Mean Radiant and Operative Temperatures

Mean radiant temperature (MRT) expresses the influence of surface temperatures in the room on occupant comfort. The area-weighted method shown in Equation (2) is a simple way to calculate MRT, but it does not reflect the geometric position, posture, and orientation of the occupant, ceiling height, or radiant asymmetry [29]. In Equation (3), the calculation of mean radiant temperature from surrounding surfaces considers the surface temperatures of the surrounding elements and the angle factor. The angle factor is a function of shape, size, and the position concerning the occupant standing or being seated. The surfaces of the room are assumed as black, with high emissivity and no reflection. In this case, the angle factors weight the enclosing surface temperatures to the fourth power [28].

$$T_{mr} = \frac{T_1A_1 + T_2A_2 + \ldots + T_NA_N}{A_1 + A_2 + \ldots + A_N}, \quad (2)$$

$$\overline{T}^4_{mr} = T^4_1F_{p-1} + T^4_2F_{p-2} + \ldots + T^4_NF_{p-N}, \quad (3)$$

where

T_{mr} = mean radiant temperature, °C,
T_N = surface temperature of surface N, °C (calculated or measured),
A_N = area of surface,
$F_{p\text{-}N}$ = is the angle factor between the person and surface N.

The angle factors quantify the amount of radiation energy that leaves the human body and reaches each surface. They were calculated according to Figures B.2 to B.5 in [28]. If the difference between the indoor surface temperatures is relatively small (<10 °C), Equation (4) can be used.

$$\overline{T}_{mr} = T_1F_{p-1} + T_2F_{p-2} + \ldots + T_NF_{p-N} \quad (4)$$

The MRT is calculated as the average value of the surrounding temperatures weighted according to the angle factors. If the temperature difference between indoor surfaces is below 10 °C, then the MRT error calculated with Equation (4) will be less than 0.2 °C [28]. Equation (5) shows the formula to calculate the angle factor [43].

$$F_{p-N} = F_{max}\left(1 - e^{-(a/c)\tau}\right)\left(1 - e^{-(b/c)\gamma}\right), \quad (5)$$

where

γ = A+$B(a/c)$,
τ = C+$D(b/c)$ + $E(a/c)$.

Parameters *a*, *b*, and *c*, defined in Figure 14, are related to dimensions and distances between the occupant and the envelope. Table 13 shows the parameters *A*, *B*, *C*, and *D* to calculate angle factors for seated persons and walls, floors, and ceilings.

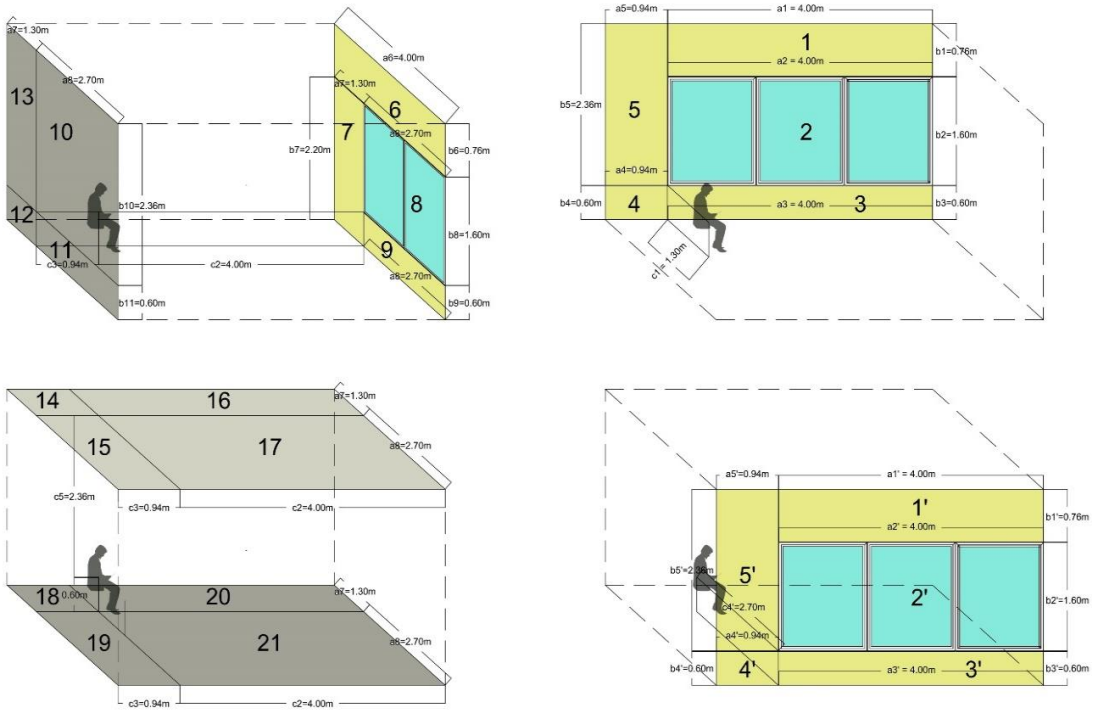

Figure 14. Geometry of the office space and occupant's position and dimensions to calculate the angle factor.

Table 13. Parameters for calculating angle factors [1].

	F_{max}	*A*	*B*	*C*	*D*	*E*
Seated person (Wall/window facing person)	0.118	1.216	0.169	0.717	0.087	0.052
Seated person (Floor/ceiling facing person)	0.116	1.396	0.130	0.951	0.080	0.055

[1] Values are taken from [28].

Figure 14 illustrates the dimensions and geometry of the office space and the different surfaces considered to calculate the MRT for a seated person. The facing direction was ignored for simplification. The temperature of each rectangle (1 to 21) was measured to calculate the MRT. Due to small differences, only five temperatures have been taken into account. $T_1 = T_6 = T_{1'} = T_{14} = T_{15} = T_{16} = T_{17} = T_{ceiling}$; $T_3 = T_{3'} = T_4 = T_{4'} = T_9 = T_{11} = T_{12} = T_{18} = T_{19} = T_{20} = T_{21} = T_{floor}$; $T_7 = T_5 = T_{5'} = T_{wall;}$ $T_8 = T_{WFG}$; $T_2 = T_{2'} = T_{WFG\_TP}$.

A rough approximation to obtain the operative temperature may be to use the arithmetic average of the mean radiant temperature (MRT) of the heated space and dry-bulb air temperature if air velocity is less than 0.2 m/s and MRT is less than 50 °C. In cases where the air velocity is between 0.2 and 1 m/s, or where the difference between mean radiant and air temperature is above 4 °C, the ASHRAE 55 provides a formula, shown in Equation (6), to calculate operative temperature [27].

$$T_{op} = A\,T_a + (1 - A)\,T_{mr}\,, \tag{6}$$

where

T_{op} = operative temperature (°C),

T_a = indoor air temperature (°C), and
T_{mr} = mean radiant temperature (°C).

The value of A can be found in Table 14 as a function of the relative air speed, v_r.

Table 14. Parameters of WFG.

vr	<0.2 m/s	0.2 to 0.6 m/s	>0.6 m/s
A	0.5	0.6	0.7

Figure 15 illustrates the indoor relative humidity (*RH*), the surface temperature of indoor surfaces, and the MRT calculated according to Equation (4). The WFG panel temperatures (T_{WFG}, $T_{WFG\text{-}TP}$) contribute to cooling the mean radiant temperature down to 20 °C when the energy management system is in operation. T_{WFG} was lower than $T_{WFG\text{-}TP}$ because the mass flow rate through the transparent panels was set to $\dot{m}$ = 2 L/min m^2, and through the translucent interior partitions, it was $\dot{m}$ = 1 L/min m^2. Another reason to explain the temperature difference was that each transparent WFG has its circulating device, whereas the translucent panels share the same circulating device. The former has proven to be more effective in delivering the cold from the heat pump than the latter. Floor, opaque walls, and ceiling temperatures (T_{floor}, T_{wall}, $T_{ceiling}$) are taken into account with their angle factors, which are calculated according to Equation (5).

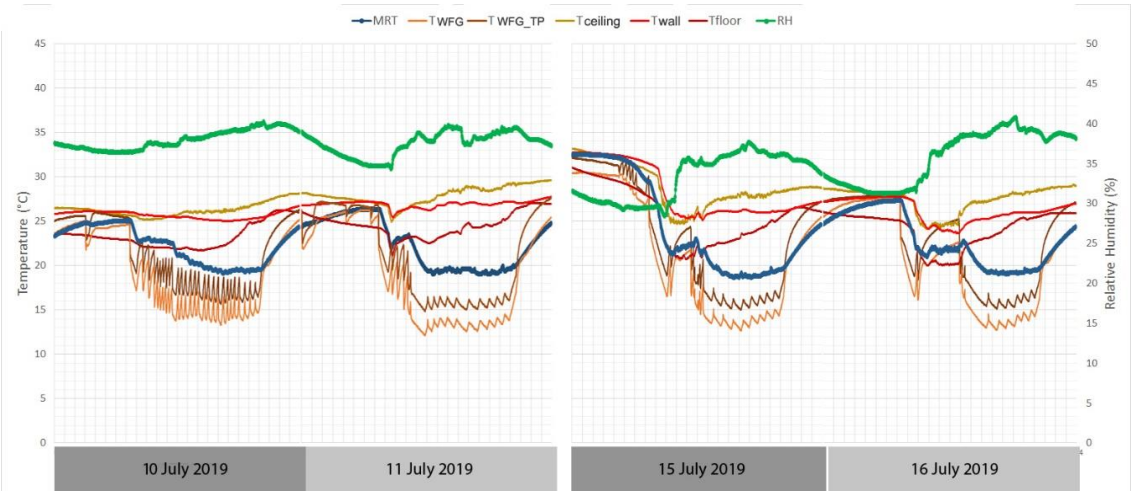

Figure 15. Surface temperatures of indoor surfaces, mean radiant temperature (*MRT*), and indoor relative humidity (*RH*)—sample days 10 July 2019 to 11 July 2019 and 15 July 2019 to 16 July 2019.

4.4. Predicted Mean Vote (PMV)

The Predicted Mean Vote (PMV) model uses six key factors to address thermal comfort: metabolic rate, clothing insulation, air temperature, radiant temperature, airspeed, and humidity. These factors may vary with time; however, in this article, the airspeed, metabolic rate, and clothing insulation are considered steady. Compliance with the ASHRAE-55 standard is tested using the CBE Thermal Comfort Tool. This tool, developed at the University of California at Berkeley, allows designers to calculate thermal comfort according to ASHRAE Standard 55-2017. The indoor air temperature and the MRT were taken from Figure 15 during operating hours. Clothing was set as 0.8 Clo (typical office indoor clothing); the metabolic rate was set as 1 Met (sedentary activity), the relative humidity was taken from Figure 14, and air velocity was set as 0.10 m/s (mean air velocity of the day). The ASHRAE-55 Comfort Zone, shaded in gray in Figure 16, represents the recommended predicted mean vote, between −0.5 and +0.5, for buildings where the occupants have metabolic rates of between 1.0 met and 1.3 met, and clothing provides between 0.5 clo and 1.0 clo of thermal insulation. Figure 16 illustrates the

variations of the predicted mean vote (PMV), mean radiant temperature (MRT), indoor air temperature ($T_{\_int}$), and operative temperature (T_{op}) on four summer days. The PMV over the working hours ranged from −0.04 to −0.42 on 10/07/2019, while the MRT ranged from 23.0 to 19.3 °C, and the indoor air temperature ranged from 25.2 to 27.4 °C. During the working hours, the highest indoor temperature was on 11 July 2019 at 8:00 p.m., when the MRT was 20.1 °C and the predicted mean vote was 0.1, very close to the optimum value. Similar values are shown over the four days.

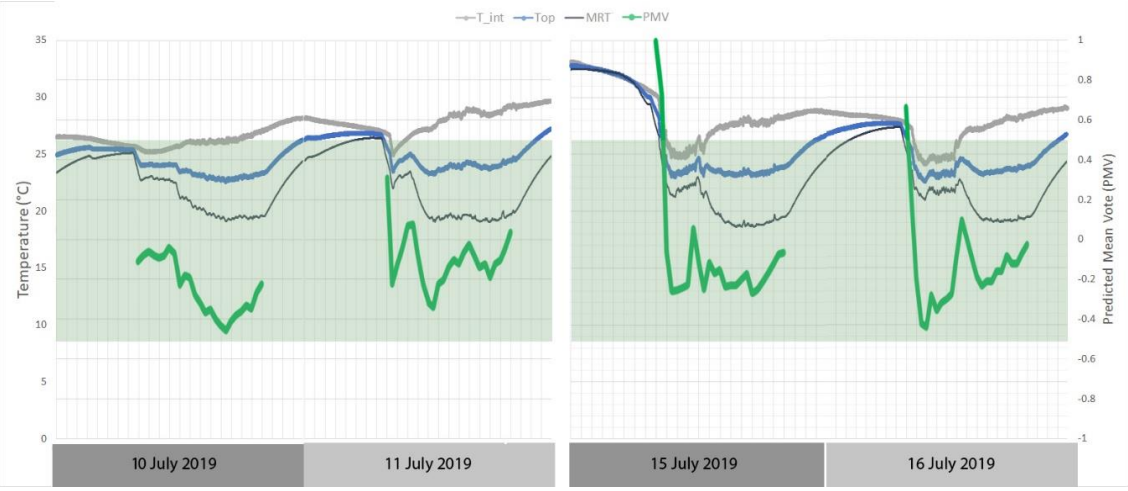

Figure 16. Operative temperature (T_{op}) and Predicted Mean Vote (*PMV*) in summer—sample days 10 July 2019 to 11 July 2019 and 15 July 2019 to 16 July 2019.

The comfort zone is defined by the combinations of the six key factors for thermal comfort. The PMV model is calculated with the air temperature and mean radiant temperature in question along with the applicable metabolic rate, clothing insulation, airspeed, and humidity. If the resulting PMV value generated by the model is within the recommended range, the conditions are within the comfort zone. Table 15 defines the PMV range for the thermal sensation scale. For 1.1% of the working hours, the PMV was above +0.4; for 6.7%, the PMV was from 0 to +0.2; for 32.3%, the PMV was from 0 to −0.2; for 54.3%, the PMV was from −0.2 to −0.4; and for 5.6% of the time, the PMV was below −0.4. Despite the high indoor air temperature, the PMV showed that occupants would describe their comfort conditions as "Slightly Cool" and always within the recommended limits specified by ASHRAE-55 (−0.5 < PMV < +0.5). The transparent WFG provided the partition exposed to solar radiation with a temperature that prevented thermal asymmetry and a lack of comfort. Hence, the results in Figure 15 indicated that the system gave consistent performance and provided comfortable conditions.

Table 15. ASHRAE thermal comfort scale [1].

Cold	Cool	Slightly Cool	Neutral	Slightly Warm	Warm	Hot
−3	−2	−1	0	+1	+2	+3

[1] Values are taken from [27].

The same comfort analysis was carried out in February. Figure 17 illustrates the variations of the predicted mean vote (PMV), mean radiant temperature (MRT), indoor air temperature ($T_{\_int}$) and operative temperature (T_{op}), and relative humidity (RH) on four February days. As shown in Figure 9, the conditions on sunny winter days are required to operate the heat pump in cooling mode in the afternoon. The indoor air temperature dropped to 20.5 °C on 19 February 2020 at 8:00 a.m., and reached 27 °C on 24 February 2020 at 7:00 p.m. The relative humidity ranged from 35% to 40%. The PMV over the working hours ranged from −1 on 19 February 2020 to 0.8 on 24 February 2020. Both values are out of the comfort range. In the morning, the PMV on the four days was below −0.5, so the occupants

would describe their comfort conditions as "Slightly Cool" or "Cool". The heat pump was set to operate in heating mode when the indoor temperature was below 20 °C, and that condition was not met. On 24 February 2020, the PMV was above 0.5 from 5:00 p.m. to 8:00 p.m. Even though the heat pump was operating in cooling mode, the occupants would describe their comfort conditions as "Slightly Warm" or "Warm". For 45% of the working hours, the predicted mean vote was below −0.5, out of the shaded area representing the recommended comfort range. For 8% of the working hours, the predicted mean vote was above the comfort range when the indoor temperature surpassed 25.5 °C, and the WFG temperature was not low enough to bring down the mean radiant temperature.

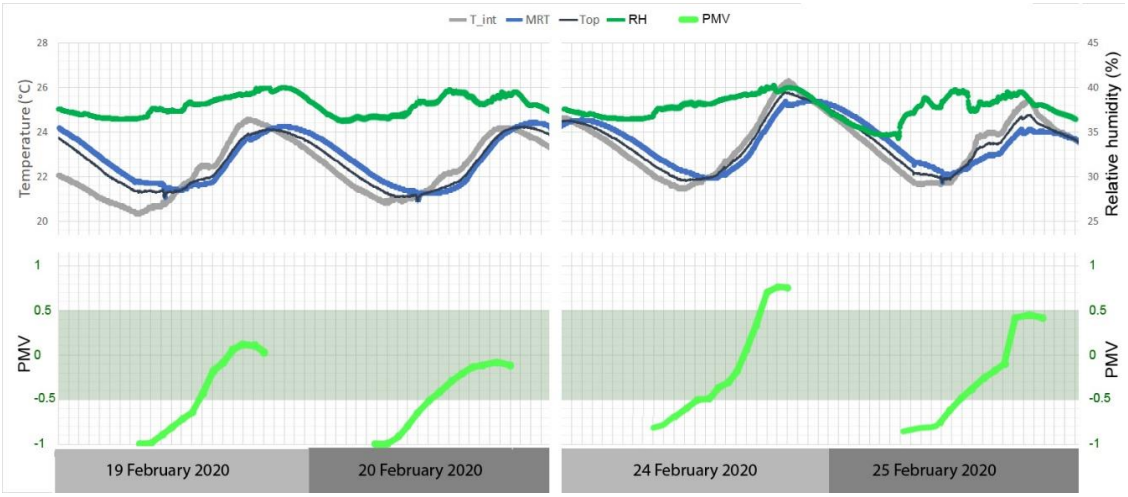

Figure 17. Operative temperature (T_{op}), Predicted Mean Vote (*PMV*), and indoor relative humidity (*RH*) in winter—sample days 19 February 2020 to 20 February 2020 and 24 February 2020 to 25 February 2020.

5. Conclusions

This paper has studied the energy performance of innovative building envelopes (facade and internal partitions), such as water flow glazing (WFG), coupled with an energy management system, as well as the relationships with steady and transient parameters. The energy strategies varied from a free-floating temperature regime on sunny winter days to the air-to-water heat pump, air heat exchanger, and buffer tank in summer conditions. A simple logic energy management system received inputs from temperature and relative humidity sensors. It controlled the heat pump and the air heat exchanger to deliver heat or cold to the buffer tank. The results included actual indoor air and glazing temperatures, heating and cooling energy consumption, and the influence of WFG in the mean radiant temperature and comfort.

Water-Flow Glazing was evaluated as a component of a hydronic radiant heating and cooling system. It showed final energy-saving potential, provided thermal comfort, and may be considered a valid option for office retrofitting. On the hottest day of the year, when the temperature ranged from 18 to 40 °C and the peak solar radiation was above 700 W/m^2, the energy system consumed 32 kWh (0.8 kWh/m^2) and the WFG managed to keep the indoor air temperature between 25 and 27 °C. The contribution of the air heat exchanger was negligible over the year because it was set to work for cooling only when the difference between the tank top temperature and outdoor temperature ($T_{\_tank\_top} - T_{\_ext}$) was above 10 °C. It complicated the piping and the control logic and did not improve the energy performance.

Radiant panels improve the performance of air-to-water heat pumps. The energy efficiency ratio (EER) reached 3.62 when the water temperature was 18 °C, and the coefficient of performance (COP) was 4.5 when the water temperature was 35 °C in heating mode. Using WFG as a radiant cooling facade and indoor partitions effectively reduced the operative temperature to comfortable levels when the indoor air temperature was between 25 and 27.5 °C.

The Predicted Mean Vote (PMV) in summer conditions was between 0 and −0.5 in working hours, within the recommended values of ASHRAE-55 standard. The MRT ranged from 19.3 to 23 °C, and the indoor air temperature ranged from 25.2 to 29.1 °C. In winter conditions, the electronic control unit was set to operate in heating mode if the indoor air temperature was below 20 °C. Then, for 45% of the working hours, the predicted mean vote was below −0.5, out of the comfort range, so the occupants would describe their comfort conditions as "Slightly Cool" or "Cool". The control unit logic should be fixed to start operating the heating mode if the indoor temperature drops below 21 °C. On mild sunny winter days, when the outdoor temperature reached 17 °C in the afternoon, the heat pump cooled down the buffer tank, but the WFG failed to deliver enough cooling power. The predicted mean vote was above 0.5, and the conditions could be described as "Warm" and out of the comfort range for more than three hours. There were two conditions to activate WFG in the cooling mode; first, indoor air temperature should be above 25 °C, and second, the difference between indoor air temperature and the bottom tank temperature should be more than 10 °C.

Water-Flow Glazing was evaluated as a component of a hydronic radiant heating and cooling system. It showed final energy-saving potential, provided thermal comfort, and may be considered a valid option for office retrofitting. The system is limited by its high initial cost and the need for an energy management system integrated with the rest of the equipment, especially the ventilation system and the heat pump. The ventilation system is an essential aspect of comfort. Controlling the relative humidity is indispensable in radiant systems to avoid condensation issues. Therefore, a more advanced ventilation device could help optimize the whole system's performance. Including a heat recovery and variable airflow would reduce the sensible and latent thermal loads and control the dew point temperature. There were uncertainties with the air-to-water heat pump operation. Although the radiant WFG panels could improve the heat pump COP and EER, there were issues with the operating cycles that could affect its performance. The selected heat pump was oversized, and frequently started and stopped because it prematurely detected that it had reached the target temperature.

After the first year of monitoring, there are uncertainties, misfunctions, and system issues that must be addressed. Firstly, due to the complexity of the elements involved in human comfort, the control unit must integrate the ventilation device. The operation logic should be able to modify the water mass flow rate and ventilation air heat flow. Secondly, the devices must be adequately dimensioned to avoid misfunctions, especially the air-to-water heat pump. Further research must include heat pump electricity monitoring to compare the actual thermal and electricity consumption and assess energy performance more accurately. Finally, further research on the standardization of its manufacturing process and deployment is needed to bring down initial costs and payback periods. Another research line would be to integrate WFG into commercial building performance simulations.

Author Contributions: Conceptualization, B.M.S., F.d.A.G., and J.A.H.R.; methodology, B.M.S. and F.d.A.G.; software, J.A.H.R.; formal analysis, B.M.S. and F.d.A.G.; data curation, J.A.H.R.; writing—original draft preparation, J.A.H.R.; writing—review and editing, F.d.A.G. and B.L.A.; visualization, B.M.S., F.d.A.G., and B.L.A.; supervision, J.A.H.R. and B.L.A.; project administration, B.M.S.; funding acquisition, F.d.A.G. All authors have read and agreed to the published version of the manuscript.

Funding: This article has been funded by the KSC Faculty Development Grant (Keene State College, New Hamshire, USA).

Acknowledgments: This work was supported by program Horizon 2020-EU.3.3.1: Reducing energy consumption and carbon footprint by smart and sustainable use, project Ref. 680441 InDeWaG: Industrialized Development of Water Flow Glazing Systems.

Conflicts of Interest: The authors declare that they have no conflict of interest.

References

1. Kamilaris, A.; Kalluri, B.; Kondepudi, S.; Kwok Wai, T. A literature survey on measuring energy usage for miscellaneous electric loads in offices and commercial buildings. *Renew. Sustain. Energy Rev.* **2014**, *34*, 536–550. [CrossRef]
2. Balaras, C.A.; Droutsa, K.; Argiriou, A.A.; Asimakopoulos, D.N. Potential for energy conservation in apartment building. *Energy Build.* **2000**, *31*, 143–154. [CrossRef]
3. Del Ama Gonzalo, F.; Ferrandiz, J.; Fonseca, D.; Hernandez, J.A. Non-intrusive electric power monitoring system in multi-purpose educational buildings. *Int. J. Power Electron. Drive Syst.* **2019**, *9*, 51–62. [CrossRef]
4. Menezes, A.C.; Cripps, A.; Buswellb, R.A.; Wright, J.; Bouchlaghem, D. Estimating the energy consumption and power demand of small power equipment in office buildings. *Energy Build.* **2014**, *75*, 199–209. [CrossRef]
5. Europe 2020 Indicators—Climate Change and Energy. Available online: http://ec.europa.eu/ (accessed on 15 June 2020).
6. Andreou, A.; Barrett, J.; Taylor, P.G.; Brockway, P.E.; Wadud, Z. Decomposing the drivers of residential space cooling energy consumption in EU-28 countries using a panel data approach. *Energy Built Environ.* **2020**, *1*, 432–442. [CrossRef]
7. Bae, W.-B.; Mun, S.-H.; Huh, J.-H. Real-Time Occupant Based Plug-in Device Control Using ICT in Office Buildings. *Energies* **2016**, *9*, 143. [CrossRef]
8. Masoso, O.T.; Grobler, L.J. The dark side of occupants' behaviour on building energy use. *Energy Build.* **2010**, *42*, 173–177. [CrossRef]
9. Muhammad, W.; Monjur, M.; David, M.; Mario, S.; Yacine, R. Building energy metering and environmental monitoring. A state-of-the-art review and directions for future research. *Energy Build.* **2016**, *120*, 85–102. [CrossRef]
10. Komor, P. Space cooling demands from office plug loads. *Ashrae J.* **1997**, *39*, 41–44.
11. BRECSU. *Energy Consumption Guide 19: Energy Use in Offices*; Building Research Energy Conservation Support Unit: Watford, UK, 2000.
12. Dunn, G.; Knight, I. Small power equipment loads in UK office environments. *Energy Build.* **2005**, *37*, 87–91. [CrossRef]
13. Izquierdo, M.; Moreno-Rodríguez, A.; González-Gil, A.; García-Hernando, N. Air conditioning in the region of Madrid, Spain: An approach to electricity consumption, economics and CO_2 emissions. *Energy* **2011**, *36*, 1630–1639. [CrossRef]
14. Menezes, A.C.; Cripps ABuswell, R.A.; Bouchlaghem, D. Benchmarking small power energy consumption in office buildings in the United Kingdom: A review of data published in CIBSE Guide F. *Build. Serv. Eng. Res. Technol.* **2013**, *34*, 73–86. [CrossRef]
15. Pezzutto, S.; Fazeli, R.; De Felice, M.; Sparber, W. Future development of the air-conditioning market in Europe: An outlook until 2020. *Wiley Interdiscip. Rev. Energy Environ.* **2016**, *5*, 649–669. [CrossRef]
16. Lanzisera, S.; Dawson-Haggertym, S.; Cheung, H.; Taneja, J.; Culler, D.; Brown, R. Methods for detailed energy data collection of miscellaneous and electronic loads in a commercial office building. *Build. Environ.* **2013**, *65*, 170–177. [CrossRef]
17. Pezzutto, S.; De Felice, M.; Fazeli, R.; Kranzl, L.; Zambotti, S. Status quo of the air-conditioning market in Europe: Assessment of the building stock. *Energies* **2017**, *10*, 1253. [CrossRef]
18. Li, D.H.W.; Wong, S.L.; Tsang CLCheung, G.H.W. A study of the daylighting performance and energy use in heavily obstructed residential buildings via computer simulation techniques. *Energy Build.* **2006**, *38*, 1343–1348. [CrossRef]
19. Hermanns, M.; del Ama, F.; Hernández, J.A. Analytical solution to the one-dimensional non-uniform absorption of solar radiation in uncoated and coated single glass panes. *Energy Build.* **2012**, *47*, 561–571. [CrossRef]
20. Taleghani, M.; Kleerekoper, L.; Tenpierik, M.; van den Dobbelsteen, A. Outdoor thermal comfort within five different urban forms in the Netherlans. *Build. Environ.* **2015**, *83*, 65–78. [CrossRef]
21. Tullie Circle, N.E. (Ed.) *Ashrae Handbook-Heating, Ventilating, and Air-Conditioning Systems and Equipment*; ASHRAE: Atlanta, GA, USA, 2012; Available online: https://app.knovel.com/web/toc.v/cid:kpASHRAEA2/viewerType:toc/ (accessed on 15 June 2020).

22. Europe 2020 Indicators—Electricity Price Statistics. Available online: https://ec.europa.eu/eurostat/statistics-explained/index.php?title=Electricity_price_statistics (accessed on 15 August 2020).
23. Mikulik, J. Energy Demand Patterns in an Office Building: A Case Study in Kraków (Southern Poland). *Sustainability* **2018**, *10*, 2901. [CrossRef]
24. Lee, S.H.; Jeon, Y.; Chung, H.J.; Cho, W.; Kim, Y. Simulation-based optimization of heating and cooling seasonal performances of an air-to-air heat pump considering operating and design parameters using genetic algorithm. *Appl. Therm. Eng.* **2018**, *144*, 362–370. [CrossRef]
25. Priarone, A.; Silenzi, F.; Fossa, M. Modelling Heat Pumps with Variable EER and COP in EnergyPlus: A Case Study Applied to Ground Source and Heat Recovery Heat Pump Systems. *Energies* **2020**, *13*, 794. [CrossRef]
26. Fanger, P.O. *Thermal Comfort, Analysis and Application in Environmental Engineering*; Danish Technical Press: Copenhagen, Denmark, 1970.
27. ASHRAE-55. *ANSI/ASHRAE Standard 55-2017: Thermal Environmental Conditions for Human Occupancy*; ASHRAE: Atlanta, GA, USA, 2017.
28. ISO 7730:2005. *Ergonomics of the Thermal Environment-Analytical Determination and Interpretation of Thermal Comfort Using Calculation of the PMV and PPD Indices and Local Thermal Comfort Criteria*; International Organization for Standardization (ISO): Geneva, Switzerland, 2005.
29. Marino, C.; Nucara, A.; Pietrafesa, M. Mapping of the indoor comfort conditions considering the effect of solar radiation. *Sol. Energy* **2015**, *113*, 63–77. [CrossRef]
30. Godbole, S. *Investigating the relationship between Mean Radiant Temperature (MRT) and Predicted Mean Vote (PMV)*; A case study in a university building; School of Architecture and the Built Environment: Stockholm, Sweden, 2018.
31. Chow, T.; Chunying, L.; Zhang, L. Thermal characteristics of water-flow double-pane window. *Int. J. Therm. Sci.* **2011**, *50*, 140–148. [CrossRef]
32. Gueymard, C.; duPont, W. Spectral effects on the transmittance, solar heat gain, and performance rating of glazing systems. *Sol. Energy* **2009**, *83*, 940–953. [CrossRef]
33. Chow, T.T.; Li, C. Liquid-filled solar glazing design for buoyant water-flow. *Build. Environ.* **2013**, *60*, 45–55. [CrossRef]
34. Gil-Lopez, T.; Gimenez-Molina, C. Environmental, economic and energy analysis of double glazing with a circulating water chamber in residential buildings. *Appl. Energy* **2013**, *101*, 572–581. [CrossRef]
35. Gutai, M.; Kheybari, A.G. Energy consumption of water-filled glass (WFG) hybrid building envelope. *Energy Build.* **2020**, *218*, 110050. [CrossRef]
36. Moreno Santamaria, B.; del Ama Gonzalo, F.; Pinette, D.; Gonzalez-Lezcano, R.-A.; Lauret Aguirregabiria, B.; Hernandez Ramos, J.A. Application and Validation of a Dynamic Energy Simulation Tool: A Case Study with Water Flow Glazing Envelope. *Energies* **2020**, *13*, 3203. [CrossRef]
37. Moreno Santamaria, B.; del Ama Gonzalo, F.; Lauret Aguirregabiria, B.; Hernandez Ramos, J.A. Experimental Validation of Water Flow Glazing: Transient Response in Real Test Rooms. *Sustainability* **2020**, *12*, 5734. [CrossRef]
38. Spanish Ministry of Development. BasicDocument on Energy Saving of the Technical Building Code (Documento Básico de Ahorro de Energía del Código Técnico de la Edificación, CTE-DB-HE). 2019. Available online: https://www.codigotecnico.org/images/stories/pdf/ahorroEnergia/DBHE.pdf (accessed on 16 August 2020).
39. European Union. Directive (EU) 2018/844 of the European Parliament and of the Council of 30 May 2018. Amending Directive 2010/31/EU on the Energy Performance of Buildings and Directive 2012/27/EU on Energy Efficiency. 2018. Available online: https://eur-lex.europa.eu/legal-content/EN/TXT/PDF/?uri=CELEX:32018L0844&from=EN (accessed on 16 August 2020).
40. Spanish Regulation of Thermal Installations in Buildings (RITE). Factores de Emisión de CO_2 y Coeficientes de Paso a Energía Primaria de Diferentes Fuentes de Energía Final Consumidas en el Sector de Edificios en España. Agencia Estatal Boletín Oficial del Estado: Madrid, Spain. 2016. Available online: https://energia.gob.es/desarrollo/EficienciaEnergetica/RITE/Reconocidos/Reconocidos/Otros%20documentos/Factores_emision_CO2.pdf (accessed on 16 August 2020).
41. Saunier Duval. Manuel d'installation. Available online: https://www.saunierduval.fr/france/download/genia-air-1/genia-air-2/saunier-duval-genia-air-6-8-12-15-unite-exterieure-notice-installation-0020117808-03-12-2012-291831.pdf (accessed on 16 August 2020).

42. Ventilación Técnica Para la Edificación. Available online: https://www.casals.com/es/productos-casals/ventilacion-tecnica-para-la-edificacion/ventiladores-in-line-y-en-caja-insonorizada/box-bd-plus// (accessed on 4 September 2020).
43. Cannistmro, G.; Franzitta, G.; Giaconia, C.; Rizzo, G. Algorithms for the calculation of the view factors between human body and rectangular surfaces in parallelepiped environments. *Energy Build.* **1992**, *19*, 51–60. [CrossRef]

4.3 Validation of Objective 3

4.3.1 Context of papers and References

This paper examined the Life Cycle Assessment (LCA) throughout the Peralveche and Sofia prototypes. The analysis comprises Life Cycle Energy (LCE), Life Cycle Cost (LCC) and Global Warming Potential (GWP) calculations for dynamic Water Flow Glazing (WFG) envelopes.

This paper has been published in *Energies*, which is a peer-reviewed, open access journal of related scientific research, technology development, engineering, and the studies in policy and management and is published semimonthly online by MDPI.

Energies is indexed in JCR, with an Impact Factor of 3.004 (2020) Q3, and in Scopus, with a CiteScore of 4.7 (2020) Q2.

Paper:

Energies

PAPER 5: *Santamaria, B.M.; Gonzalo, F.d.A.; Griffin, M.; Aguirregabiria, B.L.; Ramos, J.A.H. Life Cycle Assessment of Dynamic Water Flow Glazing Envelopes: A Case Study with Real Test Facilities. Energies 2021, 14, 2195.*

4.3.2 PAPER 5: Life Cycle Assessment of water flow glazing envelopes: A Case Study with Real Test Facilities

Overview

Life Cycle Assessment (LCA) is a comprehensive and internationally standardized method. It quantifies all relevant emissions, resources consumed, and the related environmental aspects associated with any goods or services. A Life Cycle Assessment can significantly help improve a sustainable building design by presenting how different materials or processes contribute to the building's overall environmental impact. Life Cycle Assessment considers four phases, the extraction of resources, the construction phase, the building operation, and the demolition. This paper examined the Life Cycle Assessment (LCA), Life Cycle Energy (LCE), and Life Cycle Cost (LCC) calculations for dynamic Water Flow Glazing (WFG) envelopes.

Life Cycle Energy comprises the building's operational energy, initial and recurrent embodied energy over its lifetime, and, finally, the energy for demolition and disposal. Equation 4.2 was used to calculate the Life Cycle Energy.

$$E = E_i + E_e rr + E_0(n) + E_d, \tag{4.2}$$

where E is the total energy of the building element, E_i is the initial embodied energy, Eerr is the recurrent embodied energy for future maintenance and refurbishment (5% of the initial embodied energy), E_o is the total annual operational energy, n is the lifetime of the element in years, and E_d is the embodied energy required for demolition and disposal (3% of the initial embodied energy).

The building envelope's Life Cycle Cost has included its construction cost, C_1, operation cost, C_2, and demolition cost, C_3. The present value interest factor of the annuity (PVIFA) was used to calculate the operation cost's current value. The present value interest factor (PVIF) was used to estimate the demolition and disposal cost's current value at the end of the envelope life cycle. C represents the building envelope's total Life Cycle Cost and the heating and cooling system; r represents the interest rate; n represents the design operating life in years.

$$C = C_1 + C_2 \left(\frac{1}{r} - \frac{1}{r(1+r)^n} \right) + C_3 \left(\frac{1}{(1+r)^n} \right). \tag{4.3}$$

Finally, Global Warming Potential (GWP) is a measure of the amount of heat trapped in the atmosphere. This variable is measured in carbon dioxide equivalents (kgCO_2eq). This equivalence means that the total greenhouse potential of a specific emission type is given concerning CO_2. The most common period for lifetime of buildings is 50 years in their LCE and LCC approach.

This paper showed that WFG glazing technology typically retains a higher price point for initial construction than the reference prototypes, requiring a substantial investment early on. This is because of the additional equipment needed for the successful operation of WFG panels. The steeper initial investment for WFG technology can serve as a deterrent for the technology in the eyes of building design professionals. It is not until we consider each system's overall Life Cycle Costs that the economic benefits of WFG systems become apparent. For this study, a WFG system is better over the operation phase only when it is compared with a traditional double-glazing system, as has been demonstrated in Peralveche. Another important factor that should be taken into account in the analysis between a much more traditional glazing system versus a WFG system is the Life Cycle Energy (LCE) and

global warming potential (GWP) variables. The Peralveche WFG system, as compared to the Peralveche reference prototype, has demonstrated a savings of 66% in LCE with a 70% reduction of CO_2 emission. In Sofia, there are similar results. Sofia WFG demonstrated a 36% savings in LCE with a 30% reduction in CO_2 emissions. After monitoring the WFG systems for a several years, uncertainties, mis-functions, and system issues must be addressed. WFG systems are limited by a high initial investment cost coupled with the need for an energy management system integrated with the other required equipment, especially if the system is coupled with boreholes heat exchangers combined with a ground source heat pump. The heating and cooling devices must be adequately dimensioned to avoid mis-functions, especially the Air-to-Water heat pump. Further research must include monitoring energy performance much more accurately by attaching sensors to monitor the amount of electricity powering the heat pump to compare the actual thermal and electricity consumption. In addition to this, further standardization of the manufacturing and deployment process is required to bring down upfront investment costs and payback periods. Finally, an integration of a whole evaluation protocol, including maintenance, environmental, and economic aspects, should be explored. This could be used by stakeholders involved in the design, maintenance, and monitoring process in future projects.

Published Paper

energies

MDPI

Article

Life Cycle Assessment of Dynamic Water Flow Glazing Envelopes: A Case Study with Real Test Facilities

Belen Moreno Santamaria [1], Fernando del Ama Gonzalo [2,*], Matthew Griffin [2], Benito Lauret Aguirregabiria [1] and Juan A. Hernandez Ramos [3]

[1] Department of Construction and Architectural Technology, Technical School of Architecture of Madrid, Technical University of Madrid (UPM), Av. Juan de Herrera 4, 28040 Madrid, Spain; belen.moreno@upm.es (B.M.S.); benito.lauret@upm.es (B.L.A.)
[2] Keene State College, 229 Main St, Keene, NH 03435, USA; Matthew.Griffin@ksc.keene.edu
[3] Escuela Department of Applied Mathematics, School of Aeronautical and Space Engineering, Technical University of Madrid (UPM), Plaza Cardenal Cisneros 3, 28040 Madrid, Spain; juanantonio.hernandez@upm.es
* Correspondence: fernando.delama@keene.edu

Abstract: High initial costs hinder innovative technologies for building envelopes. Life Cycle Assessment (LCA) should consider energy savings to show relevant economic benefits and potential to reduce energy consumption and CO_2 emissions. Life Cycle Cost (LCC) and Life Cycle Energy (LCE) should focus on investment, operation, maintenance, dismantling, disposal, and/or recycling for the building. This study compares the LCC and LCE analysis of Water Flow Glazing (WFG) envelopes with traditional double and triple glazing facades. The assessment considers initial, operational, and disposal costs and energy consumption as well as different energy systems for heating and cooling. Real prototypes have been built in two different locations to record real-world data of yearly operational energy. WFG systems consistently showed a higher initial investment than traditional glazing. The final Life Cycle Cost analysis demonstrates that WFG systems are better over the operation phase only when it is compared with a traditional double-glazing. However, a Life Cycle Energy assessment over 50 years concluded that energy savings between 36% and 66% and CO_2 emissions reduction between 30% and 70% could be achieved.

Keywords: water flow glazing; dynamic building envelope; life cycle assessment

Citation: Santamaria, B.M.; Gonzalo, F.d.A.; Griffin, M.; Aguirregabiria, B.L.; Hernandez Ramos, J.A. Life Cycle Assessment of Dynamic Water Flow Glazing Envelopes: A Case Study with Real Test Facilities. *Energies* **2021**, *14*, 2195. https://doi.org/10.3390/en14082195

Academic Editor: Fitsum Tariku

Received: 14 March 2021
Accepted: 8 April 2021
Published: 14 April 2021

1. Introduction

In recent years, clean energy use has steadily grown. However, energy consumption has not altered its pattern, with fossil fuels acting as the primary energy consumption and generation source. Many carbon emissions and greenhouse gasses caused by conventional energy sources have severe consequences on the environment. Therefore, building codes, regulations, and energy directives consider carbon emissions' impact when evaluating energy efficiency [1]. New technologies emerge rapidly and force building designers to act without a thorough environmental impact analysis [2]. To control the construction sector's environmental impact is the most critical challenge that the architecture, engineering, and construction (AEC) industry must face soon [3,4]. Life Cycle Assessment (LCA) is a comprehensive and internationally standardized method. It quantifies all relevant emissions, resources consumed, and the related environmental aspects associated with any goods or services [5,6].

1.1. Literature Review

Extensive investigation has been conducted to study the environmental impact of building materials [7]. A Life Cycle Assessment can significantly help improve a sustainable building design by presenting how different materials or processes contribute to the

building's overall environmental impact [8,9]. According to some authors, Life Cycle Assessment considers four phases, the extraction of resources, the construction phase, the building operation, and the building's demolition [10]. The European standards (EN) standards for Building Life Cycle Assessment maintain a list of 24 total categories that describe potential environmental impact [11–13]. A broadly accepted standard of the environmental impact of buildings is energy consumption [14]. The Life Cycle Energy analysis (LCE) only accounts for energy inputs at different life cycle stages, including the operational energy and embodied energy in buildings over their lifetime. Life Cycle Energy analysis evaluates the embodied energy of products, design modifications, and strategies used to optimize operational energy. The most common period for major renovations in the residential sector in practice is, according to some authors, 30–40 years [15]. Other authors estimate the lifetime of buildings as 50 years in their LCC approach [16]. The optimization of building envelopes should examine both the energy-saving and the Life Cycle Cost goals [17]. Different authors have proposed mathematical models to calculate each envelope material's Life Cycle Cost and heating and cooling system [18]. Construction costs, return on investment, increased market value, and maintenance and operation costs are the factors that determine consumers' response to sustainable buildings [19]. Since buildings have long lifespans, the design decisions have long-term consequences, considering that upfront costs amount to less than 30% of the total Life Cycle Costs [20,21].

Global warming potential (GWP) is a measure of the amount of heat trapped in the atmosphere. This variable is measured in carbon dioxide equivalents ($kgCO_{2eq}$). This equivalency means that the total greenhouse potential of a specific emission type is given concerning CO_2 [22]. Since the calculation for global warming potential includes the residence time of gases in the atmosphere, a total time range for an assessment can be defined at 100 years [23]. Emissions are substances that are released into the environment, which includes the air, water, and soil. This, in turn, negatively impacts human and environmental health. Emissions typically enter into the environment as a waste product from different industrial processes. The most common (and therefore well-known) emissions are called greenhouse gas (GHG) emissions [24]. Some articles have studied building envelope design from its energy-saving potential, environmental consequences, and social impacts. It is of the utmost importance to optimize the balance between the cost and energy savings [25,26].

Dynamic or active buildings adapt their thermal performance according to different inputs, such as outdoor and indoor conditions, and can produce part of the building's energy over its operational life. Technical research and numerical simulation tools on active building envelopes have increased over the last decade. However, the ratio of dynamic facades in the building industry remains stable [27]. Some dynamic envelopes change their opacity or vary their transmission or reflection properties. Electrochromic glass, Polymer dispersed liquid crystal, and Suspended Particle Devices are hindered by their high cost and non-standardized manufacturing processes [28,29]. Active envelopes can also produce renewable energy on-site. Photovoltaic panels (PV) are considered the most reliable on-site renewable energy generation technology due to the wide range of electricity use and cables' flexibility that transport the energy [30]. Solar thermal collectors are considered a renewable and CO_2 free energy source. However, the pipes' stiffness transporting warm water has limitations in their applicability as a part of the building envelope [31].

This paper will examine the Life Cycle Assessment (LCA), Life Cycle Energy (LCE), and Life Cycle Cost (LCC) calculations for dynamic Water Flow Glazing (WFG) envelopes. Coupled with a plug and play piping system, it would produce a high-performance building envelope and innovative heating and cooling system [32,33]. Water Flow Glazing is a technology that can be integrated into transparent building envelopes, either in new buildings or as a retrofit for traditional glazing [34]. Flowing water through WFG panels captures an extensive percentage of the solar infrared radiation and keeps the glazing transparency [35]. WFG can absorb solar energy to provide domestic hot water to plumbing fixtures when the solar irradiance is high enough [36,37].

1.2. Objectives and Innovation

Water Flow Glazing has proven its potential for energy savings and for increasing comfort of occupants in previous studies. The main contribution of this article has been to carry out a thorough analysis of a 50-year life cycle from the energy and cost perspectives. To accomplish this task, the authors have employed a tested methodology used in previous scientific articles. This study considered two prototypes in different locations, glazing compositions and energy systems. Real-world data were collected from these prototypes and analyzed to determine the actual energy performance of WFG systems. This paper is structured into four separate parts. Section 2 of this article provides background information on Water Flow Glazing technology, a description of the WFG test facilities, and finally the methodology of Life Cycle Energy analysis (LCE) and Life Cycle Cost (LCC) calculations. Section 3 provides an analysis of the year-long data collection that occurred at the WFG facilities. This section also contains information pertaining to the embodied energy, the operational energy, and the renewable energy production of the test facilities. Section 4 is a discussion on LCE and LCC and their impact on global warming potential based on a multi-index evaluation. In addition to this, this section has a discussion on the limitations of the methodology. The fifth and final section is the conclusions section.

2. Materials and Methods

Water flow glazing can be used as both a high-performance envelope as well as an element of the heating and cooling system. The WFG module presented in this paper is made up of three components: an extruded aluminum frame, the glazing, and a circulating device. The glazing is a compound of several layers of laminated glass and coatings, with thermal and spectral properties provided by the glass manufacturers. It combines coatings and Polyvinyl butyral layers with a variable water mass flow rate to absorb or reject incoming infrared solar radiation. The circulating device is defined by a water pump, an exchanger that can regulate heat, and different sensors (such as the water flow and water temperature) to regulate the different fluid variables involved. Finally, the aluminum assembly provides the frame with structure. Although WFG can absorb and transport thermal energy, alternative heating and cooling sources might be added to compensate for the heat losses and gains and maintain comfort conditions. The initial cost of the glazing exceeds the cost of a traditional double or triple glazing panel. However, its performance has to be evaluated over its life cycle to consider potential energy savings. In addition, the water flow captures the solar infrared radiation and increases its temperature through the window. This water is transported and eventually releases the energy in buffer tanks so that thermal energy can be used in hydronic heating systems. The renewable energy integrated into the building envelope might not be enough to meet the energy needs, so it is necessary to study different energy sources and systems to compare their final energy consumption and greenhouse gas emission potential. The Life Cycle Assessment of Water Flow Glazing includes four phases. Phase 1 is the extraction, production of construction materials, and transportation of materials from the extraction point to the construction site. Phase 2 is the construction phase, including required energy to run construction machinery, any additional materials for construction, and any waste disposal. Phase 3 includes the energy required for the building's actual operation (including all energy used during the building occupation over the total lifespan of the structure), general maintenance, repairs, and finally, any required material replacement for the building. Finally, phase 4 involves demolition and transport of waste to recycling plants or landfills.

2.1. Water Flow Glazing Thermal Properties

Heat flux through any glazing depends on the difference between the indoor and outdoor temperatures $(\theta_e - \theta_i)$ and the direct and diffuse solar radiation, i_0. Equation (1) shows the heat flow, q, in glazing panels with gas chambers depending on the thermal transmittance, U, and g-factor. Equation (2) illustrates that the variable fluid's temperature and mass flow rate impact the heat flow through the glazing. Equations (1) and (2) are

valid assuming steady conditions, constant values for convective and radiative coefficients, negligible thermal resistance and thermal mass of the glass panes and the water chamber, and the uniform flow inside the water chamber.

$$q = U(\theta_e - \theta_i) + gi_0, \tag{1}$$

$$q = U(\theta_e - \theta_i) + U_w(\theta_{IN} - \theta_i) + gi_0, \tag{2}$$

where U_w is the thermal transmittance between the water chamber and the interior, U is the glazing thermal transmittance, θ_e is the outdoor temperature, θ_i is the indoor temperature, and θ_{IN} is the inlet temperature of the fluid into the WFG system. Equations (3)–(5) are taken from a previous article [38]. They show the thermal transmittances of WFG, along with the g-factor. All the parameters depend on the mass flow rate, which is estimated uniform inside the glass pane.

$$U = \frac{U_i\, U_e}{\dot{m}c + U_e + U_i}, \tag{3}$$

$$U_w = \frac{U_i\, \dot{m}c}{\dot{m}c + U_e + U_i}, \tag{4}$$

$$g = \left(\frac{U_i}{\dot{m}c + U_e + U_i}\right)\left(\left(A_1\left(\frac{U_e}{h_e}\right) + A_2\left(\frac{1}{h_g} + \frac{1}{h_e}\right)U_e + A_3\left(\frac{U_e}{h_i}\right) + A_w\right)\right) + A_i + T. \tag{5}$$

Water flow glazing can change the thermal performance by varying the mass flow rate per unit of surface, $\dot{m}$. U and U_w are two additional thermal transmittances that depend on the mass flow rate. The product $\dot{m}c$ denotes the potential of the water to transfer energy. U_i and U_e thermal transmittances were obtained utilizing the convective heat coefficients, h_e, h_i, h_g, h_w. The thermal resistance, $(1/U_e)$ is the sum of the thermal resistances from the water chamber to the outdoors. Similarly, the thermal resistance, $(1/U_i)$, is the sum of the thermal resistances from the water chamber to indoors. Hence, U_e represents the thermal transmittance between the water chamber and outdoors, and U_i, the thermal transmittance between that water chamber and indoors. A_w is the water absorptance, whereas A_1, A_2, A_3 are the glass panes absorptances.

This study included two separate prototypes. The first one was placed in Peralveche, Spain (latitude 40°36′42″ N, longitude 2°26′57″ W, altitude 1111 MAMSL). The second one was built and tested in Sofia, Bulgaria (42°39′1″ N, 23°23′26″ E, Elevation: 590 m a.s.l.). The Peralveche WFG cabin was made of double glazing with a water chamber. Figure 1 shows the WFG cabin and energy system schematics.

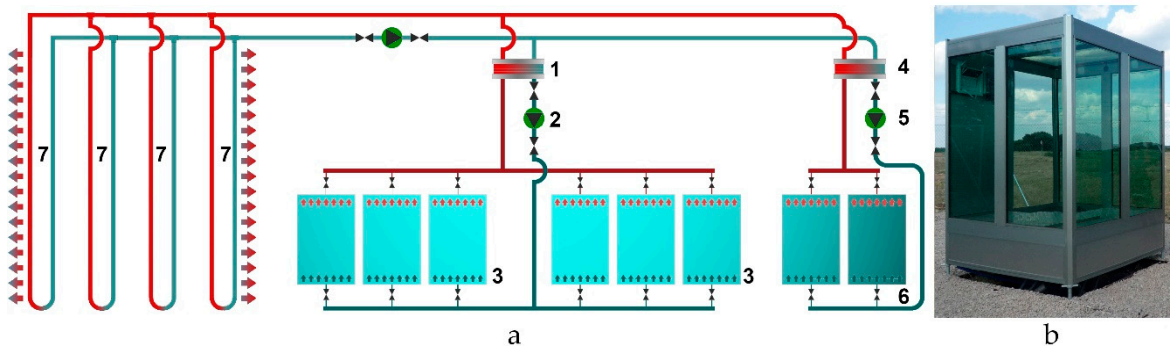

Figure 1. Peralveche prototype: (**a**) schematics of energy system: 1—plate heat exchanger, 2—water circulation pump and precision flow meters, 3—wall water flow glazing panels, 4—plate heat exchanger, 5—water circulation pump and precision flow meters, 6—roof water flow glazing panels, 7—borehole heat exchangers; (**b**) Water Flow Glazing (WFG) cabin.

The glass panes utilized to build this glazing assembly were Planiclear 6 + 6 mm with Poly-Vinyl Butyral layers (1 × 0.38 mm), a water chamber measuring 16 mm, and Planiclear 8 + 8 mm with Poly-Vinyl Butyral layers (1 × 0.38 mm). The cabin had six sides and each side was a square of 2 m × 2 m. The WFG panels were connected to four borehole heat exchangers buried 50 m underneath the cabin. The WFG cabin managed two different closed loop circulating systems. The first loop consisted of pipes that distributed refrigerant fluid from the borehole heat exchangers to the circulation pump. The WFG cabin included a second loop that circulated water through vertical facades and the horizontal roof and the mass flow rate was set to 0.9 $L \cdot min^{-1} \cdot m^{-2}$. Table 1 shows the glazing's thermal and spectral values from previous articles [38,39]. This WFG cabin was compared with another, referred to as Reference prototype, which had double glazing with an air cavity.

Table 1. Thermal properties of Peralveche glazing.

			$\dot{m}$ = 0 $L \cdot min^{-1} \cdot m^{-2}$			$\dot{m}$ = 0.9 $L \cdot min^{-1} \cdot m^{-2}$		
	Orientation	**Area (m^2)**	U ($W \cdot m^{-2} \cdot K^{-1}$)	U_w ($W \cdot m^{-2} \cdot K^{-1}$)	**g**	U ($W \cdot m^{-2} \cdot K^{-1}$)	U_w ($W \cdot m^{-2} \cdot K^{-1}$)	**g**
WFG [1]	S + E + W + roof	15.8	4.797	0.0	0.396	0.762	5.802	0.27
Reference [1]	S + E + W + roof	15.8	2.6	-	0.67	-	-	-

[1] Values taken from [39].

As per the Sofia prototype, the square plan dimensions were 7 m × 7 m. The walls are parallelograms of 7 m by 3.4 m comprised of five WFG modules facing east, west, and south, respectively. Figure 2 shows the unitized facade module. The circulating system incorporated a solar water pump and a plate heat exchanger connected to the water distribution pipes. The unitized WFG panels measured 3000 mm high and 1300 mm width, and the mass flow rate was set at 2 $L \cdot min^{-1} \cdot m^{-2}$. In the Southern glazing, the following layers were employed: a single 10 mm diamant glass pane, a 16 mm argon chamber, a low-emissivity coating Planitherm XN, Planiclear (8 mm), 2 Saflex R solar (SG41), Planiclear (8 mm), water chamber (24 mm), Planiclear (8 mm), 4 Saflex R standard clear (RB11), Planiclear (8 mm). Eastern and western glazing composition was meant to reject energy, so a highly reflective coating was included, instead of the low emissivity coating.

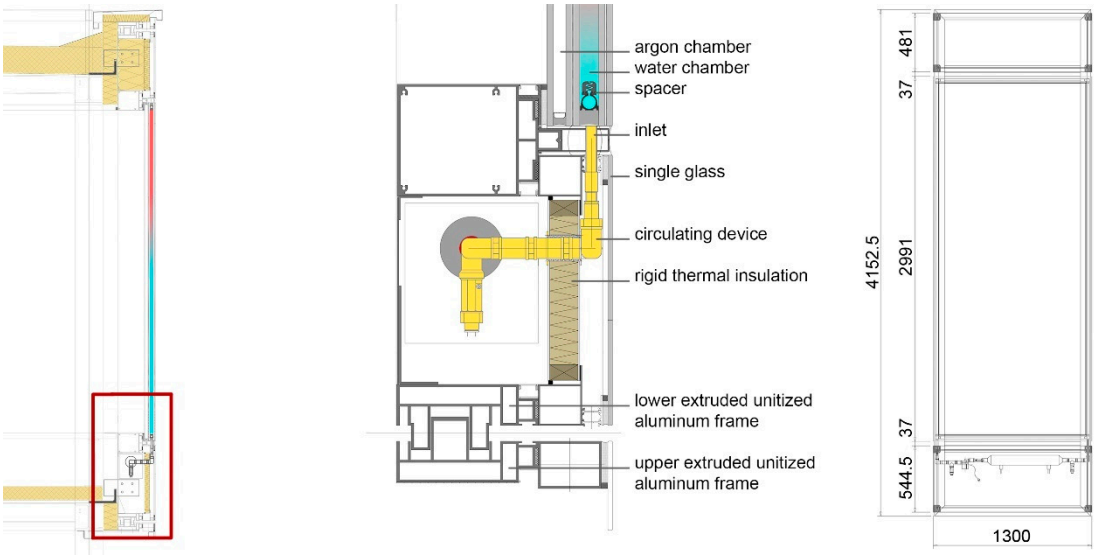

Figure 2. Sofia prototype description: (**a**) section; (**b**) detail of the unitized facade and circulating device; (**c**) elevation of the unitized module.

Table 2 shows the thermal properties of the glazing taken from a previous article [40]. The total glass area was 60 m^2. This WFG cabin was compared with another one, referred to as Reference prototype, with triple glazing with an air cavity and an argon cavity. The glass layers and coatings were the same as the WFG.

Table 2. Thermal properties of Sofia glazing.

			$\dot{m}$ = 0 L·min^{-1}·m^{-2}			$\dot{m}$ = 2 L·min^{-1}·m^{-2}		
	Area (m^2)	**Orientation**	U **(W·m^{-2}·K^{-1})**	U_w **(W·m^{-2}·K^{-1})**	**g**	U **(W·m^{-2}·K^{-1})**	U_w **(W·m^{-2}·K^{-1})**	**g**
WFG [1]	19.2	S Wall	1.041	0.0	0.59	0.066	6.459	0.24
WFG [1]	38.4	E–W Wall	0.995	0.0	0.27	0.063	6.462	0.22
Reference	19.2	S Wall	1.0	-	0.57	-	-	-
Reference	38.4	E–W Wall	1.0	-	0.30	-	-	-

[1] Values taken from [40].

2.2. Life Cycle Energy (LCE) Analysis

The total embodied energy of building elements involves the energy consumed directly at the primary material extraction, manufacturing, and assembly. These amounts of energy constitute the element's initial embodied energy, and the operational energy includes the heating and cooling energy consumption. Primary energy also considers the energy required to produce the final energy consumed in the building, and it varies according to fuel type and transportation losses. Primary energy is proportional to energy-related CO_2 emissions [41,42]. Life Cycle Energy comprises the building's operational energy, initial and recurrent embodied energy over its lifetime, and, finally, the energy for demolition and disposal. Equation (6) was used to calculate the Life Cycle Energy.

$$E = E_i + E_{err} + E_o(n) + E_d, \quad (6)$$

where E is the total energy of the building element, E_i is the initial embodied energy, E_{err} is the recurrent embodied energy for future maintenance and refurbishment (5% of the initial embodied energy), E_o is the total annual operational energy, n is the lifetime of the element in years, and E_d is the embodied energy required for demolition and disposal (3% of the initial embodied energy). Some LCE analysis studies include energy requirements such as lighting, cooking, hot water, and appliances. However, this study includes only the heating and cooling energy through the envelope. For the purposes of this paper, the energy absorbed by the WFG panels was considered as renewable energy production over the operational time in the final energy balance. Therefore, when calculating the total annual operational energy variable, this will be determined by taking the total energy consumption value and subtracting the amount of energy provided by the WFG panels in the structure.

2.3. Life Cycle Cost (LCC) Analysis

In addition to improving the thermal performance and reducing the environmental impact, the design of an efficient building envelope needs to pay attention to reducing the economic costs. Building owners demand the selection of cost-effective elements of the building envelope in a sustainable building design. Therefore, in terms of effective decision-making, it is essential to have a complete insight into the construction and running costs throughout the building's lifespan. The Life Cycle Cost (LCC) approach is based on optimizing design solutions and minimizing the sum of construction and operating expenses over the building lifetime. The building envelope's Life Cycle Cost has included its construction cost, C_1, operation cost, C_2, and demolition cost, C_3. The present value interest factor of the annuity (PVIFA) was used to calculate the operation cost's current value. The present value interest factor (PVIF) was used to estimate the demolition and disposal cost's current value at the end of the envelope life cycle. C represents the building

envelope's total Life Cycle Cost and the heating and cooling system; r represents the interest rate; n represents the design operating life in years. Therefore, the proposed Life Cycle Cost model for building facades is presented in Equation (7).

$$C = C_1 + C_2\left(\frac{1}{r} - \frac{1}{r(1+r)^n}\right) + C_3\left(\frac{1}{(1+r)^n}\right) \quad (7)$$

3. Results

This section started by defining the parameters to quantify the environmental performance: primary energy, equivalent CO_2 emissions, and cost. The building reference time was defined as 50 years.

Depending on the local context, the embodied impact may surpass the operational impact. The indicators that measure energy performance can be split into economic factors and physical energy factors.

3.1. Embodied Energy Calculation

The building elements' embodied energy has been taken from different sources, whereas the operational energy was calculated with experimental data from the prototypes. It was assumed that the structures were not renovated during this time and had no change in their usage mode throughout their useable life. Energy use, in the viewpoint of the various stages of a building's life cycle, in cold-weather temperatures, the operational stage can reach upwards of 80%. In contrast, the building materials and in-situ construction account for 10–20% [43]. For simplification purposes, the energy for demolition and disposal is a percentage of the total primary energy. Embedded Energy (EE) is the total energy needed to produce goods and services, including processing, mining and extraction, manufacturing, and transport of products. Table 3 shows the emissions associated with the EE are the result of energy and emissions quantification based on the ITeC database [18]. The following assumptions have been considered: The embodied energy associated with the replacement, refurbishment, and substitution of materials and products is assumed to be 5% every ten years [44]. The embodied energy associated with demolition and disposal was assumed to be 3% of the total building Life Cycle Energy [45–47]. The considered energy for replacement, demolition, and transportation to landfill does not exceed 10 kWh.m^{-2}.

Table 3. Embodied Energy (EE) and Embodied Carbon (EC) of materials.

Material	EE ($MJ \cdot kg^{-1}$)	EC ($kgCO_{2eq} \cdot kg^{-1}$)	Weight ($kg \cdot m^{-2}$)	EE ($MJ \cdot m^{-2}$)	EC ($kgCO_{2eq} \cdot m^{-2}$)	Cost (€$\cdot m^{-2}$)
Double Reference	12.95	1.59	69.00	1500.00	110.01	120.50
Triple Reference	15.30	1.70	104.50	2002.30	180.05	220.50
Double WFG	13.25	1.63	70.00	1666.00	114.10	239.10
Triple WFG	15.90	1.75	105.00	2299.50	183.75	370.22
Extr. Al. Stick	220.00	14.76	25.8	5676.00	380.81	110.85
Extr. Al. Stick (R)	14.60	1.02	25.8	376.68	26.32	110.85
Extr. Al. Unitized	220.00	14.76	84.00	18480.00	1239.84	415.20
Extr. Al. Unitized (R)	14.60	1.02	84.00	1226.40	85.68	415.20
Circulating device [1]	-	-	-	237.20	79.68	200.00

[1] A circulating device can serve 4 m^2 of WFG.

The energy systems used for this study were borehole heat exchangers coupled with a ground-source heat pump for the WFG Peralveche prototype, Air-to-Water heat pump for WFG Sofia prototype, and Air-to-Air heat pump for both reference prototypes. All the heat pumps are considered to be 7 to 20 kW. The chosen system boundaries include the production of the component, starting from raw materials, the use stage, and the dismantling stage of both systems, along a temporal horizon of 50 years. Closed-loop borehole heat exchangers were made of high-density polyethylene vertical pipes with water (78%) and ethylene glycol (22%) mixture flowing. The installation process included

drilling boreholes and trenches, inserting a vertical loop, and grouting operations of the borehole with concrete and bentonite mixture [48–50]. The dismantling process included the disposal of the glycol, the sealing of the borehole, and the disposal at the heat pump's end of life. Table 4 shows the embodied energy, emissions, and cost associated with the energy systems used to operate the different prototypes.

Table 4. Embodied Energy (EE) and Embodied Carbon (EC) of energy systems.

Material	EE (MJ)	EC ($kgCO_{2eq}$)	Cost (€)
Borehole heat exchangers [1]	9975.50	1661.98	5695.30
Ground-source heat pump	2193.60	390.30	7396.21
Air-to-Water heat pump	2210.50	350.70	8078.65
Air-to-Air heat pump	2393.70	380.50	3700.70

[1] Four 50 m borehole heat exchangers, diameter 118 mm.

The compressor and structure were made of reinforced steel and the evaporator and condenser from low alloyed steel. The pipes, cables, and expansion valves were made of copper. Pipes were insulated with a polymer and the cables were insulated with PVC. The refrigerant was assumed to be the same (tetrafluoroethane) for all the heat pumps. The heat pumps were considered maintenance-free, and their lifetime, 25 years.

3.2. Renewable Energy Production

Renewable primary energy (RPE in $kWh \cdot m^{-2}$) was produced as the water flowed through the glazing. The data were measured over a year. The RPE can cover part of the winter's heating needs and was subtracted from the non-renewable primary energy needed to maintain the prototype's indoor temperature within a comfort range. The heat absorption rate in the southern facades is closely related to the glazing composition and the orientation. When the solar radiation hits in the glazing units, the water chamber absorbs part of that energy. Heating was assumed to be delivered by a hydronic system using the energy absorbed by the WFG envelope. When needed, a heat pump operated to deliver the energy to keep comfort indoor conditions. Figure 3 shows the water heat gain of the prototypes' envelope. The horizontal panels in Peralveche show the largest water heat gain in July with 81.44 $kWh \cdot m^{-2}$. When it comes to the southern facades, the Sofia prototype shows the largest heat gain. The mass flow rate was set higher than any other prototypes (2 $L \cdot min^{-1} \cdot m^{-2}$), and the southern glazing properties demonstrate the highest absorptance. The peak solar heat gain in the Sofia prototype was 97.39 $kWh \cdot m^{-2}$ in July.

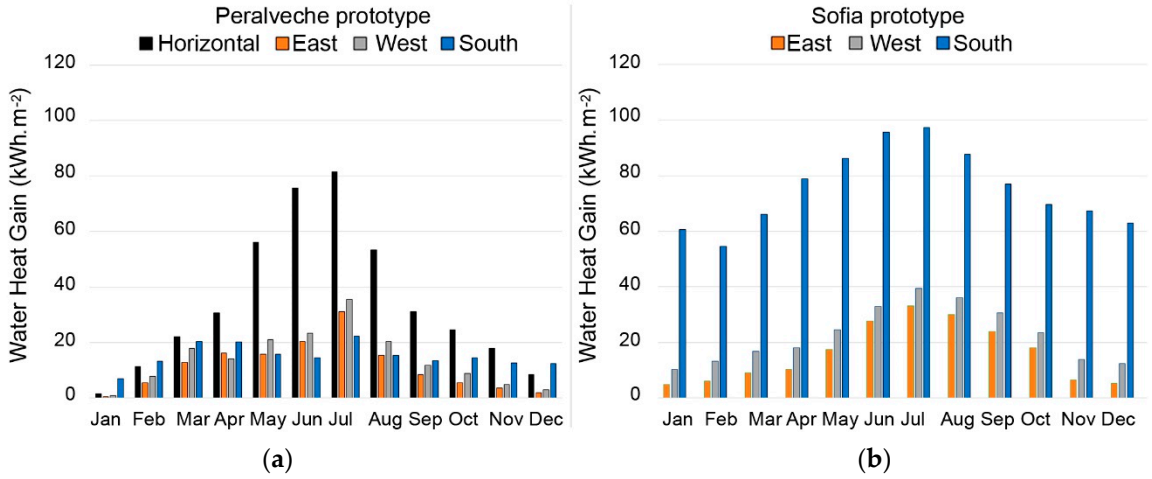

Figure 3. Experimental data. Water heat gain in WFG envelopes; (**a**) Peralveche prototype WFG; (**b**) Sofia WFG prototype in $kWh \cdot m^{-2}$.

3.3. Operational Energy

Heating and cooling energy loads (in kWh·m^{-2}) were calculated by using Equation (1) for the reference glazing and Equation (2) for WFG. The inputs were measured over a year time. Real data, obtained from the prototype throughout the year, allowed the correlation between the WFG cabin and the Reference cabin. Figure 4 shows the heating and cooling energy in kWh·m^{-2} to keep the inside within comfort temperature over the year. The figure considers only the energy that goes through the transparent envelope. The cooling load of the Peralveche Reference cabin showed by far the highest energy consumption with a peak of 118 kWh·m^{-2} in July.

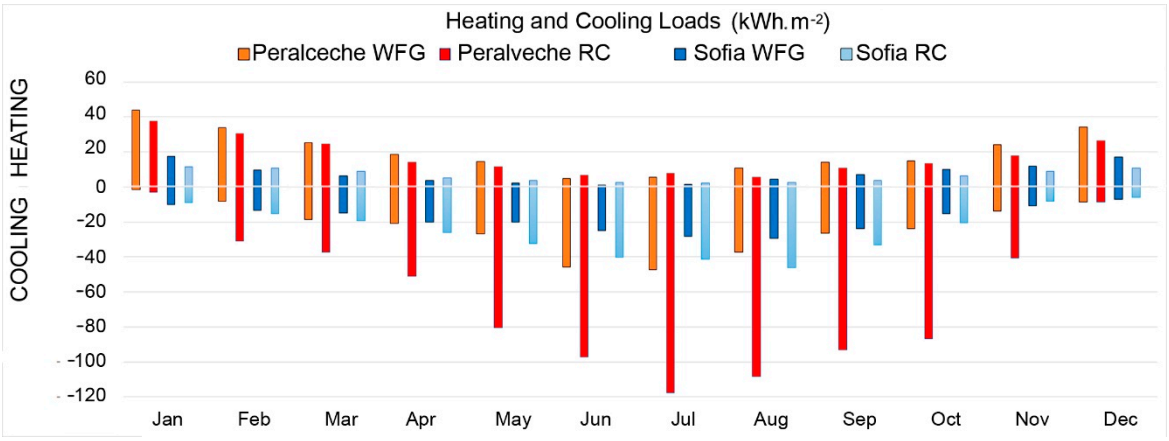

Figure 4. Experimental data. Heating and cooling energy through the transparent building envelopes in kWh·m^{-2}.

Table 5 shows conversion factors between non-renewable primary energy, NRPE, and final energy, FE (kWh$_{NRPE}$/kWh$_{FE}$), as well as CO_2 emissions conversion factors provided by the Spanish Regulation of Thermal Installations in Buildings [42]. The price per kWh of different energy carriers or fuels was taken from Eurostat documents [43].

Table 5. Conversion factor (f) from final energy (FE) to non-renewable primary energy (NRPE), CO_2 emissions, and price of energy carriers.

	f_{NRPE} (kWh$_{NRPE}$/kWh$_{FE}$)	f_{TPE} (kWh$_{TPE}$/kWh$_{FE}$)	f_{CO2} (kgCO_2/kWh$_{FE}$)	Price [1] (€/kWh)
Mainland electricity	1.954	2.368	0.331	0.239
Fuel	1.179	1.182	0.331	0.0713
Natural gas	1.190	1.195	0.252	0.102
Biomass (pellets)	0.085	1.113	0.018	0.0462

[1] values taken from [43].

The non-renewable primary energy consumption of the existing building per unit of envelope area and year, *NRPEC*, in kWh·m^{-2} per year, was calculated using Equation (8).

$$NRPE = f_{NRPE}FE_{heat} + f_{NRPE}FE_{cool}, \quad (8)$$

The equivalent CO_2 emissions of the existing building per unit of envelope area and year, in kgCO_2.m^{-2} per year, were calculated with Equation (9).

$$CO_{2eq} = f_{CO2}FE_{heat} + f_{CO2}FE_{cool}, \quad (9)$$

Tables 6 and 7 illustrate the non-renewable primary energy consumption (NRPE) with different energy generators in Peralveche and Sofia, respectively. The conversion factor between final energy and non-renewable primary energy (kWh NRPE/kWh FE) and the factor of emitted CO_2 for electricity were taken from Table 3 for mainland electricity: 1.954

for the conversion factor between final energy and non-renewable primary energy (kWh NRPE/kWh FE) and 0.331 for CO_2 emissions for electricity. In the final energy balance, the renewable energy production was subtracted from the WFG prototype heating loads. The ground-source heat pumps' performance depends on the source inlet temperature in the heat pump, and the inlet temperature in the WFG (θ_{IN}). A typical value of source inlet temperature ranges from 20 °C in ground-source heat pumps (GSHP) to 35 °C in other Water-to-Water (W-W) heat pumps. The parameters that influence Air-to-Air (A-A) heat pumps' performance are the dry bulb exterior air temperature and the dry bulb interior return air temperature [51].

Table 6. Peralveche prototype. Final energy, non-renewable primary energy, and CO_2 emissions.

	Heating		Cooling	
Peralveche	**WFG(W-W)**	**RC(A-A)**	**WFG(W-W)**	**RC(A-A)**
Energy (kWh·m^{-2})	42.12	206.95	279.70	755.05
COP [1]	6.60	4.20	5.90	3.30
FE (kWh·m^{-2})	6.38	49.27	47.41	228.80
NRPE (kWh·m^{-2})	12.47	96.28	92.63	447.08
CO_{2eq} (kgCO_2.m^{-2})	2.11	16.31	15.69	75.73
OE cost (€·m^{-2} per year)	1.53	11.78	11.33	54.68

[1] COP values are taken from [51].

Table 7. Sofia prototype. Final energy, non-renewable primary energy, and CO_2 emissions.

	Heating		Cooling	
Sofia	**WFG(W-W)**	**RC(A-A)**	**WFG(W-W)**	**RC(A-A)**
Energy (kWh·m^{-2})	0.00	76.58	219.10	298.07
COP [1]	5.30	4.20	4.60	3.30
FE (kWh·m^{-2})	0.00	18.23	47.63	90.32
NRPE (kWh·m^{-2})	0.00	35.63	93.07	176.49
CO_{2eq} (kgCO_2.m^{-2})	0.00	6.04	15.77	29.90
OE cost (€·m^{-2} per year)	0.00	4.36	11.38	21.59

[1] COP values are taken from [51].

The yearly operating energy was assumed to remain steady during the entire building operation. The resource mix supplying electricity to the buildings is assumed to be unvarying. The HVAC systems' efficiency and the operation schedule were assumed to remain unchanged during the Life Cycle Assessment.

4. Discussion

WFG can be a part of hydronic heating and cooling systems, and it is compatible with ground-source heat pumps and boilers. In this study, the authors have considered only mainland electricity as the energy source, ground source heat pumps for the Peralveche WFG prototype, Air-to-Water heat pumps for the Sofia WFG prototype, and Air-to-Air heat pumps for the reference prototypes.

4.1. Life Cycle Cost Evaluation

The method to evaluate the Life Cycle Cost (LCC) has been shown in Section 2. The parameters to calculate the envelope's Life Cycle Cost and the energy system initial cost have been discussed in Section 3. The operation cost was calculated with data provided by Table 5 and energy prices for mainland electricity. Maintenance costs for the envelope over 50 years have been calculated as a percentage of the initial cost (1% for the reference glass and 5% for WFG), whereas the heat pump's lifetime was 25 years. The cost of the studied WFG unitized facade was 985 €·m^{-2}, whereas the price for the circulating water pump was 20 €·m^{-2}. Replacing the water pumps after a 10-year cycle is included in the maintenance

cost. Finally, the demolition and disposal costs were calculated as a percentage of the initial cost (3%). Therefore, the total proposed Life Cycle Cost for the building envelope and energy system was calculated according to Equation (7). The total construction costs of the envelopes and the energy systems were calculated by multiplying each envelope component's quantity by the total unit price. The operation cost was converted to the present value based on annual heating and cooling loads through the envelope. The considered demolition and disposal values were 3% of the total construction costs and converted to the present value. This article considered a discount rate of 2% calculated as an average of the harmonized consumer price index in Spain over the last 20 years. The price of energy was taken from Eurostat reports [43]. The material prices of other components come from the ITeC database [18]. Table 8 shows the cost analysis parameters for all cases.

Table 8. Cost analysis parameters.

	C_1	C_2	C_3	Total (50 Years)
Peralveche WFG	17,529	640	7921	40,611
Peralveche RC	7373	1239	3921	47,767
Sofia WFG	65,626	1320	10,046	110,865
Sofia RC	40,795	1923	4923	103,066

Water flow glazing envelopes showed a higher Coefficient C_1. The initial cost reflected the investment in borehole heat exchangers and circulating devices. However, the coefficient C_2 reflected that the reference yearly operation cost is twice as much as the WFG cost in Peralveche and 1.5 more in Sofia. The total cost considered a 50-year life cycle by converting the operation and disposal costs to the present value. In Peralveche, the reference prototype cost surpassed the WFG one. In Sofia, the WFG is slightly higher than the reference one.

4.2. Life Cycle Energy Evaluation

Life Cycle Energy included the materials initial embodied energy, the operational energy for heating and cooling over 50 years, the recurrent embodied energy over its lifetime, and, finally, the energy for demolition and disposal. Equation (6) was used to calculate the Life Cycle Energy. Table 9 shows the initial embodied energy E_i, the recurrent embodied energy for future maintenance E_{err}, calculated as a percentage of the initial embodied energy, the total annual operational energy, and the embodied energy required for demolition and disposal E_d.

Table 9. Life Cycle Energy parameters in GJ.

	E_1	E_{err}	E_o	E_d	Total (50 Years)
Peralveche WFG	193	19	300	58	571
Peralveche RC	116	12	1553	35	1716
Sofia WFG	1216	122	978	61	2377
Sofia RC	1198	120	2230	60	3608

The most considerable initial embodied energy *Ei* was shown in both WFG prototypes. It was more significant in the Peralveche prototype than in Sofia because of the high embodied energy in the borehole heat exchangers. However, the lower operational energy over 50 years compensated for the higher initial energy consumption. Table 10 illustrates the CO_2 emissions, which is the parameter used to assess the global warming potential (GWP) in $kgCO_{2eq}$. The life cycle emissions included the same phases: manufacture and transport of construction materials, maintenance, operation of the building, and waste disposal.

Table 10. Life cycle Embodied Carbon in $kgCO_{2eq}$.

	EC_1	EC_{err}	EC_o	EC_d	Total (50 Years)
Peralveche WFG	10,107	707	14,133	505	25,452
Peralveche RC	8145	3654	73,080	407	85,286
Sofia WFG	83,713	2302	46,048	4186	136,250
Sofia RC	83,269	5247	104,945	4163	197,625

Improving the thermal performance of the building envelope with WFG caused an increase in the initial cost. However, the amount of energy and CO_2 emissions declined in both cases over the considered life cycle.

4.3. Multi-Index Evaluation Model

Usually, the optimum building envelope's thermal performance is often accompanied by an increase in the cost and environmental load. This study established a multi-index evaluation model, including non-renewable primary energy consumption NRPE, global warming potential GWP, and cost, as indicators of the environment's aspects to evaluate a building envelope. Figure 5 shows that the initial cost of the WFG prototype in Peralveche doubled the reference one's cost because of the investment in borehole heat exchangers. Over a 50-year lifetime cycle, the reference prototype's accumulative cost surpasses the WFG prototype, due to the operational cost difference. When it comes to the Life Cycle Energy and the global warming potential the WFG showed a better performance. The reference prototype consumed three times as much energy as the WFG. The accumulative CO_2 emissions for the WFG envelope were 25,247 $kgCO_{2eq}$, whereas the reference glass envelope was responsible for 85,286 $kgCO_{2eq}$. When the cost is increased by 100%, the total Life Cycle Energy decreased by 1145 GJ. It has been estimated that the initial investment for the WFG system would cost €17,529, while the Reference system would require an initial investment of €7373. The WFG system would require €640.88 for maintenance per year, with an end-of-product, total demolition, and removal cost of €7921. Summing together these values and the initial investment for the system, the final total Life Cycle Cost of the Peralveche WFG system is €40,611. Meanwhile, for Peralveche RC, this system would cost €1239 in maintenance costs per year, with an end-of-product, total demolition, and removal cost of €3921. Combining these values with the initial investment cost shows that the final total Life Cycle Cost of the Peralveche RC system would be €47,767. Therefore, in the Peralveche case, it is apparent that the successful construction and implementation of the WFG system would save the owner a total of €7156 over the total building life cycle period. When it comes to Life Cycle Energy assessment and global warming potential, the WFG system in the Peralveche prototype used 571 GJ of energy during its lifetime. It was also determined that the system would contain 25,452 $kgCO_{2eq}$ during its 50 years of use. Meanwhile, for the Peralveche RC prototype, the system was calculated to use 1716 GJ of energy, while containing 85,286 $kgCO_{2eq}$ during its 50 years of use. Therefore, the Peralveche WFG system, when compared to the RC, will save 1145 GJ of energy as well as 59,834 $kgCO_{2eq}$ of Embodied Carbon over its entire lifetime.

Figure 6 shows that the HVAC operation cost over 50 years did not compensate for the higher initial cost of the WFG prototype. Over a 50-year lifetime cycle, the WFG envelope showed a better performance in the Life Cycle Energy and the global warming potential. The accumulative Life Cycle Energy for the WFG envelope was 2377 GJ, whereas the Life Cycle Energy of the reference glass was 3608 GJ. A model integrating Life Cycle Cost with Life Cycle Energy is used to assess the envelope schemes and select the optimal one in the decision-making process. The Sofia WFG system is estimated to initially cost €65,626, while the Sofia Reference system would cost €40,795.

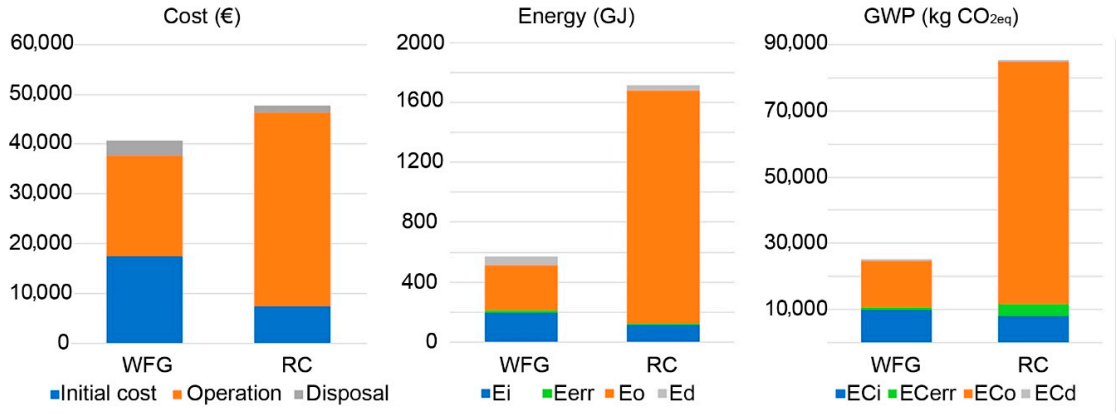

Figure 5. Life Cycle Assessment outcomes of the Peralveche prototype.

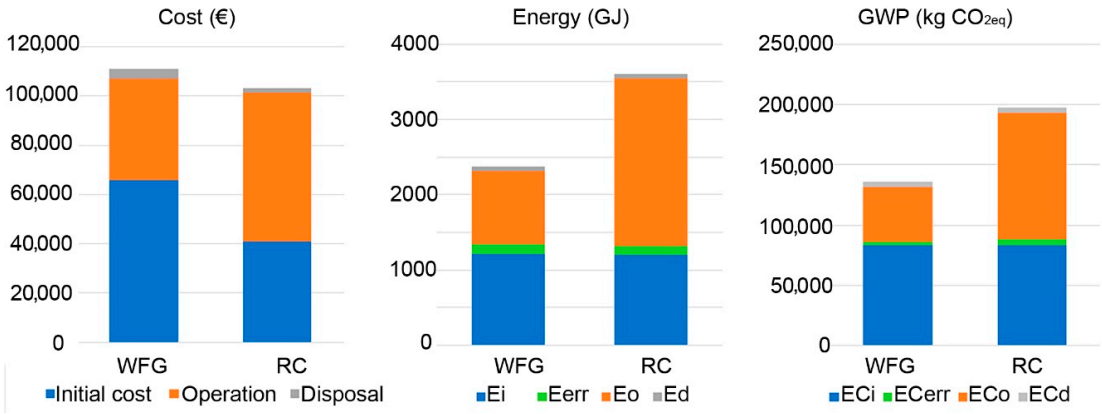

Figure 6. Life Cycle Assessment outcomes of the Sofia prototype.

For Sofia prototypes, the WFG system would require €1320 for maintenance per year, with an end-of-product, total demolition, and removal cost of €10,046. Summing together these values, as well as the initial investment for the system, it can be seen that the final total Life Cycle Cost of the Sofia WFG system is €110,865. Meanwhile, for Sofia RC, this system would cost €1923 in maintenance costs per year, with an end-of-product, total demolition and removal cost of €4923. Combining these values with the initial investment cost, the final total Life Cycle Cost of the Sofia RC system would be €103,066. The Sofia WFG system would cost an additional €33,184 compared to Sofia RC over the structure's lifespan.

The WFG system in the Sofia prototype used 2377 GJ of energy, so the system would contain 136,250 $kgCO_{2eq}$ during its 50 years of use. Meanwhile, for the Sofia RC prototype, the system used 3608 GJ of energy while containing 197,625 $kgCO_{2eq}$ during its 50 years of service. In this case, the WFG system will save 1231 GJ of energy while also containing 6137 $kgCO_{2eq}$ less of Embodied Carbon over its entire lifetime as compared to the Reference system.

5. Conclusions and Limitations

This paper aimed to develop a conceptual framework to assess the building envelope energy consumption throughout their entire life cycle. By analyzing two case studies, the results can assist building designers during the decision-making process at early stages and consider water flow glazing as an option to reduce energy consumption and CO_2 emissions.

As has been demonstrated, WFG glazing technology typically retains a higher price point for initial construction than the reference prototypes, requiring a substantial investment early on. This is because of the additional equipment needed for the successful operation of WFG panels. The Peralveche reference prototype's initial cost is 42% of the

Peralveche WFG cost, whereas the Sofia reference prototype initial cost is 62% of the WFG initial cost. The steeper initial investment for WFG technology can serve as a deterrent for the technology in the eyes of building design professionals. However, when the total Life Cycle Costs of the WFG and RC are also taken into account, WFG can potentially be a much more economical option.

It is not until we consider each system's overall Life Cycle Costs that the economic benefits of WFG systems become apparent. For this study, the building lifespan was determined to be 50 years. The total Life Cycle Cost (LCC) of the Peralveche WFG is 85% of the total Reference system LCC. Meanwhile, the Sofia Reference LCC is 92% of the total WFG LCC. The conclusion derived from these findings is that selecting high-performance triple glazing is better than a WFG in Life Cycle Cost. A WFG system is better over the operation phase only when it is compared with a traditional double-glazing system, as has been demonstrated in Peralveche.

Another important factor that should be taken into account in the analysis between a much more traditional glazing system versus a WFG system is the Life Cycle Energy (LCE) and global warming potential (GWP) variables. The Peralveche WFG system, as compared to the Peralveche reference prototype, has demonstrated a savings of 66% in LCE with a 70% reduction of CO_2 emission. In Sofia, there are similar results. Sofia WFG demonstrated a 36% savings in LCE with a 30% reduction in CO_2 emissions. This analysis shows that a high-performance triple glazing system improves the Reference prototype performance, but WFG performs better in LCE and GWP in both cases.

The WFG system, however, does have several limitations. Firstly, there is an apparent lack of interoperability with the rest of the building systems present in modern structures, especially concerning the ventilation system. In addition to this, it is not always possible to retrieve all the detailed information needed as input for Water Flow Glazing operation. The maintenance of the building systems operation and the control of the building's indoor environmental conditions according to its user's comfort is of the utmost importance, and smart meters can assist in this. However, these devices pose considerable limitations concerning the quality, frequency, and accuracy of data. Therefore, taking these limitations into account, several future steps of research should be undertaken. Firstly, a development of a testing method to evaluate the performance of the unitized module components should be explored. In addition to this, more case studies in several different climate regions should be analyzed. Thirdly, the development of a management system to control the water pump in the circulating device should be realized. The life cycle of the water pump, which is another point of future research, depends on the operating hours and the on-off cycle. Finally, an integration of a whole evaluation protocol, including maintenance, environmental, and economic aspects, should be explored. This could be used by stakeholders involved in the design, maintenance, and monitoring process in future, potential projects.

After monitoring the WFG systems for a year, several uncertainties, misfunctions, and system issues must be addressed. WFG systems are limited by a high initial investment cost coupled with the need for an energy management system integrated with the other required equipment, especially if the system is coupled with borehole heat exchangers combined with a ground source heat pump. The heating and cooling devices must be adequately dimensioned to avoid misfunctions, especially the Air-to-Water heat pump. Further research must include monitoring energy performance much more accurately by attaching sensors to monitor the amount of electricity powering the heat pump to compare the actual thermal and electricity consumption. In addition to this, further standardization of the manufacturing and deployment process is required to bring down upfront investment costs and payback periods. Finally, another potential further research component would be to control indoor relative humidity, which would be achieved by integrating WFG with efficient ventilation systems.

Author Contributions: Conceptualization, B.M.S., F.d.A.G., J.A.H.R.; methodology, B.M.S., F.d.A.G.; software, J.A.H.R.; formal analysis, M.G., F.d.A.G.; data curation, F.d.A.G., J.A.H.R.; writing—original draft preparation, B.M.S., F.d.A.G., J.A.H.R.; writing—review and editing, M.G., B.M.S.; visualization, M.G., B.M.S., B.L.A.; supervision, J.A.H.R., B.L.A.; project administration, F.d.A.G.; funding acquisition, F.d.A.G. All authors have read and agreed to the published version of the manuscript.

Funding: This article has been funded by KSC Faculty Development Grant (Keene State College, NH, USA).

Acknowledgments: This work was supported by program Horizon 2020-EU.3.3.1: Reducing energy consumption and carbon footprint by smart and sustainable use, project Ref. 680441 InDeWaG: Industrialized Development of Water Flow Glazing Systems. The authors wish to thank the municipality of Peralveche, Spain, for its generous support.

Conflicts of Interest: The authors declare that they have no conflict of interest.

Abbreviations

Symbol	Meaning
AEC	Architecture, engineering, and construction.
EE	Embedded energy.
FE	Final energy.
GHG	Greenhouse gas.
GSHP	Ground source heat pump.
GWP	Global warming potential.
LCA	Life Cycle Assessment.
LCC	Life Cycle Cost.
LCE	Life Cycle Energy.
NRPE	Non-renewable primary energy.
PV	Photovoltaic
PVIF	Present value interest factor.
PVIFA	Present value interest factor of the annuity.
RC	Reference cabin.
RPE	Renewable primary energy.
WFG	Water Flow Glazing.
A_j	Absorptance of glass layers.
C_1	Construction cost.
C_2	Operation cost.
C_3	Demolition cost.
E	Total energy of the building element.
E_i	Initial embodied energy.
E_{err}	Recurrent embodied energy for future maintenance and refurbishment.
E_o	Total annual operational energy.
E_d	embodied energy required for demolition and disposal.
h_j	Convective heat coefficients.
i_0	Solar irradiance ($W \cdot m^{-2} \cdot K^{-1}$).
$\dot{m}$	Mass flow rate per unit of surface ($Liter \cdot min^{-1} \cdot m^{-2}$).
n	Lifetime of the element in years.
P	Heat gain in the water chamber (W).
q	Heat flow ($W \cdot m^{-2} \cdot K^{-1}$).
r	Interest rate.
θ_i	Interior temperature (K).
θ_e	Exterior temperature (K).
θ_{IN}	Inlet temperature of the water chamber (K).
U	Thermal transmittance ($W \cdot m^{-2} \cdot K^{-1}$).
U_i	Interior thermal transmittance ($W \cdot m^{-2} \cdot K^{-1}$).
U_e	Exterior thermal transmittance ($W \cdot m^{-2} \cdot K^{-1}$).
U_w	Thermal transmittance (water chamber–interior) (K).

References

1. Wu, J.; Yin, P.Z.; Sun, J.S.; Chu, J.F.; Liang, L. Evaluating the environmental efficiency of a two-stage system with undesired outputs by a DEA approach: An interest preference perspective. *Eur. J. Oper. Res.* **2016**, *254*, 1047–1062. [CrossRef]
2. Webler, T.; Holewinski, M.; Orrick, B.; Kaur, R. Toward a method for the rapid collection of public concerns and benefits of emerging energy technologies. *J. Risk Res.* **2020**, *23*, 35–46. [CrossRef]
3. Manfren, M.; Sibilla, M.; Tronchin, L. Energy Modelling and Analytics in the Built Environment—A Review of Their Role for Energy Transitions in the Construction Sector. *Energies* **2021**, *14*, 679. [CrossRef]
4. Jezierski, W.; Sadowska, B.; Pawłowski, K. Impact of Changes in the Required Thermal Insulation of Building Envelope on Energy Demand, Heating Costs, Emissions, and Temperature in Buildings. *Energies* **2021**, *14*, 56. [CrossRef]
5. Oshiro, K.; Fujimori, S. Stranded investment associated with rapid energy system changes under the mid-century strategy in Japan. *Sustain. Sci.* **2021**, *16*, 477–487. [CrossRef]
6. Wang, H.; Chen, W.; Zhang, H.; Li, N. Modeling of power sector decarbonization in China: Comparisons of early and delayed mitigation towards 2-degree target. *Clim. Chang.* **2020**, *62*, 1843–1856. [CrossRef]
7. Allan, K.; Phillips, A.R. Comparative Cradle-to-Grave Life Cycle Assessment of Low and Mid-Rise Mass Timber Buildings with Equivalent Structural Steel Alternatives. *Sustainability* **2021**, *13*, 3401. [CrossRef]
8. Omrany, H.; Soebarto, V.; Sharifi, E.; Soltani, A. Application of Life Cycle Energy Assessment in Residential Buildings: A Critical Review of Recent Trends. *Sustainability* **2020**, *12*, 351. [CrossRef]
9. Zabalza-Bribián, I.; Aranda-Usón, A.; Scarpellini, S. Life cycle assessment in buildings: State-of-the-art and simplified LCA methodology as a complement for building certification. *Build. Environ.* **2009**, *44*, 2510–2520. [CrossRef]
10. Bruce-Hyrkäs, T.; Pasanen, P.; Castro, R. Overview of Whole Building Life-Cycle Assessment for Green Building Certification and Ecodesign through Industry Surveys and Interviews. *Procedia CIRP* **2018**, *69*, 178–183. [CrossRef]
11. European Commission, Joint Research Centre, Institute for Environment and Sustainability. *International Reference Life Cycle Data System (ILCD) Handbook—General Guide for Life Cycle Assessment—Detailed Guidance*, 1st ed.; EUR 24708 EN; Publications Office of the European Union: Luxembourg, 2010.
12. ISO 14044:2006. *Environmental Management—Life Cycle Assessment—Requirements and Guidelines*; International Organization for Standardization: Geneva, Switzerland, 2006.
13. EN 15978 (2012). *Sustainability of Construction Works—Assessment of Environmental Performance of Buildings—Calculation Method. European Committee for Standardisation*; International Organization for Standardization: Geneva, Switzerland, 2012.
14. Chau, C.K.; Leung, T.M.; Ng, W.Y. A review on life-cycle assessment, life-cycle energy assessment and life-cycle carbon emissions assessment on buildings. *Appl. Energy* **2015**, *143*, 395–413. [CrossRef]
15. Jausovec, M.; Sitar, M. Comparative Evaluation Model Framework for Cost-Optimal Evaluation of Prefabricated Lightweight System Envelopes in the Early Design Phase. *Sustainability* **2019**, *11*, 5106. [CrossRef]
16. Gluch, P.; Baumann, H. The Life Cycle Costing (LCC) Approach: A Conceptual Discussion of Its Usefulness for Environmental Decision-Making. *Build. Environ.* **2004**, *39*, 571–580. [CrossRef]
17. Hu, M. A Building Life-Cycle Embodied Performance Index—The Relationship between Embodied Energy, Embodied Carbon and Environmental Impact. *Energies* **2020**, *13*, 1905. [CrossRef]
18. ITeC (Instituto de la Tecnología de la Construcción de Cataluña). Available online: https://itec.es/servicios/bedec/ (accessed on 3 February 2021).
19. Oyedele, L.; Tham, K.; Fadeyi, M.; Jaiyeoba, B. Total Building Performance Approach in Building Evaluation: Case Study of an Office Building in Singapore. *J. Energy Eng.* **2012**, *138*, 25–30. [CrossRef]
20. Sharma, A.; Saxena, A.; Sethi, M.; Varun, V.S. Life cycle assessment of buildings: A review. *Renew. Sustain. Energy Rev.* **2011**, *15*, 871–875. [CrossRef]
21. Ferrara, M.; Fabrizio, E.; Virgone, J.; Filippi, M. Energy Systems in Cost-Optimized Design of Nearly Zero-Energy Buildings. *Autom. Constr.* **2016**, *70*, 109. [CrossRef]
22. EN-European Standard. *EN15978-Sustainability of Construction Works-Assessment of Environmental Performance of Buildings-Calculation Method*; No. EN 15978:2011; European Committee for Standarization. s.l.: Brussels, Belgium, 2011.
23. Connolly, R.; Connolly, M.; Carter, R.M.; Soon, W. How Much Human-Caused Global Warming Should We Expect with Business-As-Usual (BAU) Climate Policies? A Semi-Empirical Assessment. *Energies* **2020**, *13*, 1365. [CrossRef]
24. Wang, X.; Jiang, D.; Lang, X. Climate Change of 4 °C Global Warming above Pre-industrial Levels. *Adv. Atmos. Sci.* **2018**, *35*, 757–770. [CrossRef]
25. Lu, S.L.; Wang, Z.C.; Zhang, T.S. Quantitative analysis and multi-index evaluation of the green building envelope performance in the cold area of China. *Sustainability* **2020**, *12*, 437. [CrossRef]
26. Chiradeja, P.; Ngaopitakkul, A. Energy and economic analysis of tropical building envelope material in compliance with thailand's building energy code. *Sustainability* **2019**, *11*, 6872. [CrossRef]
27. Luo, Y.; Zhang, L.; Bozlar, M.; Liu, Z.; Guo, H.; Meggers, F. Active building envelope systems toward renewable and sustainable energy. *Renew. Sustain. Energy Rev.* **2019**, *104*, 470–491. [CrossRef]
28. Abdulmohsin, H.; Aritra, G.; Senthilarasu, S.; Tapas, K.M. Evaluation of thermal performance for a smart switchable adaptive polymer dispersed liquid crystal (PDLC) glazing. *Sol. Energy* **2020**, *195*, 185–193.

29. Ghosh, A.; Norton, B.; Duffy, A. Behaviour of a SPD switchable glazing in an outdoor test cell with heat removal under varying weather conditions. *Appl. Energy* **2016**, *180*, 695–706. [CrossRef]
30. Frattolillo, A.; Canale, L.; Ficco, G.; Mastino, C.C.; Dell'Isola, M. Potential for Building Façade-Integrated Solar Thermal Collectors in a Highly Urbanized Context. *Energies* **2020**, *13*, 5801. [CrossRef]
31. Arpino, F.; Cortellessa, G.; Frattolillo, A. Experimental and numerical assessment of photovoltaic collectors performance dependence on frame size and installation technique. *Sol. Energy* **2015**, *118*, 7–19. [CrossRef]
32. Gutai, M.; Kheybari, A.G. Energy consumption of water-filled glass (WFG) hybrid building envelope. *Energy Build.* **2020**, *218*, 110050. [CrossRef]
33. Gil-Lopez, T.; Gimenez-Molina, C. Influence of double glazing with a circulating water chamber on the thermal energy savings in buildings. *Energy Build.* **2013**, *56*, 56–65. [CrossRef]
34. Moreno Santamaria, B.; Ama Gonzalo, F.; Lauret Aguirregabiria, B.; Hernandez Ramos, J.A. Evaluation of Thermal Comfort and Energy Consumption of Water Flow Glazing as a Radiant Heating and Cooling System: A Case Study of an Office Space. *Sustainability* **2020**, *12*, 7596. [CrossRef]
35. Gutai, M.; Kheybari, A.G. Energy consumption of hybrid smart water-filled glass (SWFG) building envelope. *Energy Build.* **2021**, *230*, 110508. [CrossRef]
36. Lyu, Y.L.; Chow, T.T.; Wang, J.L. Numerical prediction of thermal performance of liquid-flow window in different climates with anti-freeze. *Energy* **2018**, *157*, 412–423. [CrossRef]
37. Chow, T.T.; Li, C. Liquid-filled solar glazing design for buoyant water-flow. *Build. Environ.* **2013**, *60*, 45–55. [CrossRef]
38. Sierra, P.; Hernandez, J.A. Solar heat gain coefficient of water flow glazing. *Energy Build.* **2017**, *139*, 133–145. [CrossRef]
39. Moreno Santamaria, B.; del Ama Gonzalo, F.; Pinette, D.; Gonzalez-Lezcano, R.-A.; Lauret Aguirregabiria, B.; Hernandez Ramos, J.A. Application and Validation of a Dynamic Energy Simulation Tool: A Case Study with Water Flow Glazing Envelope. *Energies* **2020**, *13*, 3203. [CrossRef]
40. Moreno Santamaria, B.; del Ama Gonzalo, F.; Pinette, D.; Lauret Aguirregabiria, B.; Hernandez Ramos, J.A. Industrialization and Thermal Performance of a New Unitized Water Flow Glazing Facade. *Sustainability* **2020**, *12*, 7564. [CrossRef]
41. López-Ochoa, L.M.; Las-Heras-Casas, J.; López-González, L.M.; García-Lozano, C. Energy Renovation of Residential Buildings in Cold Mediterranean Zones Using Optimized Thermal Envelope Insulation Thicknesses: The Case of Spain. *Sustainability* **2020**, *12*, 2287. [CrossRef]
42. Spanish Regulation of Thermal Installations in Buildings RITE. *Factores de Emisión de CO2 y Coeficientes de paso a Energía Primaria de Diferentes Fuentes de Energía Final Consumidas en el Sector de Edificios en España*; Instituto para la Diversificación y Ahorro de la Energía (IDAE): Madrid, Spain, 2016.
43. Energy Prices in 2019 Household Energy Prices in the EU Increased Compared with 2018. Available online: https://ec.europa.eu/eurostat/documents/2995521/10826603/8-07052020-AP-EN.pdf/2c418ef5-7307-5217-43a6-4bd063bf7f44 (accessed on 3 February 2021).
44. Yuan, Z.; Zhou, J.; Qiao, Y.; Zhang, Y.; Liu, D.; Zhu, H. BIM-VE-Based Optimization of Green Building Envelope from the Perspective of both Energy Saving and Life Cycle Cost. *Sustainability* **2020**, *12*, 7862. [CrossRef]
45. Copiello, S. Economic implications of the energy issue: Evidence for a positive non-linear relation between embodied energy and construction cost. *Energy Build.* **2016**, *123*, 59–70. [CrossRef]
46. Crawford, R.H. Post-occupancy life cycle energy assessment of a residential building in Australia. *Archit. Sci. Rev.* **2014**, *57*, 114–124. [CrossRef]
47. Crawford, R.H.; Bontinck, P.A.; Stephan, A.; Wiedmann, T.; Yu, M. Hybrid life cycle inventory methods—A review. *J. Clean. Prod.* **2018**, *172*, 1273–1288. [CrossRef]
48. Bonamente, E.; Aquino, A. Life-Cycle Assessment of an Innovative Ground-Source Heat Pump System with Upstream Thermal Storage. *Energies* **2017**, *10*, 1854. [CrossRef]
49. Bonamente, E.; Aquino, A. Environmental Performance of Innovative Ground-Source Heat Pumps with PCM Energy Storage. *Energies* **2020**, *13*, 117. [CrossRef]
50. Saner, D.; Juraske, R.; Kübert, M.; Blum, P.; Hellweg, S.; Bayer, P. Is it only CO_2 that matters? A life cycle perspective on shallow geothermal systems. *Renew. Sustain. Energy Rev.* **2010**, *14*, 1798–1813. [CrossRef]
51. Priarone, A.; Silenzi, F.; Fossa, M. Modelling Heat Pumps with Variable EER and COP in EnergyPlus: A Case Study Applied to Ground Source and Heat Recovery Heat Pump Systems. *Energies* **2020**, *13*, 794. [CrossRef]

Chapter 5

CONCLUSIONS

5.1 Conclusions

Traditional curtain walls can accomplish a passive role in managing the interior environment of a structure by employing measures such as different glazing coatings and gas cavities. Water flow glazing technology acts as an active element to manage the incoming solar radiation on the building and provide its occupants with comfort conditions.

Mathematical models have two different approaches. The simplified one, a set of algebraic equations, helps architects understand the thermal problem. The other one is the complete model, which is more accurate and considers all aspects of reality. The former seems to be the most important one because it is used to start making decisions at the early stages of the project. The latter is used to verify a hypothesis in a transient state. In this research, actual data from prototypes have been used to validate a set of algebraic equations.

The next step is to analyze energy strategies to improve the transparent envelope's behavior based on the previous algebraic equations. On the one hand, the glazing has to maximize the power absorbed by the water flow (P) to harvest thermal energy. On the other hand, reducing the absorptance of the glazing contributes to energy rejection. Furthermore, different orientations and winter and summer conditions must been analyzed.

Equations 5.1 and and 5.2 were presented in Chapter 3.

$$P = \dot{m}\ c\ (\theta_{OUT} - \theta_{IN}), \tag{5.1}$$

$$\theta_{OUT} = \frac{i_0\ A_v + U_i\ \theta_i + U_e\ \theta_e + \dot{m}\ c\ \theta_{IN}}{\dot{m}\ c + U_e + U_i}, \tag{5.2}$$

where P is the total power that is absorbed by the water, θ_{OUT} is the temperature of the water leaving the glazing assembly while θ_{IN} is the temperature of the water entering the glazing assembly.

Equation 5.3 is the result of combining equations 5.1 and 5.2.

$$P = \frac{\dot{m}\ c}{\dot{m}\ c + U_e + U_i}\ (i_0\ A_v + U_i\ (\theta_i - \theta_{IN}) + U_e\ (\theta_e - \theta_{IN})). \tag{5.3}$$

To maximize the water heat gain (P), the value of the product ($\dot{m}\ c$) must be higher than the sum of (U_e) and (U_i) ($\dot{m}\ c > \ > U_e + U_i$)

In this case, the power absorbed (P), turns to be the maximum power (P_{max}).

In addition, if the total absoptance of the glazing (A_v) increases, P also increases.

The difference between the outdoor temperature and the inlet temperature of the glazing (θ_e - θ_{IN}) must be controlled in order to avoid energy losses.

Therefore, Southern facades in cold climates in winter conditions would make the most of solar radiation maximizing the water heat gain. The energy absorbed in the water chamber provides hot water for the heating system or DHW.

In contrast, during summer, energy rejection strategies would be desirable, specially in Eastern and Western facades. For this strategy, the optimum solution would be to reduce the total absoptance of the glazing (A_v) keeping the energy absorption of water in order to avoid energy transmittance indoors.

GENERAL CONCLUSIONS: ENERGY

1. The WFG modular facade bestows high performance on triple glazing thickness: Thermal transmittance (U) ranges from 1.041 to 0.066, while the Solar Heat Coefficient (g) ranges from 0.592 to 0.24, when varying the mass flow rate from 0 L/m2 min to 2 L/m2 min. The Visible Transmittance (T_v) is 0.529 and the Transmittance (T) is 0.214.

2. The WFG prototype developed in Peralveche employed the dual utilization of renewable solar energy production and borehole heat exchangers. The most prevalent advantage is the cooling effect that is apparent during the summer months. During the sample summer week for the WFG cabin, the exterior environment reached a temperature of 36.5 $°C$, while the WFG cabin was able to produce a temperature reduction of 16 $°C$ as compared to the Reference Cabin.

3. WFG technology can be coupled with air-to-water heat pumps to increase efficiency. The Coefficient of Performance (COP) of water-to-water heat pumps is higher due to the lower temperature difference between the source (outdoor air) and load (WFG) sides. The DMAIA prototype results showed that WFG radiant panels improved the performance of air-to-water heat pumps. In Summer conditions, with an outdoor air temperature of 35 $°C$, the COP increased from 2.90 to 3.62 when the water temperature through the WFG was 18$°C$.

4. Water heat gain depends on several variables, including the orientation, the glass composition, and the mass flow rate. The higher the absorptance and mass flow rate, the higher the water heat gain. A triple-pane system with an argon chamber outdoors and a low-emissivity coating has shown promising results in absorbing solar energy. Data from the Sofia prototype showed that the daily solar energy absorbed by the Southern facade in winter is 2.73 kWh/m^2 with a peak solar irradiance of 380 W/m^2 and average outdoor temperature of 1.5 $°C$. However, if the goal is to reject solar energy, a triple pane system with an argon chamber closest to the exterior combined with a solar-control coating has performed well. The daily solar energy absorbed by the Eastern and Western facades in summer is 2.16 kWh/m^2 with a peak solar irradiance of 525 W/m^2 average outdoor temperature of 27 $°C$.

5. The potential of WFG as a means to reduce the cooling loads in summer has been tested. A prototype with WFG in facades and the roof, connected to borehole heat exchangers, was built along with another prototype with the same dimensions and made of traditional double glazing. The effect of thermal inertia derived from geothermal boreholes contributes to flattening the WFG prototype's temperature curve compared with the Reference one. The WFG cabin temperature peaked at 37 $°C$ during the day and 15 $°C$ at night, whereas the RC ranged from 52 $°C$ during the day to 13 $°C$ at night.

6. The damping effect on the WFG cabin's temperature is shown in the Madrid prototype. The WFG system provided the facade with thermal inertia, and the cabin did not suffer drastic thermal oscillations between day and night. The air temperature of the WFG cabin reached a peak value of 27 $°C$, during the day and 18 $°C$ by night, whereas the air temperature of the RC was 37 $°C$ during the day and 15 $°C$ by night. This effect can increase the thermal comfort inside

the building and reduce energy consumption. Once the maximum temperature was reached, the interior of the WFG cabin cooled down more slowly than the Reference cabin did.

PARTICULAR CONCLUSIONS: METHODS

1. Building prototypes proved to be very useful as they have been an essential part of the methodology that has allowed to validate the hypotheses and objectives. Likewise, the mathematical model, provided by researchers of the School of Aeronautics and Space Engineers, has been crucial to compare simulated results with actual data.

2. The reliability of the mathematical model to predicting the behavior of WFG was tested by developing real prototypes. In the Peralveche prototype, the outlet temperature in the WFG roof panels was predicted and compared with the actual results. The mean error (ME) and the mean percentage error (MPE) were measured. The ME of the outlet temperature, θ_{OUT}, was $0.29°C$, and the MPE was 2.1%.

PARTICULAR CONCLUSIONS: ARCHITECTURE AND CONSTRUCTION

1. The study of the Sofia prototype demonstrated that industrialized water flow glazing unitized facade is ready to be used in architecture, engineering, and construction industries.

2. Water flow glazing (WFG), as an advanced facade technology, combines passive (coatings and polyvinyl butyral (PVB) layers) and active solutions (variable water mass flow rate) to absorb or reject infrared radiation and reduce the temperature of the interior glass pane.

3. The WFG module reaches dimensions up to 3 x 1.3 m vertically, allowing freedom in facade design. In addition, every module is autonomous and independent from each other, enabling facade breakdowns that do not depend on hydrostatic pressure.

4. As we have seen in all the prototypes, the WFG modular facade maintains the properties of glass in terms of its transparency, luminosity, lightness, and smoothness.

PARTICULAR CONCLUSIONS: SUSTAINABILITY

1. Thermal comfort can be achieved in summer using WFG radiant surfaces. With indoor air temperatures between 25 and 27°C and MRT between 18 and 22°C, the PMV ranges from -0.5 and +0.1. Those values fall into ASHRAE Thermal Comfort Scale as "Slightly cold."

2. Life Cycle Assessment (LCA) of WFG systems consistently showed a higher initial investment than traditional glazing. The final Life Cycle Cost analysis demonstrates that WFG systems are better through the operational phase only when it is compared with a traditional double-glazing. However, a Life Cycle Energy assessment over 50 years concluded that energy savings between 36% and 66% and CO2 emissions reduction between 30% and 70% could be achieved.

Overall, this thesis has shown that a set of algebraic equations from a simplified mathematical model helps architects and engineers understand the complex behavior of dynamic WFG envelopes at an early stage of the project. Future research could develop a complete mathematical model and its integration in commercial software to validate the hypothesis in a transient state over the years.

5.2 Critical Reflections

The WFG system has several challenges to address. Firstly, retrieving detailed inputs is necessary to assess Water Flow Glazing operation. An advanced energy management system with smart meters and actuators should be deployed along with the WFG facade to integrate the heat pump operation and the ventilation system. These devices show limitations concerning the regularity and precision of data. Secondly, more case studies in several different climate regions should be analyzed. The system is originally meant to operate in areas with mild winters and warm summers. When the freezing risk is high, the performance in the harsh wintertime has to be tested. Finally, a whole commissioning protocol, including design, manufacturing, and maintenance, should be explored to involve construction stakeholders in adopting this product.

The market adoption of the WFG system is limited by its high initial cost, particularly when coupled with borehole heat exchangers. Production and deployment processes must be standardized to bring down initial costs and payback periods.

Water-Flow Glazing was evaluated as a component of a hydronic radiant heating and cooling system. It showed final energy-saving potential, provided thermal comfort, and may be considered a valid option for office retrofitting. However, the

system is limited by its high initial cost and the need for an energy management system integrated with the rest of the equipment, especially the ventilation system and the heat pump. The ventilation system is an essential aspect of comfort. Controlling the relative humidity is indispensable in radiant systems to avoid condensation issues. Therefore, a more advanced ventilation device could help optimize the whole system's performance. Including a heat recovery and variable airflow would reduce the sensible and latent thermal loads and control the dew point temperature. There were uncertainties with the air-to-water heat pump operation. Although the radiant WFG panels could improve the heat pump COP and EER, there were issues with the operating cycles that could affect its performance. The selected heat pump was oversized and frequently started and stopped because it prematurely detected that it had reached the target temperature.

After the first year of monitoring, uncertainties, misfunctions, and system issues must be addressed. Firstly, due to the complexity of the elements involved in human comfort, the control unit must integrate the ventilation device. The operation logic should be able to modify the water mass flow rate and ventilation air heat flow. Secondly, the devices must be adequately dimensioned to avoid misfunctions, especially the air-to-water heat pump. Further research must include heat pump electricity monitoring to compare thermal and electricity consumption and assess energy performance more accurately. Finally, further research on the standardization of its manufacturing process and deployment is needed to bring down initial costs and payback periods. Another research line would be to integrate WFG into commercial building performance simulations.

5.3 Future Research

This thesis studies water flow glazing as a key technology to achieve Net-Zero Energy Buildings (NetZEB), reducing energy consumption and greenhouse gas emissions. The aqueous medium of WFG technology offers multiple advantages in terms of energy savings in buildings. It provides an opportunity for transparent facades to show a real solution to climate change.

When solar radiation penetrates the WFG glazing, a certain amount of this energy is absorbed into the water chamber and later distributed to other parts of the building. Furthermore, another amount of solar energy is transmitted indoors. This energy is reflected diffusely inside the room, creating irradiance. The inner walls absorb some part of the transmitted beam radiation and some diffuse irradiance. Moreno and Hernández (2018) demonstrated that glass panes absorb beam and diffuse solar radiation, together with diffuse irradiance created inside the room

after multiple reflections. This absorbed energy contributes to increasing the indoor temperature. Hence, future research includes evaluating water flow glazing as an effective technology to alleviate overheating inside the buildings.

Energy harvesting strategies may yield considerable energy surplus stored through geothermal borehole heat exchangers or water tanks. The former produces heat with high energy efficiency but needs sufficient ground area and has a high initial cost. The latter allows a cost effective solution, although it requires a significant water volume within an insulated tank. However, Phase Change Materials (PCM) application presents a potential advantage in increasing storage capacity. Chow and Lyu (2017) highlighted that PCM has 5 to 14 times as much storage capacity per unit volume as water. Likewise, more hot water can be harvested during off-work hours for residential use in typical summer and winter weeks using PCM. A fascinating future research project is to implement PCM heat exchangers to enhance WFG energy management.

Some dynamic envelopes react to diverse outdoor conditions by changing their opacity or varying transmission or reflection properties. Gutai and Kheybari (2021) introduces the Smart Water-filled Glass (SWFG) control method, which enables the change of the façade element's opacity by coloring the fluid over a year regarding seasonal changes. A promising future research includes the evaluation of dynamic thermochromic dyes through the glazing.

The simplified mathematical model defines the energy balance in a macro-scale situation to measure the energy that enters the building and its loses. A mezzo-scale situation for the different elements of the building will provide an algorithm defining the specific operations that should be carried out to solve the problem, by means of numerical methods. A very interesting future research will be to implement the algorithm in a commercial tool in order to develop a whole year validation, as it is shown in Figure 5.1.

During the InDeWaG Project, the tests corresponding to the UNE-EN 13830 standard (air permeability, water tightness and resistance to wind load) were carried out. It would be interesting to continue in this way to test the WFG module against impact and fire.

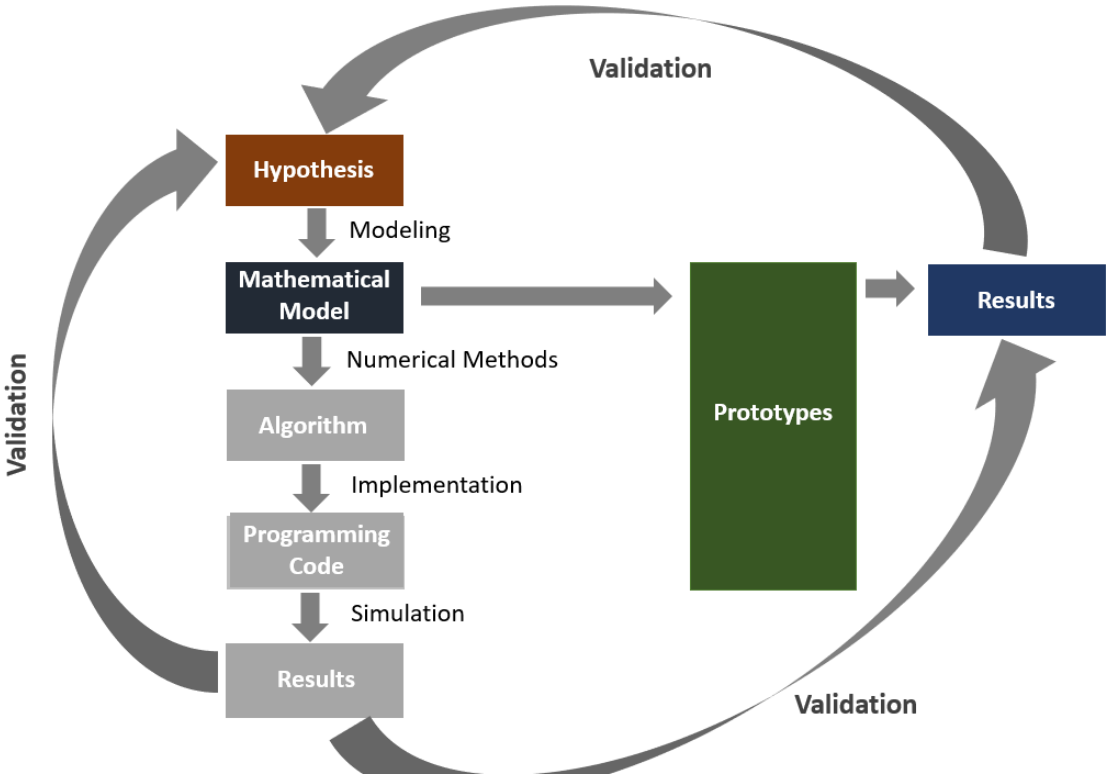

Figure 5.1: Methodology based in the comparison of real data and simulation results

Every day more users, companies and organizations decide to develop their projects following ecological construction standards, and with almost zero energy consumption. This need is what has given rise to the Green Certificates, which are certifications made by experts based on standardized, clear and objective criteria, which allow to ensure or attest to the good environmental performance of the building or construction. An attractive and striking future research will be to evaluate the suitability of the WFG facades in relation to the Green Certificates: LEED, BREAM, etc.

The industrialized facade becomes extremely relevant in nowadays' architecture due to several advantages such as: freedom of geometries because the design is fully computerized, reduction of assembly elements or pieces on-site, reduction of labor costs, execution times are shortened, the use of water is reduced and the work is "cleaner", the quality control is exhaustive, etc. Hence, a very promising future research will be to optimize the design in order to reduce manufacturing costs.

Appendix A

CONFERENCES, PUBLICATIONS, R&D PROJECTS AND DOCTORAL STAY

2019-2020

CONFERENCES

From 2019 to 2020, I have participated in 3 International Conferences, as part of the work to disseminate the results of the Research Project, entitled *Industrial Development of Water Flow Glazing Systems* (IndeWaG), funded by the program Horizon 2020-EU.3.3.1: Reducing energy consumption and carbon footprint by smart and sustainable use, project Ref. 680441.

1. **International Conference on Innovative Applied Energy (IAPE 2019). Oxford, United Kingdom (14-15 March 2019)**

   The IAPE international conference provides a forum for both researchers and industrials to present and share their latest findings in all aspects of applied energy. This provides a unique opportunity to investigate the intersections and the inter-play of the various approaches and solutions developed across this domain.

2. **VII European Conference on Renewable Energy Systems (ECRES 2019). Madrid, Spain (11-12 June 2019)**

   Within the framework of this conference a special session, related to WFG

technology, has been organized in which I participated as chairman.

Session title: *Achieving nearly Zero Energy Buildings with Water Flow Glazing facades*

Conveners: B. Moreno Santamaria, Technical University of Madrid, Spain/ Prof. Dr. J.A. Hernandez, Technical University of Madrid, Spain Dr. T.T. Chow, City University of Hong Kong, Hong Kong

The goal of this session was to attract building energy experts, researchers and industrialists to present and discuss their recent works on water-flow glazing facades and the related technologies, referring to (but not limited to) the scope outlined below.

Scope of the session:

- Theoretical heat and fluid flow analysis in water flow glazing (WFG)
- WFG materials selection and optical properties
- Solar engineering, energy storage and services system integration
- WFG product and system design optimization
- Architectural design, prefabrication and site installation matters
- Long-term reliability and life-cycle analysis
- Operation, maintenance, and services management
- Industrial applications and demonstration projects
- Social and technological barriers on WFG applications

3. **14th Conference on Advanced Building Skins (ABS 2019). Bern, Suitzerland (28-29 October 2019)**

Within the framework of this conference a special session related to WFG technology has been organized.

Session title: *Fluid-flow Façade Technology for Advanced Environmental Performance*

Conveners: Dr. T.T. Chow, City University of Hong Kong, Hong Kong Prof. J.A. Hernandez, Technical University of Madrid, Spain/ B. Moreno Santamaria, Technical University of Madrid, Spain

The two organizing parties in the past decade have accumulated considerable research experiences, technical knowledge, and invention patents on this topic, including the fluid-flow channeled glazing as the transparent façade surfaces and the building-integrated hybrid-solar panels as the opaque wall surfaces. In recent years, more and more academic publications, innovative ideas and practical solutions have been released. New applications were reported in

different countries and meetings. This proposed session is to gather the experts and co-workers of this field to review the state-of-the-arts, to disseminate the technology advancements, to invite for valuable industrial feedback, and to bridge the gap for industrialization.

The scope of the session includes, but is not limited to the following:

- Theoretical heat and fluid flow analysis of Fluid-flow Facade (FF)
- FF materials selection and properties evaluation
- FF product and system design optimization
- Architectural design, prefabrication and site installation matters
- Long-term reliability and life-cycle analysis
- Operation, maintenance, and services management
- Practical applications and demonstration projects

4. **5th World Multidisciplinary Civil Engineering-Architecture-Urban Planning Symposium – WMCAUS 15-19 June 2020, Prague, Czech Republic**

   The main mission of *World Multidisciplinary Civil Engineering-Architecture-Urban Planning Symposium - WMCAUS* is to contribute in multidisciplinary studies related with Civil Engineering, Architecture, City and Urban Planning and to improve interactions between people within these fields. As another mission it will provide a forum for this diverse range of studies which report very latest results and document emerging understanding of the related systems and our place in it.

2019-2020

PUBLICATIONS

The above-mentioned Conferences, yielded the following publications:

Rapado, M.A. Moreno, B. y Hernández, J.A. Battery-less wireless low consumption sensor powered by PV cells and buffered by an ultra-capacitor. Con ISBN: 978-1-912532-05-6. International Conference on Innovative Applied Energy (IAPE 2019). Oxford, United Kingdom (14-15 March 2019).

Del Ama, F., Ferrandiz, J.A., y Moreno, B. Building Energy Modeling by means of BIM software. A case study with Water Flow Glazing. Proceedings ISBN: 978-605-86911-7-9. VII European Conference on Renewable Energy Systems (ECRES 2019). Madrid, Spain (11-12 June 2019).

Belen Moreno, Benito Lauret y Juan A. Hernandez. Industrialization of Water Flow Glazing facades by means of modular units. Proceedings ISBN: 9878-605-86911-7-9. VII European Conference on Renewable Energy Systems (ECRES 2019). Madrid, Spain (11-12 June 2019).

Belen Moreno y Juan A. Hernandez. Software Tool for the design of Water Flow Glazing envelopes. Proceedings ISBN: 9878-605-86911-7-9. VII European Conference on Renewable Energy Systems (ECRES 2019). Madrid, Spain (11-12 June 2019).

Diego Garcia, Belen Moreno, Benito Lauret y Juan A. Hernandez. Commissioning process of Water Flow Glazing facades. Proceedings ISBN: 9878-605-86911-7-9. VII European Conference on Renewable Energy Systems (ECRES 2019). Madrid, Spain (11-12 June 2019).

Belen Moreno, Fernando del Ama y Juan A. Hernandez. Achieving nZEB by means of Water Flow Glazing. Energy balance and thermal behaviour in buildings for advanced performance. 14th Conference on Advanced Building Skins (ABS 2019). Bern, Switzerland (28-29 de octubre de 2019).

Belen Moreno, Fernando del Ama y Juan A. Hernandez. Spectral and thermal problems of Water Flow Glazing. A case of study of an office space. 14th Conference on Advanced Building Skins (ABS 2019). Bern, Switzerland (28-29 de octubre de 2019).

Moreno, B., Del Ama Gonzalo, F., Fernandiz, JA., Lauret, B. Hernandez, JA. A building energy simulation methodology to validate energy balance and comfort in zero energy buildings. Journal of Energy Systems 2019, 3(4), 168-182, DOI: 10.30521/jes. 623285.

Fernando del Ama, Hunter Davis, Benito Lauret, Belen Moreno, Juan A. Hernandez. Building energy simulation. Case studies with water flow glazing. IOP Conf. Series: Materials Science and Engineering, 960 (2020) 022006, doi:10.1088/1757-899X/960/2/022006.

2020-2021

PUBLICATIONS INDEXED IN JCR AND SCOPUS

Moreno Santamaria, B.; del Ama Gonzalo, F.; Pinette, D.; Gonzalez-Lezcano, R.-A.; Lauret Aguirregabiria, B.; Hernandez Ramos, J.A. Application and Validation of a Dynamic Energy Simulation Tool: A Case Study with Water Flow Glazing Envelope. Energies 2020, 13, 3203. (Section 4.1.2)

Moreno Santamaria, B.; del Ama Gonzalo, F.; Lauret Aguirregabiria, B.; Hernandez Ramos, J.A. Experimental Validation of Water Flow Glazing: Transient Response in Real Test Rooms. Sustainability 2020, 12, 5734. (Section 4.1.3)

Moreno Santamaria, B.; Ama Gonzalo, F.; Lauret Aguirregabiria, B.; Hernandez Ramos, J.A. Evaluation of Thermal Comfort and Energy Consumption of Water Flow Glazing as a Radiant Heating and Cooling System: A Case Study of an Office Space. Sustainability 2020, 12, 7596. (Section 4.2.2)

Moreno Santamaria, B.; del Ama Gonzalo, F.; Pinette, D.; Lauret Aguirregabiria, B.; Hernandez Ramos, J.A. Industrialization and Thermal Performance of a New Unitized Water Flow Glazing Facade. Sustainability 2020, 12, 7564. (Section 4.1.4)

Santamaria, B.M.; Gonzalo, F.d.A.; Griffin, M.; Aguirregabiria, B.L.; Ramos, J.A.H. Life Cycle Assessment of Dynamic Water Flow Glazing Envelopes: A Case Study with Real Test Facilities. Energies 2021, 14, 2195. (Section 4.3.2)

2010-2020

R&D PROJECTS

During the last ten years I have been involved in several R & D Projects at a National and European level, focused on Energy Efficiency in Buildings:

RESEARCH PROJECT InDeWaG – INDUSTRIAL DEVELOPMENT OF WATER FLOW GLAZING SYSTEMS. Financed by the European Commission. Horizon 2020. Call: H2020-EE-2015-1-PPP. Topic: EE-02-2015. Type of action: IA. Proposal number: 680441. Start/ End: 2015/2020.

PROYECTO ADIMET – AUTÓMATA DIGITAL MINIATURIZADO DE BAJO COSTE DOTADO DE FIRMWARE INTELIGENTE PARA MONITORIZACIÓN,

EL CONTROL DEL CONSUMO PORMENORIZADO DE APARATOS ELÉCTRICOS EN EDIFICACIÓN CON EL OBJETIVO DEL AHORRO ENERGÉTICO. Entidad financiadora: Ministerio de Industria, Turismo y Comercio. Plan de Investigación Científica y Técnica y de Innovación 2013-2016. Descripción: AEESD 2014 – Acción estratégica de Economía y Sociedad Digital Inicio/Fin: 2014/2015.

PROYECTO SOHIRE – SOLUCIÓN HÍBRIDA REACTIVA PARA ENVOLVENTES SOSTENIBLES. Entidad financiadora: MINISTERIO DE ECONOMÍA Y COMPETITIVIDAD. Centro para el Desarrollo Tecnológico Industrial CDTI Descripción: Proyecto de Cooperación Interempresas Nacional Inicio/Fin: 2013/2015.

PROYECTO SILEDs–NUEVO SISTEMA DE ILUMINACIÓN TRANSPARENTE MEDIANTE LA INTEGRACIÓN DE LEDs EN EL CANTO DE VIDRIOS CURVOS. Entidad financiadora: MINISTERIO DE ECONOMÍA Y COMPETITIVIDAD. Centro para el Desarrollo Tecnológico Industrial CDTI Descripción: Proyecto de Investigación y Desarrollo (PID) Inicio/Fin: 2012/2015.

PROYECTO SINGER - SISTEMA INTELIGENTE PARA LA GESTIÓN Y LA EFICIENCIA ENERGÉTICA EN REHABILITACIÓN DE ENVOLVENTES ARQUITECTÓNICAS BASADO EN TECNOLOGÍA INTELLIGLASS. Entidad financiadora: MINISTERIO DE CIENCIA E INNOVACIÓN subprograma INNPACTO Descripción: IPT-2011-1764-920000 Inicio/Fin: 2011/2014.

PROYECTO SIGLAS. SISTEMA INTELIGENTE DE GESTIÓN ENERGÉTICA EN EDIFICIOS BASADOS EN TECNOLOGÍA RADIAGLASS. Entidad financiadora: Ministerio de Industria, Turismo y Comercio. Subprograma Avanza Competitividad I+D+i. Descripción: TSI-020302-2010-118 Inicio/Fin: 2010/2013.

2019-2020

DOCTORAL STAY

I have participated in the Faculty Development Grant project, Keene State College, New Hampshire, USA, supervised by Dr. Fernando del Ama Gonzalo.

The research project took two semesters: fall 2019 and spring 2020. On this regard I was able to become familiar with the Architecture program and successfully collaborated with faculty and students. I stayed at Keene State College for 6 weeks from August 16, 2019. The collaboration continued on-line over the spring Semester due to COVID-19 outbreak.

Overview of the Department:

This project's first objective was to understand energy consumption and carbon emission patterns in the building sector. ARTICLE 1 and ARTICLE 2 showed detailed reports on energy consumption patterns in buildings.

The second objective was to evaluate comfort parameters related to occupant behavior and mean radiant temperature in non-residential buildings. ARTICLE 1 showed a building energy management system's design and operation coupled with Water Flow Glazing throughout a year in an actual office space. Temperature, relative humidity, and solar radiation sensors were connected to a control unit that actuated the different devices to keep comfortable conditions with minimum energy consumption.

The final objective was to validate a Building Energy Management system that collected data at a specified time interval at designated measurement points. ARTICLE 2 showed that the accuracy of the system has proven to be adequate. However, using borehole heat exchangers as a renewable source of energy comes at a high deployment cost.

The dissemination of results plan included the submission of articles to peer-reviewed journals. Two articles co-authored by the senior KSC students, Hunter Davis and Danielle Pinette, have been submitted to open-access indexed journals:

- ARTICLE 1: Moreno Santamaria, B.; del Ama Gonzalo, F.; Pinette, D.; Gonzalez-Lezcano, R.-A.; Lauret Aguirregabiria, B.; Hernandez Ramos, J.A. Application and Validation of a Dynamic Energy Simulation Tool: A Case Study with Water Flow Glazing Envelope. Energies 2020, 13, 3203. (Section 4.1.2)
- ARTICLE 2: Fernando del Ama, Hunter Davis, Benito Lauret, Belen Moreno, Juan A. Hernandez. Building energy simulation. Case studies with water flow glazing. IOP Conf. Series: Materials Science and Engineering, 960 (2020) 022006, doi:10.1088/1757-899X/960/2/022006.

As a result of this publications, we participated at World Multidisciplinary Civil Engineering Architecture and Urban planning Symposium (WMCAUS) held in Prague in 2020. As explained in previous paragraph, the aim of this symposium was to provide a forum for discussion of the latest findings and technologies in different fields of Civil Engineering, Architecture and Urban Planning. The original date of the conference was postponed, and it was finally held on-line.

In addition to the scientific articles, I overviewed KSC students John Mc Mahon and Mike Downing participation at the Academic Excellence Conference, held at

Keene State College in spring 2020. The presentation title was: The unintentional air and moisture movement through buildings.

References

Abdulmohsin, H., Aritra, G., Senthilarasu, S., Tapas, K., 2020. Evaluation of thermal performance for a smart switchable adaptive polymer dispersed liquid crystal (pdlc) glazing. Solar Energy 195, 185–193.

AENOR, . Asociación española de normalización y certificación. https://www.aenor.com/. [Online; accessed on 16 August 2021].

AENOR, 2006. Sistemas solares térmicos y componentes. captadores solares. parte 2: Métodos de ensayo. https://www.aenor.es/.

Allen, K., Connelly, K., Rutherford, P., Wu, Y., 2017. Smart windows—dynamic control of building energy performance. Energy Build 139, 535–546.

Andresen, I., 2018. Handbook of Energy Systems in Green Buildings. Springer, Berlin, Heidelberg.

Arpino, F., Cortellessa, G., Frattolillo, A., 2015. Experimental and numerical assessment of photovoltaic collectors performance dependence on frame size and installation technique. Solar Energy 118, 7–19.

Attia, H., Gonzalo, F.D.A., 2019. Stand-alone pv system with mppt function based on fuzzy logic control for remote building applications. International Journal of Power Electronics and Drive Systems 10(2), 842–851.

Baranzelli, C., Lavalle, C., Sgobbi, A., Aurambout, J., Trombetti, M., Jacobs, C., Garcia, J.C., Kancs, D., Kavalov, B., 2016. Regional patterns of energy production and consumption factors in europe—exploratory project erebiland—european regional energy balance and innovation landscape. Publications Office of the European Union: Luxembourg EUR 27697.

Bertsch, S., Oppliger, D., Menzi, T., 2013. Facade element.

BOE, . Boletín oficial del estado, españa. https://www.boe.es/. [Online; accessed on 16 August 2021].

Boemi, S., Tziogas, C., 2013. Energy Performance of Buildings. Springer, Cham.

Buonomano, A., Forzano, C., Kalogirou, S., Palombo, A., 2019. Building-façade integrated solar thermal collectors: Energy-economic performance and indoor comfort simulation model of a water based prototype for heating, cooling, and dhw production. Renewable Energy 137, 20–36.

Casini, M., 2015. Smart windows for energy efficiency of buildings. International Journal of Civil and Structural Engineering 2, 230–238.

CDTI, . Centro para el desarrollo tecnológico industrial. https://www.cdti.es/. [Online; accessed on 16 August 2021].

Chiapale, J., Bavel, C.V., Sadler, E., 1983. Comparison on calculated and measured performance of a fluid-roof and a standard greenhouse. Energy in Architecture 2, 75–89.

Chow, T., Li, C., 2013. Liquid-filled solar glazing design for buoyant water-flow. Building and Environment 60, 45–55.

Chow, T., Li, C., Lin, Z., 2009. Innovative solar windows for cooling demand climate. Solar Energy Materials and Solar Cells 94, 212–220.

Chow, T., Li, C., Lin, Z., 2011a. The function of solar absorbing window as water-heating device. Building and Environment 46, 955–960.

Chow, T., Li, C., Lin, Z., 2011b. Numerical prediction of water-flow glazing performance with reflective coating. Proceedings of the Conference of International Building Performance Simulation Association, Sydney .

Chow, T., Li, C., Lin, Z., 2011c. Thermal characteristics of water-flow double-pane window. International Journal of Thermal Sciences 50, 140–148.

Chow, T., Lyu, Y., 2017. Numerical analysis on the advantage of using pcm heat exchanger in liquid-flow window. Applied Thermal Engineering 125, 1218–1227.

CORDIS, . European research results. https://cordis.europa.eu/es. [Online; accessed on 16 August 2021].

CTE DBHE, S.M.o.D., 2019. Basicdocument on energy saving of the technical building code (documento básico de ahorro de energía del código técnico de la edificación, cte-db-he). https://www.codigotecnico.org/images/stories/pdf/ahorroEnergia/DBHE.pdf (. [Online; accessed on 16 August 2021].

Damagnez, J., Bavel, C.V., Sadler, E., 1984. Simulation of the effect of storage characteristics upon the dynamic response of the fluid-roof solar greenhouse. Acta Hrotic 106, 27–38.

Directive 2018/844, E.U., 2018. Directive (eu) 2018/844 of the european parliament and of the council of 30 may 2018. amending directive 2010/31/eu on the energy performance of buildings and directive 2012/27/eu on energy efficiency. https://eur-lex.europa.eu/legal-content/EN/TXT/PDF/?uri=CELEX:32018L0844&from=EN. [Online; accessed on 24 November 2020].

Edwards, R., Larivé, J., Rickeard, D., Weindorf, W., 2014. Well-to-tank report version 4.a. well-to-wheels analysis of future automotive fuels and powertrains in the european context. Publications Office of the European Union: Luxembourg .

EN410, 2011. Glass in building—determination of luminous and solar characteristics of glazing. German Institute for Standardization: Berlin, Germany .

EN673, 2011. Glass in building—determination of thermal transmittance (u value)—calculation method. German Institute for Standardization: Berlin, Germany .

Frattolillo, A., Canale, L., Ficco, G., Mastino, C., Dell'Isola, M., 2020. Potential for building façade-integrated solar thermal collectors in a highly urbanized context. Energies 13, 5801.

Garzia, F., 2013. Modelling and simulation of fluidized glazing elements for office buildings. Tesi di Dottorato, Scuola di Ingegneria Industriale, Politecnico di Milano .

Ghosh, A., Norton, B., Duffy, A., 2016. Behaviour of a spd switchable glazing in an outdoor test cell with heat removal under varying weather conditions. Applied Energy 180, 695–706.

Gil-Lopez, T., Gimenez-Molina, C., 2013. Influence of double glazing with a circulating water chamber on the thermal energy savings in buildings. Energy and Buildings 56, 56–65.

Gil-Lopez, T., Molina, C.G., 2013. Environmental, economic and energy analysis of double glazing with a circulating water chamber in residential buildings. Applied Energy 101, 572–581.

Giménez-Molina, C., 2011. Alternatives for the improvement of the energy efficiency of glazing: Dynamic glasses. Tesis Doctoral, Departamento de Construcción y Tecnología Arquitectónicas .

Glass, R.S.S.T., . Robin sun solar thermal glass. https://www.robinsun.co/en/technology/. [Online; accessed on 16 August 2021].

Glassx, . Glassx ag. https://www.glassx.ch. [Online; accessed on 16 August 2021].

Gstoehl, D., Stopper, J., Bertsch, S., Schwarz, D., 2011. Fluidised glass facade elements for an active energy transmission control. Proceedings of the World Engineers Convention, Geneva, Switzerland .

Gutai, M., Kheybari, A., 2020. Energy consumption of water-filled glass (wfg) hybrid building envelope. Energy and Buildings 218, 110050.

Gutai, M., Kheybari, A.G., 2021. Energy consumption of hybrid smart water-filled glass (swfg) building envelope. Energy and Buildings 230, 110508.

Hernandez, J., Hermanns, M., Ama, F., Hernandez, C., 2010. Active transparent or translucent enclosures with energy control capacity.

InDeWaG, . Industrial development of water flow glazing systems. https://http://www.indewag.eu/. [Online; accessed on 16 August 2021].

Ji, J., Luo, C., Chow, T., Sun, W., He, W., 2011. Thermal characteristics of a building-integrated dual-function solar collector in water heating mode with natural circulation. Energy 36(1), 566–574.

Kerskes, H., Heidemann, W., Müller-Steinhagen, H., 2004. Investigation of a solar active glass facade. Proceedings of the EroSun Conference Freiburg Germany .

Koffi, B., Cerutti, A., Duerr, M., Iancu, A., Kona, A., Janssens-Maenhout, G., 2017. Com default emission factors for the member states of the european union - version 2017, european commission, joint research centre (jrc) [dataset]. http://data.europa.eu/89h/jrc-com-ef-comw-ef-2017. [Online; accessed on 24 November 2020].

Lauret, B., Ovando, G., Gimenez, C., 2010. Cerramiento para el control de las cargas térmicas de edificios.

Li, C., 2012. Performance evaluation of water-flow window glazing. Ph.D. Thesis, Department of Civil and Architectural Engineering, City University of Hong Kong .

Li, C., Chow, T., 2011. Water-filled double reflective window and its year-round performance. Procedia Environmental Sciences 11, 1039–1047.

Lyu, Y., Chow, T., Wang, J., 2018. Numerical prediction of thermal performance of liquid-flow window in different climates with anti-freeze. Energy 157, 412–423.

Lyu, Y., Wu, X., Li, C., Su, H., He, L., 2019. Numerical analysis on the effectiveness of warm water supply in water flow window for room heating. Solar Energy 177, 347–354.

McGlew, J., 1985. Building structure and building panel and method of controlling appearance and lighting of a building.

McKee, F., 1985. Windows.

Moreno, B., Ama, F., Lauret, B., Hernandez, J., 2020a. Evaluation of thermal comfort and energy consumption of water flow glazing as a radiant heating and cooling system: A case study of an office space. Sustainability 12, 7596.

Moreno, B., Ama, F., Lauret, B., Hernandez, J., 2020b. Experimental validation of water flow glazing: Transient response in real test rooms. Sustainability 12, 5734.

Moreno, B., Hernández, J., 2018. Analytical solutions to evaluate solar radiation overheating in simplified glazed rooms. Building and Environment 140, 162–172.

Patentscope, . Patentscope. https://patentscope.wipo.int/search/es/search.jsf. [Online; accessed on 16 August 2021].

Peterson, K., Torcellini, P., Grant, R., 2015. A common definition for zero energy buildings. U.S Department of energy, Energy Efficiency and Renewable Energy, USA .

Pilkinton Brothers, L., 1973. Improvements in or relating to liquid filled double glazed units.

Platzer, W., Hube, W., Adelmann, W., Crisinel, M., Vollmar, T., 2005. Development of a glass facade with internal fluid flow. Proceedings of the International Conference Glass Processing Days, Tampere, Finland .

Pérez-Pujazón, B., 2015. The architectural implementation of active glazing with circulating water, and its contribution to nearly zero energy buildings. Tesis Doctoral, Departamento de Construcción y Tecnología Arquitectónicas .

RITE, 2016. Factores de emisión de co2 y coeficientes de paso a energía primaria de diferentes fuentes de energía final consumidas en el sector de edificios en españa. Instituto para la Diversificación y Ahorro de la Energía (IDAE), Madrid .

Sartori, I., Napolitano, A., Voss, K., 2012. Net zero energy buildings: a consistent definition framework. Energy and Buildings 139, 220–232.

Schwarz, D., 1998. Method of transparent heat insulation in a building.

Schwarz, D., 2001. Method of transparent heat insulation in a building.

Seemann, R., 1982. All season window.

Sierra, P., Hernandez, J., 2017. Solar heat gain coefficient of water flow glazing. Energy and Buildings 139, 133–145.

TRNSYS, . Transient system simulation tool. https://www.trnsys.com/. [Online; accessed on 16 August 2021].

Walter, H., 1998. Composite window.